Thermoset based polymer composites for self-sensing structures and coatings

Ricardo José da Silva Lima

UMinho | 2025

Universidade do Minho

Escola de Engenharia

Ricardo José da Silva Lima

Thermoset based polymer composites for self-sensing structures and coatings

março de 2025

Universidade do Minho
Escola de Engenharia

Thermoset based polymer composites for self-sensing structures and coatings

Ricardo José da Silva Lima

Tese de Doutoramento
Engenharia de Materiais

Trabalho efetuado sob a orientação de:

Professor Doutor Senentxu Lanceros -Méndez

Doutor Pedro Filipe Ribeiro da Costa

Doutor João Pedro Nunes Pereira

Março 2025

DIREITOS DE AUTOR E CONDIÇÕES DE UTILIZAÇÃO DO TRABALHO POR TERCEIROS

Este é um trabalho académico que pode ser utilizado por terceiros desde que respeitadas as regras e boas práticas internacionalmente aceites, no que concerne aos direitos de autor e direitos conexos.

Assim, o presente trabalho pode ser utilizado nos termos previstos na licença abaixo indicada.

Caso o utilizador necessite de permissão para poder fazer um uso do trabalho em condições não previstas no licenciamento indicado, deverá contactar o autor, através do RepositóriUM da Universidade do Minho.

Licença concedida aos utilizadores deste trabalho



Atribuição-NãoComercial
CC BY-NC

https://creativecommons.org/licenses/by-nc/4.0/

ACKNOWLEDGEMENTS

This PhD thesis was developed with the invaluable support, encouragement, and expertise of numerous individuals. Each person, whether directly involved in the research or providing support behind the scenes, has played an essential role in this journey, contributing in ways that I will forever be grateful for.

First, I want to thank the members of the Electroactive Smart Materials group, who made each day in the lab both productive and enjoyable. Their camaraderie and dedication turned the challenges of research into rewarding experiences. I am particularly grateful to Pedro Costa, João Pereira, and Professor Senentxu, who not only offered their knowledge and mentorship but also gave me the chance to be part of a group whose work is making a meaningful impact in our field. Their guidance has been instrumental in shaping the direction of this research, and I am honoured to have had the opportunity to work under their influence.

Special recognition is also due to Juliana Oliveira and Jivago Nunes from Nanopaint. Their trust and faith in my capabilities were not only encouraging but foundational for my journey. They took a chance by hiring me as their first employee, allowing me early entry into the professional world and enabling my re-connection with the Electroactive Smart Materials group. This opportunity provided both practical experience and a network of supportive colleagues, both of which were pivotal in my development as a researcher. Their support exemplifies the collaborative spirit of this project and was a key part of making this work possible. Special thanks to Estela Carvalho and Rita Policia for her help with the small but important details of academic services help and thesis formatting.

To my family, I owe a debt of gratitude that words cannot fully capture. They are the core of my life, always standing by me with unyielding patience and love, no matter how challenging the journey became. Their emotional support has been a constant source of strength, and their dedication to meeting my needs has been particularly meaningful during the past two years, which brought their own set of difficulties. Through their generosity, understanding, and encouragement, they have helped me stay focused on my goals. My family's unwavering belief in me has been, and always will be, the foundation of my accomplishments.

To my beloved wife, I extend my deepest and most heartfelt thanks. For 23 years, she has stood by my side, sharing every joy and every hardship, and has supported me through countless challenges. Her belief in me has been a source of resilience, and her encouragement has been a guiding light through every battle. Her presence is a testament to the power of love, patience, and perseverance. Through her,

I have learned that it is never too late to grow, to embrace new dreams, and to become the person I aspire to be. She has not only been my partner but my greatest inspiration and source of strength.

To my daughters, I give thanks for the unique and invaluable support they have provided, even indirectly. Their laughter, curiosity, and joy have been a reminder of life's simple pleasures and have offered me moments of calm, fun, and relaxation amid the intensity of research. They remind me daily of what truly matters and bring balance to my life, helping me stay grounded and energized.

I would also like to acknowledge and express my appreciation to the Fundação para a Ciência e a Tecnologia for their financial support. Their contribution has been essential in enabling the continuation and completion of my studies, and I am deeply appreciative of the role they have played in facilitating this research. Their investment in my work reflects their commitment to advancing scientific knowledge, and I am grateful for their trust and belief in this project.

To everyone who has touched my life and this work in ways big and small, whether mentioned by name or not, I am deeply grateful. This thesis is as much a product of your kindness, guidance, and generosity as it is of my own efforts. Thank you all for being part of this journey.

STATEMENT OF INTEGRITY

I hereby declare having conducted this academic work with integrity. I confirm that I have not used plagiarism or any form of undue use of information or falsification of results along the process leading to its elaboration.

I further declare that I have fully acknowledged the Code of Ethical Conduct of the University of Minho.

Resumo

As resinas epóxi são amplamente utilizadas em várias indústrias devido à sua resistência mecânica, adesividade e versatilidade. Elas formam estruturas com ligações cruzadas aumentando rigidez e durabilidade. Contudo, estas propriedades podem ser melhoradas com a incorporação de nanopartículas condutoras, como os nanotubos de parede múltipla (MWCNTs), o carbono negro (CB) e o grafeno (G), resultando em compósitos avançados com características térmicas, mecânicas e elétricas. Esta dissertação centra-se no desenvolvimento de compósitos termoendurecidos para aplicações estruturais e revestimentos. Foram escolhidas três resinas epóxi (ERs), duas tradicionais e uma sustentável. Apesar dos seus benefícios, estas resinas podem ser frágeis em aplicações que requerem flexibilidade. A adição de nanopartículas condutoras, como os MWCNTs, CB e G concederam capacidades de deteção intrínsecas para monitorizar a deformação e a variação de temperatura. A preparação dos compósitos incluiu a dispersão das nanopartículas, utilizando dispersão ultrassónica e dissolução mecânica, com amostras preparadas através de doctor blade e serigrafia. A funcionalização garantiu resposta piezo- e termoresistiva notável, sendo que a resistividade elétrica diminui para cerca de 100 Ω/sq à concentração máxima. Os resultados revelaram uma boa resposta piezoresistiva com um gauge factor (GF) máximo de 15, e uma sensibilidade termoresistiva de 0,61 %.°C^{-1} para os compósitos 15G/ER. As estruturas coladas apresentaram uma boa resposta mecânica, apresentando excelentes propriedades adesivas, atingindo uma tensão de corte 40 MPa para a resina sustentável. Os testes morfológicos evidenciaram nanopartículas bem dispersas na matriz. Os testes mecânicos provaram capacidades de deformação variáveis, com os melhores resultados próximos do limite de percolação. Vários sensores foram fabricados por serigrafia e colagem, tendo sido realizadas avaliações de deformação e variação de temperatura que demonstraram linearidade em diferentes concentrações. As estruturas coladas apresentaram variações de resistência mais elevadas em comparação com os filmes finos, evidenciando a versatilidade da configuração estrutural. Os compósitos multifuncionais foram também testados para aplicações adesivas através de ensaios de cisalhamento. Por fim, foi desenvolvido um sistema cantilever com as resinas selecionadas, destacando o potencial auto sensível sob deformações de flexão. No geral, o trabalho desenvolvido demonstra de forma convincente a adequação das resinas epóxi para aplicações estruturais que necessitem de características adesivas com sensibilidade elétrica às deformações mecânicas e à variação de temperatura

Palavras-chave: Adesivos; Multifuncional; Piezoresistivo; Revestimentos; Resina epóxi; Sustentável Serigrafia; Termoresistivo;

Abstract

Epoxy resin (ERs) are widely used in various industries due to their excellent mechanical strength, adhesive properties, and versatility. As thermosetting polymers, they form cross-linked structures that enhance their rigidity and durability. These properties can be improved and, more important, can acquire additional functionality with the incorporation of nanoparticles, such as conductive carbonaceous resulting in advanced composites with tailored thermal, mechanical, and electrical properties.

This thesis focuses on developing self-sensing materials to be used in structural applications and coatings. Two traditional resins with different viscosities and a sustainable resin were selected for their high mechanical strength. Nanoparticles including multiwall carbon nanotubes (MWCNTs), carbon black (CB), and graphene (G) were incorporated to grant electric response without losing mechanical properties and introduce intrinsic sensing capabilities for monitoring deformation and temperature. The composite preparation involved dispersing nanoparticles in varying concentrations within each resin. Ultrasonic sonication and mechanical dissolution were chosen, and the samples were prepared by doctor blade and screen-printing. Morphological analysis showed well-dispersed nanoparticles within the matrix is all cases. Mechanical testing revealed varying strain capacities, depending on filler type and content. The formulations obtained exhibited low electrical resistivity of 100 Ω/sq at higher filler concentrations.

To assess the sensing capabilities of the materials, piezoresistive and thermoresistive response was evaluated. Tests included deformation and temperature variation evaluations, demonstrating linearity across different filler concentrations and deformation levels.

A maximum piezoresistive response with a gauge factor up to 15, and thermoresistive sensibility up to 0.61 $\%.C^{-1}$ were obtained for 15G/ER composite. Bonded structures and a cantilever prototype demonstrated both sensing properties with excellent adhesive lap shear force of 40 MPa for the bio-resin. Overall, the developed work convincingly demonstrates the suitability of epoxy resins with adhesive and self-sensing mechanical and temperature characteristics, for structural bonding applications.

Keywords: Adhesives; Coatings; Epoxy resin; Multifunctional; Piezoresistive; Screen-printing; Thermoresistive; Sustainable.

Index

Chapter 1 - Introduction 1

1.1 Overview 2

1.2 Thermosetting Polymers: Characteristics and Applications 4

1.2.1 Epoxy resins: Classification, Properties and Applications 6

1.2.3 Biobased ERs: Sustainability and Applications 9

1.3 Screen-printing Technology: Principles and Applications 10

1.3.1 Industrial Applications of Screen-Printed ERs 12

1.4 Multifunctionality of ERs Reinforced with Carbon Nanofillers 13

1.4.1 Piezoresistive Effect 14

1.4.2 Thermoresistive Effect 15

1.4.3 Carbon Nanofillers in Multifunctional Systems 16

1.4.4 Piezoresistive ERs-Based composites 18

1.5 Objectives and Methodology 19

1.6 Thesis Structure 19

1.7 References 21

Chapter 2 - Additive manufacturing of multifunctional epoxy adhesives with self-sensing piezoresistive and thermoresistive capabilities 29

2.1 Introduction 30

2.2 Experimental 32

2.2.1 Materials 32

2.3 Production of the ERs and composites adhesives 32

2.4 Fabrication of adhesively bonded joints with sensing capabilities 34

2.5 Characterization techniques and procedures 34

2.5.1 Physical-chemical characterization 34

2.5.2 Functional response characterization. 35

2.6 Results and Discussion 38

2.6.1 Physical-chemical properties of resin and composites 38
2.7 Piezoresistive and thermoresistive functional response 42
2.8 Multifunctional adhesively bonded joints 45
2.9 Piezoresistive prototype for cantilever applications 48
2.10 Conclusions 49
2.11 References 51
Chapter 3 - Develop of thermo- and piezoresistive responses in epoxy resins-based adhesives 55
3.1 Introduction 56
3.2 Experimental 58
3.2.1 Materials 58
3.3 ERs and composites process 58
3.4 Production of adhesively bonded joints for functional applications 60
3.5 Samples Characterization 60
3.6 Results and Discussion 63
3.6.1 Morphology, chemical structure, and contact angle properties 63
3.7 Mechanical and electrical measurements 65
3.8 Functional composites: piezoresistive and thermoresistive sensing 67
3.9 Adhesion and sensing properties 70
3.10 Self-sensing piezoresistive adhesive for cantilever applications 73
3.11 Conclusions 75
3.12 References 77
3.13 Graphical Abstract 80
Chapter 4 - Effect of carbonaceous filler type content on the piezo- and thermoresistive response of screen-printing sustainable adhesive epoxy composites 81
4.1 Introduction 82
4.2 Experimental details 84
4.2.1 Materials 84

4.2.2 Production of the ERs and composite adhesives 84
4.3 Fabrication of adhesively bonded joints and coatings with sensing capabilities 85
4.4 Characterization procedures 86
4.5 Results and Discussion 88
4.5.1 Physicochemical properties of bio-resin and composite adhesives 88
4.6 Functional piezoresistive and thermoresistive response 94
4.7 Adhesion and piezoresistive sensing properties of bonded joints 96
4.8 Conclusions 98
Chapter 5 - Conclusions and Future Works 104
5.1 Conclusions 105
5.2 Future Directions for Research: 107

List of Figures

Figure 1.1 - Utilization of ERs across different industries, reproduced from [11]. 3
Figure 1.2 - Schematic of polymers before and after crosslinking, reproduced from [19]. 4
Figure 1.3 - Uses of ERs divided by sector in global using applications, produced acording to [30]. 6
Figure 1.4 - Representation of Thermoplastic and Thermoset Polymeric Materials: (left) Thermoplastics featuring weak intermolecular forces between polymer chains; (right) Thermosets characterized by strong covalent bonds. Reproduced from [32]. 7
Figure 1.5 - ERs-based applications, including: A) Flexible temperature sensor, B) plastic film that integrates organic transistors with pressure-sensitive rubber, C) demonstration platform for multifunctional electronics showcasing physical properties, D) model hand covered in temperature-sensitive artificial skin, completed with an enlarged view of skin thermoreceptors, and E) a flexible temperature sensor embedded within the fibres of a textile yarn [38]. 8
Figure 1.6 - Illustration of some bio-based. Reproduced from [43]. 9
Figure 1.7 - Illustration of screen-printing process. Reproduced from [54]. 10
Figure 1.8 - Illustration of a UV process, where a liquid or past ERs is turned into a polymerized solid. Reproduced from [56]. 11
Figure 1.9 - Illustration of A) MWCNTs, B) G and C) CB, reproduced from [30], [69] and [70], respectively. 14
Figure 1.10 - Illustration of the piezoresistive effect, when matrix with conductive particles is subjected to mechanical solicitation, reproduced from [79]. A) Refers to uncompressed matrix and B) refers to compressed matrix. 15
Figure 1.11 - A) 3D representation of the proposed flow sensor; B) Illustration demonstrating the deflection of the sensor as a result of increased flow. Reproduced from [86]. 16
Figure 1.12 - Application areas of ERs matrix composites and the most relevant characteristics. Reproduced from [91]. 19
Figure 2.1 - Schematic illustration of the samples manufacturing procedure by the doctor blade and screen-printing techniques. 33
Figure 2.2 Schematic illustration of the evaluation of the functional sensing response of the samples: A) four-point-bend piezoresistive and B) thermoresistive measurements. 37
Figure 2.3 - Cross-section SEM micrographs of 3-layer screen-printed samples: resin (A and B), 3MWCNTs/RE (C and D), 5MWCNTs/RE (E and F) and 10MWCNTs/RE (G and H) composites. Magnifications from 130x to 20,000×. 39

Ilustração 2.4 - A) FTIR spectra and B) contact angle of resin and corresponding composites prepared by screen-printing and doctor blade. 39
Figure 2.5 - Representative tensile stress-strain measurements showing the elongation at break for A) screen-printing and B) doctor blade prepared samples. C) stress and strain at break and D) Initial elastic modulus measured up to 1% for all samples. 41
Figure 2.6 - Electrical sheet resistance for pristine resin and polymer composites up to 10 wt.% MWCNTs content. Films are processed both by screen-printing and doctor blade. 42
Figure 2.7 - Representative piezoresistive response under cyclic bending tests at 3 mm maximum displacement for A) 3MWCNTs/RE, B) 5MWCNTs/RE and C) 10MWCNTs/RE composites. D) Repeated bending tests for 100 cycles at maximum vertical deformation of 1 mm for the 5MWCNTs/RE composite. 43
Figure 2.8 - Piezoresistive gauge factors of composites with 3, 5 and 10 wt.% MWCNTs content for maximum bending strains from 0.1 to 5 mm at 3 mm/min. 44
Figure 2.9 - Thermoresistive response of the 5MWCNTs/RE composite for temperature variations in the A) human body regime (32 to 40 °C) and B) higher temperatures (60 to 90 °C)..... 45
Figure 2.10 - A) Schematic illustration of the bonded joint with uniaxial shear test setup. B) Shear strength of CFRP and aluminum bonded joints. 46
Figure 2.11 - Piezoresistive response of a bonded joint with 5MWCNTs/RE during 10 loading-unloading bending cycles for A) maximum bending of 0.1, 0.3, 0.5 mm; B) and 1, 3, and 5 mm. C) 500 cycles at 1 mm bending; D) corresponding GF for maximum bending displacements. 47
Figure 2.12 - Thermoresistive response of a 5MWCNTs/RE composite bonded joint between A) 32 to 50 °C and B) 60 to 90 °C for 5 cycles. 48
Figure 2.13 - A) Schematic representation of the prototype to evaluate the ERs composite as a self-sensing adhesive in a cantilever structure. Piezoresistive response of the 5MWCNTs/RE composite as a cantilever bending sensor for B) 1, 3, and 5 mm maximum displacement. 49
Figure 3.1 - Representation of the ERs and respective composites preparation by doctor blade and screen-printing methods. 60
Figure 3.2 - Representation of the A) piezoresistive (0.1 to 5 mm of bending) and B) thermoresistive tests. The lower row shows the placement of the electrodes in the samples for the corresponding tests. 63
Figure 3.3 - Cross section (above) and surface (below) SEM images of the screen-printed ERs (A and B) and composites with 3 wt.% (C and D), 5 wt.% (E and F), and 10 wt.% (G and H) MWCNTs content. 64

Figure 3.4 - Representative FTIR spectra A) and contact angle B) for ERs matrix and composites with different MWCNTs contents. 65
Figure 3.5 - Representative uniaxial stress-strain curves for screen-printed A) and doctor blade B) samples. C) Performance of initial modulus calculated up to 1% for all samples and D) stress and strain at fracture. 66
Figure 3.6 - Electrical sheet resistance as a function of MWCNTs filler concentration for samples prepared by doctor blade and screen-printing methods. The line is for guiding the eyes. 67
Figure 3.7 - Piezoresistive response of the ERs composites (3MWCNTs/ER) under 10 cyclic 4-point bending tests for small bending (0.1, 0.3, and 0.5 mm) A) and larger bending deformations of 1, 3, and 5 mm in B). C) Gauge Factor of the 3MWCNTs/ER, 5MWCNTs/ER, and 10 MWCNTs/ER composites as a function of bending deformation. D) Piezoresistive response of the 3MWCNTs/ER composite under cyclic bending up to a maximum bending of 1 mm for 100 cycles. Thermoresistive response of the screen-printed 3MWCNTs/ER composites to temperature ranges close to the human body (35 to 40 °C) E) and for industrial applications (60 to 90 °C) in F). 69
Figure 3.8 - Illustration of the uniaxial shear lap tests. B) Shear strength of bonded carbon fibre and aluminum adhesive joints for ERs and 3MWCNTs/ER composite. 71
Figure 3.9 - Piezoresistive response of screen-printed bonded adherent systems with 3MWCNTs/ER for low displacement 0.1, 0.3 and 0.5 mm A) and for 1, 3 and 5 mm B). Piezoresistive response at 1 mm maximum bending displacement C) and Piezoresistive gauge factors D). Thermoresistive response of screen-printed 3MWCNTs/ER composite as bonding for aluminum stripes between 35 to 40 °C E) and 60 to 90 °C F). 73
Figure 3.10 - A) Schematic of the structure developed for monitoring bending in cantilever mode using a 3MWCNTs/ER composite to bond together two glass fibres as adherents. Piezoresistive response for bending of 0.1, 0.3 and 0.5 mm B), and cycling stability for 100 cycles at 1 mm of bending C).....74
Figure 4.1 - Schematic representation of: A) functionalization of ERs by incorporation of nanocarbons and preparation of samples by screen-printing; B) tensile stress-strain test; C) piezoresistive bending tests.85
Figure 4.2 - SEM images of screen-printed samples with two layers, for resin (A in cross section and B in surface modes), 3MWCNTs/ER (C and D), 10G/ER (E and F), 3CB/ER (G and H), composites in cross section mode..... 89
Figure 4.3 - Resin and respective composites with different filler type and content evaluated by: A) FTIR-ATR, B) contact angle, C) DSC and D) TGA. 90

Figure 4.4 - A) Representative stress-strain curves of the resin and composites, B) maximum strength and strain, and C) Young's modulus..... 92
Figure 4.5 - Sheet resistivity measured by the four-point method for ERs composites with MWCNTs, CB and G with different filler contents in two-layer screen-printed samples..... 93
Figure 4.6 - A) Load applied during the indentation procedures as a function of displacement and for the 3MWCNTs/ER sample and the corresponding B) hardness for the different samples, as obtained from the indentation curves. 94
Figure 4.7 - Piezoresistive response under mechanical bending for A) 3MWCNTs/ER; B), 5CB/ER and C) 15G/ER at 0.5, 1- and 3-mm maximum displacement..... 95
Figure 4.8 - Shear test diagram and B) lap shear strength of bioresin and composite bonded joints. C) Piezoresistive behaviour from 0.1 to 5 mm of displacements in a bonded joint for 3MWCNTs/ER, 5CB/ER, and 15G/ER composites prepared by screen-printing. 97

List of Tables

Table 2.1 - Samples nomenclature and compositions 38

Table 3.1 - Nomenclature and main processing characteristics of the samples. 59

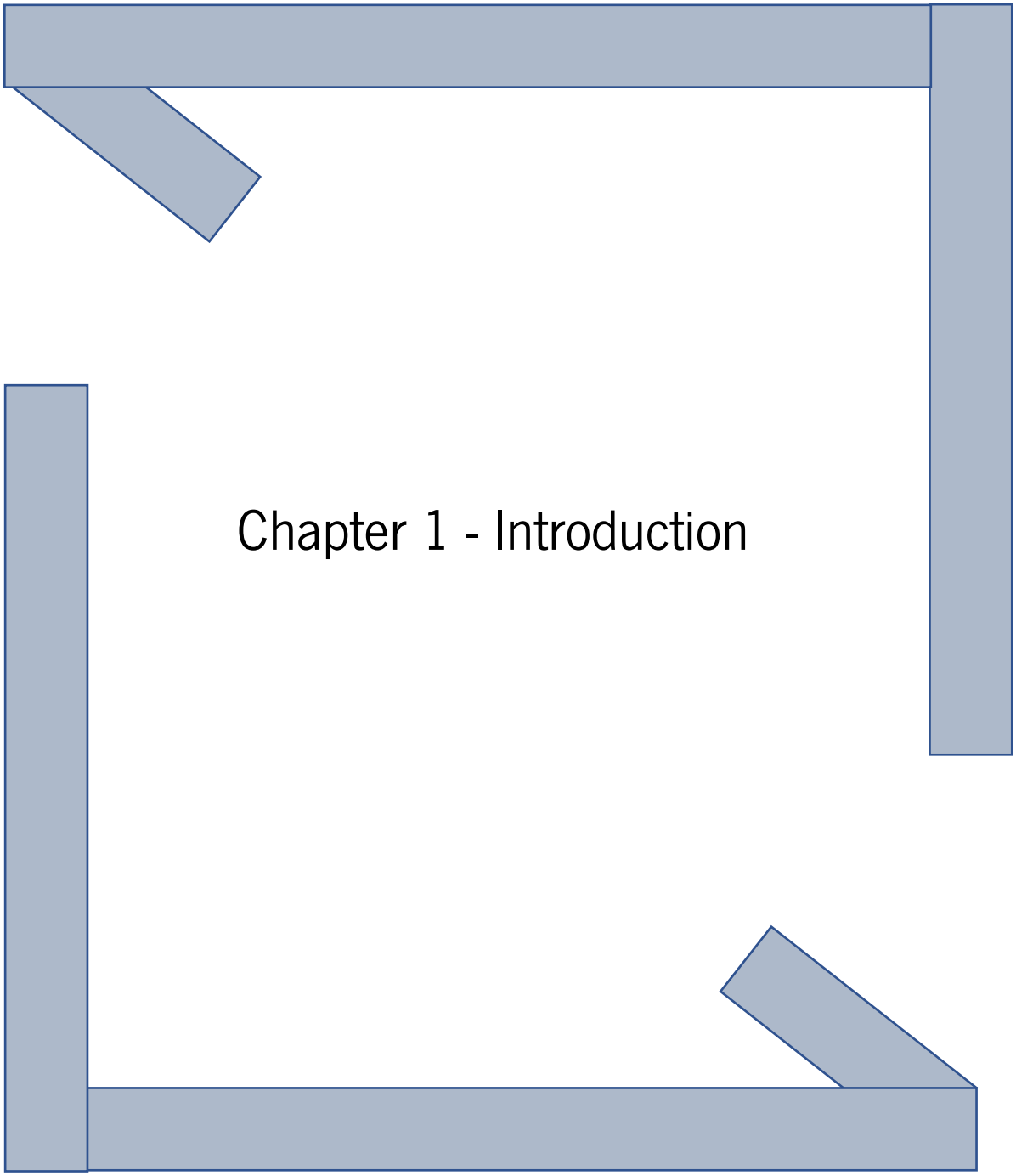
Table 4.1 - Sample nomenclature as a function of filler type and content in the ERs. 84

List of abbreviators and symbols

ΔL	Gage marks distance increase
ΔV	Voltage variation
DR	Electrical resistance variation
ΔT	Temperature variation
ρ	Electrical resistivity
π	Pi
τ	Shear strength
υ	Poisson's coefficient
0 – 10	
1CNTs/RE	1% carbon nanotubes with epoxy resin
21st	21 Century
2D	2-Dimensional
3CB/ER	3% carbon black with epoxy resin
3CNTs/RE	3% carbon nanotubes with epoxy resin
5CB/ER	5% carbon black with epoxy resin
5CNTs/RE	5% carbon nanotubes with epoxy resin
7CNTs/ER	7% carbon nanotubes with epoxy resin
7CB/ER	7% carbon black with epoxy resin
7G/ER	7% graphene with epoxy resin
10G/ER	10% graphene with epoxy resin
10 CB/ER	10% carbon black with epoxy resin
10CNTs/RE,	10% carbon nanotubes with epoxy resin
12CB/ER	12% carbon black with epoxy resin
12G/ER	12% graphene with epoxy resin
15G/ER	15% graphene with epoxy resin
20G/ER	20% graphene with epoxy resin
A	
A	Area
A_0	Overlap area
AR	Argon
ATR	Attenuated total reflectance
B	
B-ERs	Bioresins
BPA	Bisphenol A
BPF	Bisphenol F
C	
C	Carbon
CNTs	Carbon nanotubes
CB	Carbon Black
CH_2	Methylene
CH_3	Methyl

CNFs	Carbon nanofibers
CNTs	Carbon nanotubes
CFRP	Carbon fibre reinforced plastics
D	
d	Thickness
DSC	Differential scanning calorimetry
E	
ε	Strain
ε_t	Tensile strain
ERs	Epoxy resins
F	
FTIR	Fourier transform infrared spectroscopy
G	
G	Graphene
GF	Gauge factor
GFRP	Glass fibre reinforced polymer
GNPs	Graphene nanoplatelets
GO	Graphene oxide
H	
H	Hydrogen
I	
I	Current
I.E	That is
E.G	For example
IoT	Internet of things
L	
L_0	Distance between the gauges
L_t	Distance at any given moment
M	
MWCNTs	Multiwall carbon nanotubes
N	
N	Nitrogen
O	
O	Oxygen
P	
P	Cell load
PCBs	Printed circuit boards
PET	Polyethylene terephthalate
P_{max}	Maximum load
PP	Polypropylene
PUs	Polyurethane thermosetting resins
Q	

R	
RF	Radio frequency
R_0	Initial resistance
R_s	Electrical resistance
S	
S	Sensitivity
SEM	Scanning electron microscopy
SHM	Structural health monitoring
SWCNTs	Single-walled
T	
T	Temperature
Tg	Glass transition temperature
U	
UPRs	Unsaturated polyester resins
UV	Ultraviolet
X	
XIX	Nineteen century
Z	
z	Vertical displacement



Chapter 1 - Introduction

1.1 Overview

The 21st century has been characterised by a significant increase in technological innovation, profoundly transforming the ways in which human beings live, work, and interact. Over the past decades, revolutionary advancements in fields such as artificial intelligence, nanotechnology, renewable energy, and communications have driven societal and industrial change [1]. Among these developments, Industry 5.0, the Internet of Things (IoT), and 5G networks have emerged as key enablers of enhanced interconnectivity, facilitating the advancement of smart cities, autonomous vehicles, and intelligent infrastructure [2, 3].

The development of functional materials has been instrumental in facilitating these technological transformations. The increasing emphasis on materials that prioritise comfort, portability, human interaction, and seamless integration into various applications [4] is a testament to this progress. A fundamental aspect of this development is the ability of materials to interact intelligently with their environments, thereby enhancing their usability and adaptability. This has prompted research to focus on the development of flexible, soft, and stretchable materials, in conjunction with advanced manufacturing techniques, to facilitate their integration into sensors, actuators, and wearable technologies [5, 6].

In the domain of material science, ERs has emerged as a particularly promising material due to its advantageous properties, including high mechanical strength, chemical resistance, and adhesive qualities. However, conventional ERs are limited in terms of electrical and thermal conductivity, a deficit that can be addressed through functionalization with nanomaterials, thereby expanding their applicability in advanced technological applications [7, 8]. The integration of carbon-based nanomaterials, including carbon nanotubes (CNTs), graphene (G), and carbon black (CB), into ERs matrices has been demonstrated to result in a substantial enhancement of their electrical, thermal, and mechanical properties, rendering them highly suitable for sensor applications [9, 10]. Figure 1.1 presents representative applications of ERs and their Composites.



Figure 1.1 - Utilization of ERs across different industries, reproduced from [11].

Among the different functional responses, the piezoresistive and thermoresistive properties of these modified ERs nano composites are of particular interest, as they enable real-time monitoring of mechanical strain and temperature variations, rendering them ideal for applications in structural health monitoring, flexible electronics, and intelligent coatings [12, 13]. The development of these functional composites is in alignment with the growing demand for printed, flexible, and scalable sensor technologies, particularly in the context of IoT-enabled smart sensing systems.

On possibility for the fabrication of those sensors is additive manufacturing and, in particular, the screen-printing, a well-established and cost-effective 2D method of manufacturing that allows the precise deposition of functional inks and composites onto flexible substrates [14]. In comparison with traditional fabrication methods, screen-printing offers several advantages, including high customisability, large-area coverage, and compatibility with a wide range of materials and viscosities. This renders it an attractive approach for the scalable production of printed piezoresistive and thermoresistive sensors [15, 16]. However, the successful implementation of nanocarbon-enhanced ERs by screen-printing requires the resolution of key challenges, such as rheological control, dispersion stability, and substrate adhesion, which necessitate further research and optimisation [17].

The present research focuses on the development, characterisation, and optimisation of nanocarbon-functionalised ERs for sensor applications, leveraging screen-printing as the primary fabrication technique. The study investigates the impact of different nanocarbon fillers (MWCNTs, G, and CB) on the electrical, mechanical, and sensing properties of ERs composites. The objective of this research is to produce high-performance printable materials suitable for the next-generation multifunctional sensors.

1.2 Thermosetting Polymers: Characteristics and Applications

Thermosetting polymers, also referred to as thermosets, are a class of polymers that undergo an irreversible curing process, forming a highly crosslinked molecular network Figure 1.2. This unique characteristic endows them with high mechanical strength, thermal stability, and chemical resistance, making them highly relevant in various industrial applications [18].

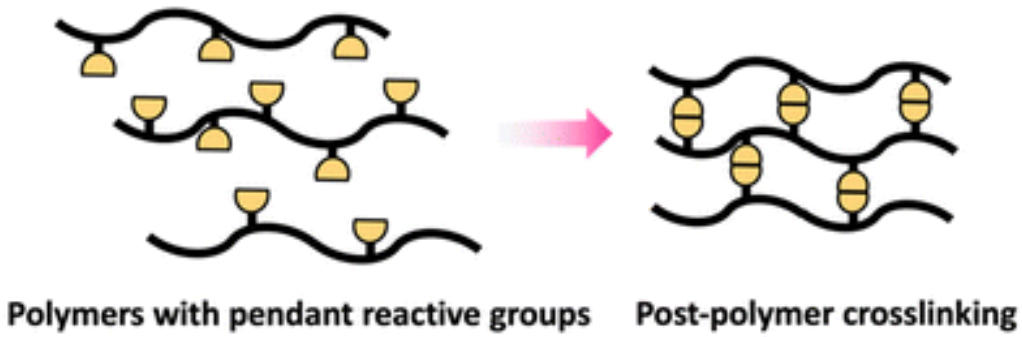


Figure 1.2 - Schematic of polymers before and after crosslinking, reproduced from [19].

Recent advances in thermosetting polymers have focused on enhancing their sustainability, recyclability, and performance through innovative synthesis and modification techniques [20]. ERs are considered to be among the most widely used thermosetting polymers. They are renowned for their exceptional mechanical strength, superlative adhesive properties, and remarkable resistance to chemicals and moisture. Typically, ERs are formed through a reaction between epoxide groups and hardeners, such as amines or anhydrides, thereby creating a highly durable structure. The wide range of applications of ERs include structural adhesives, coatings, printed circuit boards, and aerospace components, where their ability to maintain performance under extreme conditions is highly valued [21].

Similarly, phenolic resins, which are derived from the polymerisation of phenol and formaldehyde, exhibit excellent thermal and chemical resistance, making them ideal for applications requiring fire resistance, such as electrical switches, laminates, and automotive brake linings [22]. Polyurethane thermosetting resins (PUs) also play a significant role in various industries due to their versatility. The formation of PUs is achieved by the reaction between polyols and isocyanates, resulting in notable properties such as excellent abrasion resistance, impact resistance, and elasticity. These characteristics render PUs a preferred material for a wide range of applications, including insulation foams, elastomers, coatings, and adhesives [23]. Another widely used class of thermosetting polymers is that of unsaturated polyester resins (UPRs). These resins undergo a curing process in the presence of a peroxide catalyst, resulting in

the formation of a strong and durable material. The reasons for the widespread use of UPRs are threefold: their high strength-to-weight ratio, good chemical resistance, and cost-effectiveness. Consequently, they are employed in a variety of outdoor applications, including marine components, and construction materials [24].

Melamine-formaldehyde resins represent a significant category, with extensive utilisation in surface coatings, adhesives, and decorative laminates. These resins offer superior hardness and chemical resistance, rendering them particularly well-suited for high-wear applications, including laminates, kitchenware, automotive coatings, and decorative panels [22]. Furthermore, cyanate ester resins have garnered attention for their exceptional thermal stability, low moisture absorption, and superior dielectric properties, rendering them ideal for high-performance applications such as aerospace components, printed circuit boards, and high-frequency electronic devices [22].

Considering environmental concerns, researchers are being engaged in the development of bio-based thermosetting resins as sustainable alternatives to conventional synthetic resins. These bio-based resins are derived from renewable sources, including vegetable oils, lignin, and tannins, providing reduced carbon footprints and tunable mechanical properties [25]. These developments have enabled the creation of sustainable composites, biodegradable coatings, and eco-friendly adhesives, indicating a potentially effective approach to reducing the environmental impact of polymeric materials [25]. Moreover, recent studies have concentrated on enhancing the recyclability of thermosetting polymers through innovative strategies such as thermally degradable linkages and upcycling processes [26].

The extensive use of thermosetting polymers in a variety of industrial sectors highlights their crucial role in modern material science. Their ability to withstand high temperatures, their resistance to chemical degradation, and their structural integrity makes them essential components in numerous applications, including aerospace engineering and biomedical devices.

Despite their numerous advantages, conventional thermosets do pose challenges related to recyclability and environmental impact. However, ongoing research into alternative formulations and recycling methods is expected to address these limitations, paving the way for more sustainable and innovative thermosetting materials [24]. This continuous evolution in polymer science is expected to lead to novel applications and improved material properties, ensuring that thermosetting polymers remain an essential component of advanced engineering solutions.

1.2.1 Epoxy resins: Classification, Properties and Applications

ERs represent a subclass of polymeric materials that have gained widespread popularity due to their superior mechanical properties, adhesion strength, and chemical resistance. These materials have found application in a diverse range of industries. The classification of ERs is primarily based on their chemical composition, which determines their specific characteristics and suitability for different applications [27].

The following ERs are the most commonly utilised: bisphenol-A (BPA) ERs, bisphenol-F (BPF) ERs, novolac ERs, cycloaliphatic ERs, and fluorinated ERs [28].

Among these, bisphenol-A ERs are the most commonly employed due to their outstanding thermal stability, chemical resistance, and mechanical strength. They are synthesised through the reaction of bisphenol-A with epichlorohydrin, leading to a polymer with excellent adhesive properties, electrical insulation capabilities, and structural integrity. Consequently, these resins find extensive use in a variety of applications, including coatings 39%, adhesives and sealants 17%, electronics 12%, and fibre-reinforced composites 15%, followed by construction with 10% and 7% in other applications, as represented in Figure 1.3 [29, 30].

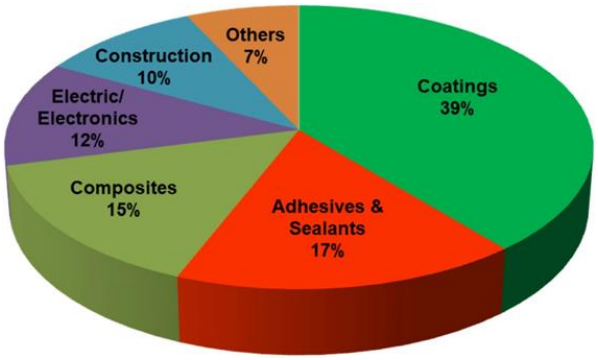


Figure 1.3 - Uses of ERs divided by sector in global using applications, produced acording to [30].

However, in instances where lower viscosity and enhanced handling properties are prioritised, bisphenol-F ERs emerge as a suitable alternative. Their enhanced chemical resistance renders them especially advantageous for use in marine coatings, construction materials, and protective applications [31]. In Figure 1.4 there's an example of polymer chains of a thermoplastic polymer (left) and of ERs polymer chains with their cross-linked structure (right).

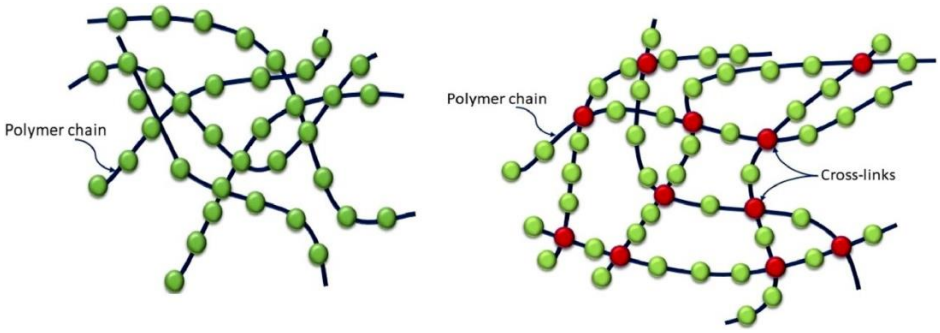


Figure 1.4 - Representation of Thermoplastic and Thermoset Polymeric Materials: (left) Thermoplastics featuring weak intermolecular forces between polymer chains; (right) Thermosets characterized by strong covalent bonds. Reproduced from [32].

In addition to BPA and BPF resins, novolac ERs offer enhanced thermal stability and superior chemical resistance, rendering them ideal for use in high-performance coatings, semiconductor encapsulation, and aerospace structures. Their high cross-linking density results in excellent mechanical strength and durability, ensuring their suitability for demanding environments [31]. A different approach is found in cycloaliphatic ERs, which lack aromatic rings, giving them superior ultraviolet (UV) resistance and lower viscosity. These characteristics render them particularly useful for outdoor applications, such as light emitting diode. encapsulation, coatings for solar panels, and electrical insulation materials, where weathering resistance and dielectric properties are essential [33].

The field of ERs has witnessed substantial advancements, with the advent of fluorinated ERs constituting a noteworthy development. These resins possess a unique category status, characterised by exceptional chemical resistance and low surface energy, thereby enhancing their hydrophobic properties. Their utility is particularly evident in applications such as anti-corrosive coatings, aerospace components, and biomedical materials. The presence of fluorine within their structure has been demonstrated to reduce surface tension, thereby enhancing their performance in challenging environments [34].

Furthermore, ERs play a crucial role in structural applications as adhesives in composite materials, bonding various substrates, including metals, plastics, and ceramics. The aerospace industry benefits significantly from ERs-based composites due to their high strength-to-weight ratio and thermal stability, making them essential in the fabrication of lightweight, high-performance components [35]. In civil engineering, ERs-modified concrete is used to enhance strength, durability, and corrosion resistance, particularly in high-exposure environments, thereby extending the lifespan of infrastructure [36].

As research continues, the development and modification of ERs through polymer chemistry and nanotechnology has expanded their potential applications. By incorporating nanofillers, such as silica or CNT ERs can achieve improved mechanical strength, thermal stability, and electrical conductivity. These advancements are of crucial importance for the development of next-generation high-performance materials required in various industries and applications [37], as represented in Figure 1.5.

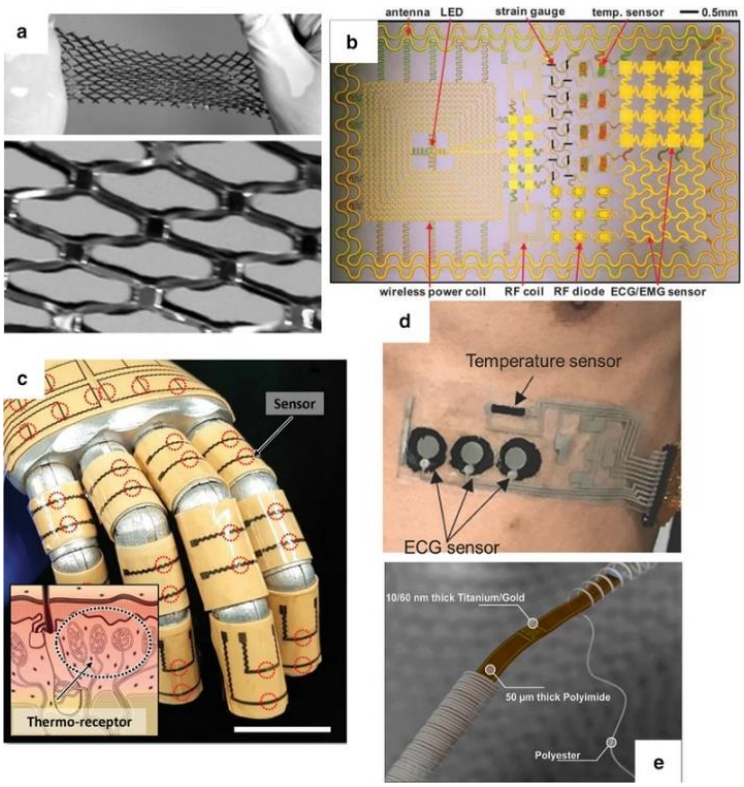


Figure 1.5 - ERs-based applications, including: A) Flexible temperature sensor, B) plastic film that integrates organic transistors with pressure-sensitive rubber, C) demonstration platform for multifunctional electronics showcasing physical properties, D) model hand covered in temperature-sensitive artificial skin, completed with an enlarged view of skin thermoreceptors, and E) a flexible temperature sensor embedded within the fibres of a textile yarn [38].

ERs are considered to be a cornerstone of modern material science. This is due to a number of factors, including their adaptability, superior properties, and wide range of applications. Their ability to be tailored through molecular engineering ensures their continued dominance in sectors requiring high-performance materials. This makes them indispensable for industrial and technological advancements [38].

1.2.3 Biobased ERs: Sustainability and Applications

Conventional ERs, which are typically derived from petrochemical sources, have significant environmental implications due to their non-renewable origin and limited biodegradability. In light of these concerns, there has been a growing interest in biobased ERs as sustainable alternatives, offering the potential to reduce environmental impact while maintaining desirable mechanical and thermal properties [39].

Biobased ERs are derived from renewable resources such as vegetable oils, lignin, rosin, vanillin, and itaconic acid [40]. Of these, vegetable oil-based epoxies, including epoxidised soybean oil and linseed oil, are of particular interest due to their high availability and low-cost. Additionally, lignin-derived epoxies offer enhanced thermal stability and rigidity, rendering them suitable for high-performance applications, in Figure 1.6 lignin illustrate some process to obtain ERs thermosets origins [41]. Rosin-based epoxies, derived from pine tree resins, are another sustainable option that provides excellent adhesion properties [42].

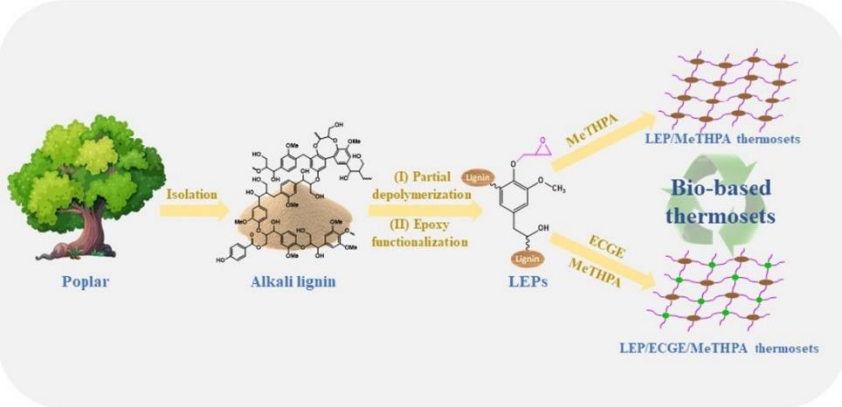


Figure 1.6 - Illustration of some bio-based. Reproduced from [43].

The properties of biobased ERs are contingent on the source material and synthesis methods employed. A significant number of these resins demonstrate competitive mechanical properties in comparison to petroleum-based epoxies, exhibiting high tensile strength and exceptional adhesion [44]. Furthermore, they demonstrate enhanced thermal stability and flame retardancy, particularly when modified with silicone or phosphorus-based [45]. Furthermore, certain formulations have been shown to exhibit reduced viscosity, thereby facilitating their processing and application in composite manufacturing [46].

Biobased ERs similar to petroleum-based ones, find application in a variety of industries, including coatings, adhesives, and structural composites. In the field of coatings, they demonstrate excellent chemical resistance and durability, rendering them suitable for use in protective finishes within the automotive and marine sectors [47]. In the field of adhesive applications, ERs demonstrate notable

bonding capabilities, particularly when used with wood and metal substrates, thereby contributing to the development of sustainable construction materials [48]. Moreover, in the composite industry, biobased epoxies function as matrix materials for natural fibre-reinforced composites, enhancing mechanical properties while reducing environmental impact [49].

The utilisation of biobased ERs plays a substantial role in enhancing environmental sustainability by reducing reliance on fossil resources and decreasing carbon emissions [50]. In contrast to conventional ERs, biobased alternatives frequently demonstrate reduced toxicity and enhanced biodegradability, thereby minimising the environmental impact at the conclusion of their life cycle [51]. Furthermore, their production from renewable materials supports circular economy initiatives [52]. Consequently, biobased ERs are a promising avenue for sustainable polymer development. Their diverse sources, competitive properties and broad applications highlight their potential to replace petroleum-derived counterparts while mitigating environmental concerns. It is therefore recommended that research into the optimisation of their synthesis and performance is continued, in order to further advance their adoption across industries and thereby promote a more sustainable future for polymer-based materials.

1.3 Screen-printing Technology: Principles and Applications

Screen-printing illustrated in Figure 1.7, is a versatile and widely utilised printing technique that employs a mesh-based stencil system to transfer ink onto a substrate. The serigraphy process is predicated on the principle of forcing ink through a permeable mesh in areas not obstructed by a stencil, thereby enabling the precise reproduction of specific designs. The technique's adaptability is evidenced by its wide range of applications, including textiles, paper, plastics, glass, ceramics, and metal surfaces [53].

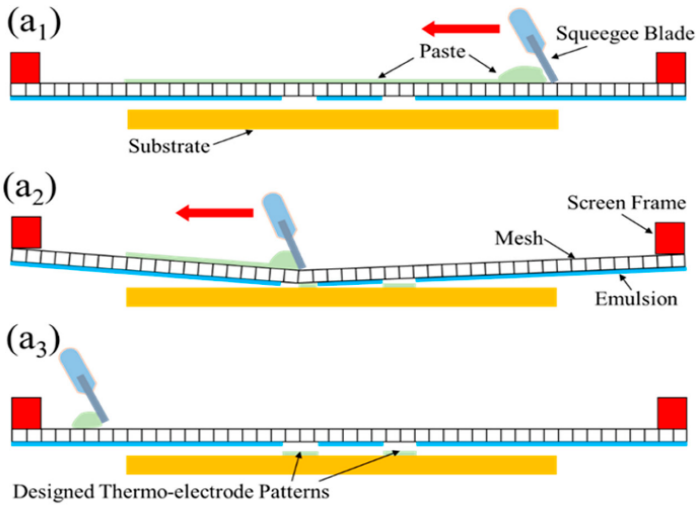


Figure 1.7 - Illustration of screen-printing process. Reproduced from [54].

The screen-printing process is comprised of several stages, including stencil preparation, ink formulation, screen selection and the actual printing process. Stencil preparation is of particular significance, as it determines the print pattern and the manner in which ink is deposited. Recent advances in the field have led to the use of photochemically, as can be seeing in Figure 1.8, treated stencils, which allow for highly detailed and repeatable patterns. The ink formulation is critical and must be carefully considered, as different substrates require specific ink properties for adhesion, durability and resistance to environmental factors [55].

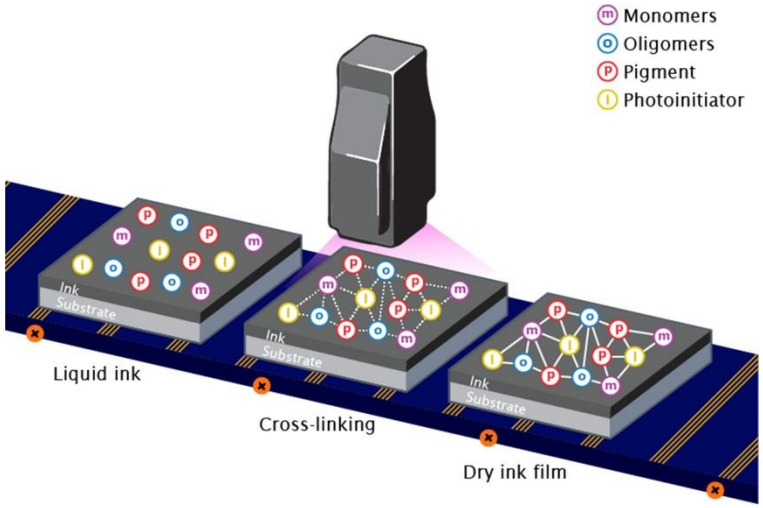


Figure 1.8 - Illustration of a UV process, where a liquid or past ERs is turned into a polymerized solid. Reproduced from [56].

The ability to produce high-quality and consistent prints with excellent characteristics is one of the key advantages of screen-printing, particularly in applications where vibrant colours and durable prints are required, such as textile printing, electronic circuit manufacturing and biomedical applications. In comparison with alternative printing techniques, screen-printing enables the deposition of thicker ink layers, thereby ensuring larger area applications with high scale potential for industry [57].

The industrial applications of screen-printing are manifold. Within the domain of printed electronics, screen-printing is employed to produce conductors, sensors and circuit boards. Due to its scalability, cost efficiency and compatibility with various conductive inks, the technique is widely utilised in flexible electronics, photovoltaic and energy storage devices [58]. Another significant application is the manufacture of radio frequency (RF) antennas, where screen-printing facilitates the production of lightweight, low-cost and flexible antenna structures for radio frequency applications.

Notwithstanding its numerous advantages, screen-printing is subject to certain limitations, with screen resolution and ink viscosity being a primary concern. This is due to the fact that screen resolution is constrained by mesh count and stencil thickness, both related with ink viscosity. While advancements in stencil fabrication have led to improvements in resolution, screen-printing remains less precise than others techniques for micro-scale applications. In addition, ink rheology and curing processes must be carefully controlled to ensure print consistency and durability [59].

The adaptability of screen-printing to automation has made it an attractive proposition for high-volume production. The advent of modern automatic screen-printing machines has been instrumental in enhancing efficiency, curtailing material wastage, and enabling elevated production rates while maintaining consistent quality [60]. These automated systems have found widespread application in the domains of textile printing and industrial marking, contributing to an augmentation in productivity and a reduction in costs.

Screen-printing is an invaluable technology across a wide range of industries due to its versatility, cost effectiveness and ability to produce high quality prints on a variety of substrates. Its continued evolution, particularly in the domains of printed electronics, biomedical applications and automation, ensures its relevance in modern manufacturing. While challenges remain, such as resolution limitations and ink formulation, ongoing research and technological advances continue to expand the potential applications of this robust printing process.

1.3.1 Industrial Applications of Screen-Printed ERs

The screen-printing of ERs has attracted considerable attention in a variety of industrial applications, due to its capacity to yield highly precise, reproducible, and durable coatings. ERs find wide application in coatings, adhesives, and composite materials, due to their excellent mechanical strength, chemical resistance, and electrical insulating properties [31]. The integration of ERs with screen-printing techniques has facilitated substantial advancements in the fabrication of electronic components, protective coatings, and biomedical applications.

Screen-printing is a well-established serigraphy method. The properties of the ink, including viscosity, thixotropic, and rheological behaviour, play a crucial role in determining the quality and performance of the printed films [61]. ERs-based inks require meticulous formulation to ensure stability during printing while maintaining adhesion, durability, and mechanical integrity. The capacity of ERs to form robust cross-linked networks after curing renders them optimal candidates for high-performance applications, including printed circuit boards (PCBs), where they provide insulation and structural reinforcement [62].

In the domain of electronics, screen-printed ERs have a well-established presence in the realm of PCBs manufacturing. The process entails the deposition of ERs-based solder masks, which function to insulate conductive pathways while safeguarding against environmental degradation. These solder masks are predominantly cured through UV exposure or thermal processes to attain the desired mechanical properties [31]. Furthermore, ERs-based screen-printing finds applications in the fabrication of flexible electronic devices and sensors, where precision and material robustness are critical [59].

Furthermore, the curing conditions have been shown to exert a substantial influence on the ultimate properties of the resultant films. Thermal curing, for instance, has been demonstrated to enhance mechanical strength and adhesion, although it is often associated with extended processing times. Conversely, UV curing offers accelerated solidification and less expensive process, but it is susceptible to limitations imposed by penetration depth and exposure uniformity [63].

Furthermore, a consideration of the occupational health and environmental impact of ERs in screen-printing is imperative. Exposure to ERs has been associated with allergic contact dermatitis, respiratory issues, and other occupational health hazards [64].

In conclusion, it is evident that screen-printing of ERs is a pivotal technology in a variety of industries, offering distinct advantages such as precision, reproducibility, and material robustness. Nevertheless, challenges pertaining to ink formulation or curing processes, and health considerations must be addressed in order to optimise performance and safety. Further research in advanced formulations, alternative curing techniques, and environmentally friendly materials will be instrumental in enhancing the applicability and sustainability of screen-printed ERs.

1.4 Multifunctionality of ERs Reinforced with Carbon Nanofillers

The integration of advanced sensing functionalities into structural materials represents a significant area of interest within the broader field of materials engineering. Among these functionalities, piezoresistive and thermoresistive effects have demonstrated considerable potential for the development of multifunctional materials with self-sensing capabilities. These effects, which describe changes in electrical resistance due to mechanical stress (piezoresistive) or temperature variations (thermoresistive), have been extensively studied in semiconductor materials and nanostructured composites [65, 66]. In recent years, the incorporation of carbon-based nanofillers, including CNTs, G, and CB (Figure 1.9), among others, has facilitated the development of polymer composites that exhibit enhanced electrical, thermal, and mechanical properties [67, 68].

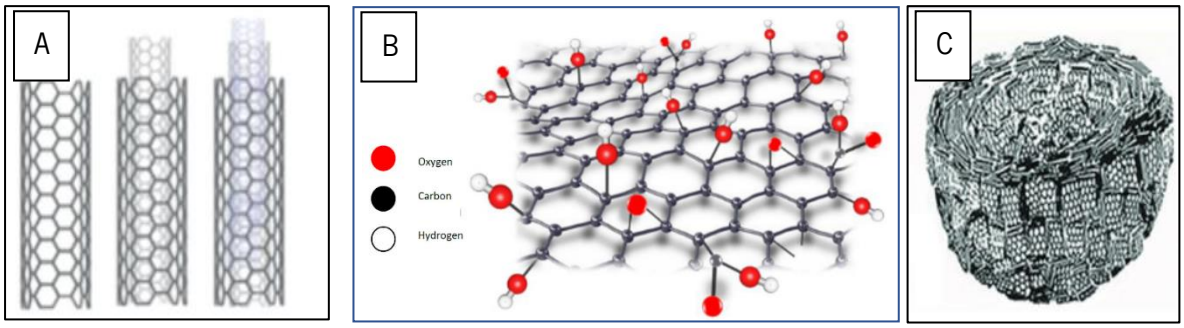


Figure 1.9 - Illustration of A) MWCNTs, B) G and C) CB, reproduced from [30], [69] and [70], respectively.

This thesis investigates the integration of carbon-based nanofillers into ERs with a view to improving their piezoresistive and thermoresistive characteristics. The experimental chapters present a detailed overview of the current state of the art in relation to the materials employed in the piezoresistive and thermoresistive systems that have been studied.

1.4.1 Piezoresistive Effect

The piezoresistive effect refers to the change in electrical resistivity of a material under mechanical strain. This phenomenon is extensively employed in strain sensors and structural health monitoring applications. The gauge factor (GF) is a critical parameter defining the sensitivity of a piezoresistive material, commonly

given by equation 1.1:

$$GF = \frac{\Delta R/R_0}{\varepsilon} \tag{1.1}$$

Where $\Delta R/R_0$ is the relative change in electrical resistance and ε is the applied strain. Higher GF values indicate greater sensitivity, making them desirable for advanced sensing applications [71].

The incorporation of carbon nanofillers into polymer matrices significantly enhances piezoresistive properties, which is related to percolation network variations under mechanical solicitation. Carbon-based nanofillers such as CNTs, graphene nanoplatelets (GNPs), and carbon nanofibres (CNFs) also introduce quantum tunnelling effects, which contribute to the electrical conductivity variation of the nano composites [72].

Nanofillers contribute to piezoresistivity through two primary mechanisms: the intrinsic piezoresistivity, an inherently piezoresistive properties exhibited by carbon nanostructures, in which mechanical

deformation alters their electronic band structure, modulating electrical resistance [73]; and the reconfiguration of the conductive network, in which under strain, the inter-nanoparticle spacing changes under strain, which affects electron hopping across nanofillers, significantly influencing the gauge factor [74]. Generally, nanocomposites strain sensors exhibit piezoresistive sensitivities between 1 up to some hundreds, depending on the filler content, type and dispersion quality [75-78]. Figure 1.10 shows a schematic representation on how the conductive path is formed in ERs matrix carbonaceous composites.

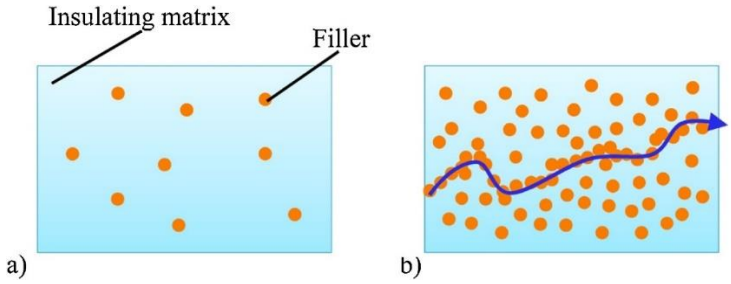


Figure 1.10 - Illustration of the piezoresistive effect, when matrix with conductive particles is subjected to mechanical solicitation, reproduced from [79]. A) Refers to uncompressed matrix and B) refers to compressed matrix.

1.4.2 Thermoresistive Effect

The term "thermoresistive effect" refers to the variation of electrical resistance as a function of temperature [66]. This property has been extensively explored in the development of advanced sensing devices and smart materials. The thermoresistive sensitivity quantifies the overall variation in resistance and is influenced by multiple factors, including material composition, morphology, and filler dispersion, in the case of nano composites. Thermoresistive sensitivity (S) is typically expressed as the fractional change in electrical resistance per unit change in temperature, given by equation 1.2:

$$S = \frac{\Delta R/R_0}{\Delta T} \times 100 \qquad (1.2)$$

Where $\Delta R/R_0$ is the relative variation of the electrical resistance and ΔT is the temperature variation. Thermoresistive sensitivity is responsible for nonlinear dependencies and external influences such as thermal expansion, polymer segmental motion, and electron transport mechanisms, critically dependent on filler type and content [66, 80, 81].

Carbon-based nanofillers, including CNTs, GNPs, and CNFs, have been shown to enhance the thermoresistive properties of polymer composites [82]. This enhancement is attributed to the percolating conductive networks, which modify the electrical response with temperature variations. Empirical studies

have demonstrated that thermoresistive sensitivity varies significantly with filler type, polymer matrix, and environmental conditions. Different matrices, such as vinyl ester, polysulfone, and polypropylene, lead to variations in sensitivity and hysteresis due to their mechanical and thermal properties [83].

1.4.3 Carbon Nanofillers in Multifunctional Systems

Epoxy resins, which are extensively utilized in high-performance structural applications, have undergone extensive modification through the incorporation of carbon-based nanofillers to achieve multifunctional properties, including piezoresistivity and thermoresistivity. A systematic study of the mechanical, electrical, and thermal properties of ERs-based nano composites has been undertaken, utilising carbon nanofillers such as G, graphene oxide (GO), CNTs, CNFs, and hybrid carbon nanofillers [84].

The employment of G and G-based nanofillers has become increasingly prevalent, owing to their exceptional mechanical strength, electrical conductivity and thermal stability. GNPs and GO have been employed to reinforce ERs matrices, resulting in enhanced electrical percolation, mechanical robustness and piezoresistive behaviour. The high aspect ratio and superior electron mobility of G enable the formation of efficient conductive networks at low filler loadings, thus enabling effective use in piezoresistive sensing applications. Figure 1.11 shows a flow sensor based on piezoresistive materials [85].

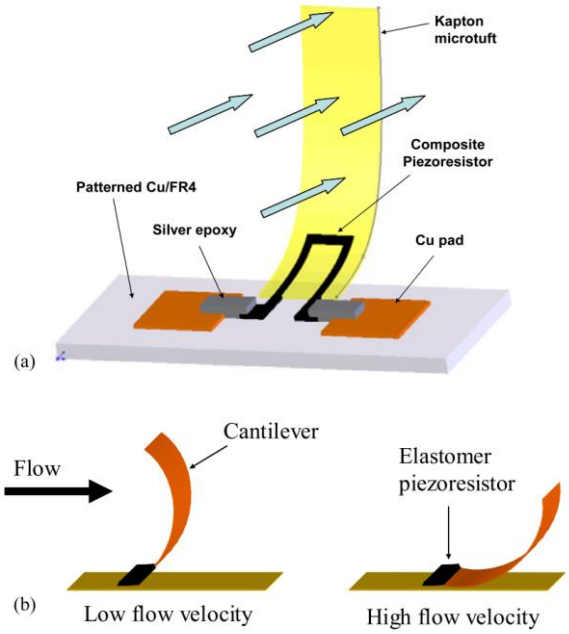


Figure 1.11 - A) 3D representation of the proposed flow sensor; B) Illustration demonstrating the deflection of the sensor as a result of increased flow. Reproduced from [86].

CNTs, comprising both single-walled (SWCNTs) and MWCNTs variants, demonstrate noteworthy mechanical flexibility, electrical conductivity, and thermal conductivity. Their integration into ERs matrices has led to the formation of nano composites that exhibit enhanced thermoresistive performance and piezoresistive sensitivity. The dispersion of CNTs plays a crucial role in defining the overall performance, as uniform distribution reduces percolation thresholds, maximises conductivity or ink viscosity [87, 88]. Additionally, CNT-reinforced ERs composites have demonstrated high sensitivity to mechanical strain, rendering them promising candidates for structural health monitoring applications [87-89].

Carbon nanofibres represent another class of nanofiller employed in ERs-based nano composites with a view to enhancing both electrical conductivity and mechanical properties. CNFs possess a higher aspect ratio than conventional microfillers, a factor which leads to a lower percolation threshold and better dispersion within the ERs matrix. Their incorporation into the polymer matrix has led to interesting piezoresistive response and thermal stability, rendering them suitable for applications necessitating real-time strain monitoring and resistance to elevated temperatures, being also a low-cost material [90].

Hybrid carbon nanofillers, consisting of combinations of CNTs, G, and CNFs, have attracted significant attention due to their ability to offer synergistic effects that enhance the piezoresistive and thermoresistive properties of ERs nano composites. The hybridization approach optimises the electrical percolation threshold while maintaining high mechanical strength and thermal stability. Studies have indicated that combining G with CNTs significantly improves the uniformity of the conductive network, thereby enhancing piezoresistive sensitivity [91].

The mechanisms governing the piezoresistive response of carbon-based nano composites are closely related to the formation of conductive pathways [92]. Under applied stress or strain, the resistance of the nanocomposites varies due to the rearrangement of conductive filler networks, allowing for real-time strain detection. Furthermore, thermoresistive behaviour is governed by the temperature-dependent electron mobility in the nanofillers, with higher filler loadings contributing to improved thermal stability [93].

Despite the considerable progress achieved in the field of carbon nanofiller-reinforced ERs composites, challenges persist with regard to the uniform dispersion of nanofillers, interfacial adhesion, and processing techniques. In order to enhance the compatibility of the nanofillers with the ERs matrix, surface functionalization has been explored, with the aim of improving mechanical integrity and stability [94]. Further research is required in order to optimise processing methods and tailor the functional properties of nano composites for specific engineering applications.

1.4.4 Piezoresistive ERs-Based composites

Piezoresistive ERs have attracted significant attention due to their capacity to function as self-sensing materials. These resins, when integrated with conductive nanofillers, demonstrate an alteration in electrical resistance upon mechanical deformation, rendering them optimal for strain sensing applications. Carbon-based nanofillers, have been the subject of extensive research to enhance the piezoresistive response of ERs-based nano composites [74, 95-97].

Carbon nanotubes, are among the most extensively utilised nanofillers, a consequence of their exceptional electrical conductivity and mechanical strength. It has been shown that CNT-ERs composites demonstrate superior piezoresistive performance, with gauge factors ranging from 2.5 to 78, contingent on the CNT content and dispersion quality [98, 99]. The high aspect ratio of CNTs facilitates and decreases the formation of percolative networks, significantly enhancing the electrical conductivity and strain sensitivity of ERs.

Carbon nanofibres have also been employed to improve the piezoresistive properties of ERs, with CNF reinforced ERs composites exhibiting gauge factors ranging from 5.5 to 37.1 depending on the CNF concentration and processing methods [100, 101]. CNFs have been demonstrated to enhance both mechanical and electrical properties, rendering them suitable for utilization in high-performance strain sensors.

GNPs also have the capacity to enhance the piezoresistive behaviour of ERs composites. The incorporation of GNPs with CNTs has been shown to result in synergistic effects, achieving the highest gauge factors reported among carbon nanofillers. For instance, CNT-GNPs hybrids have yielded a GF of up to 13.9 [95]. This enhancement is attributed to the formation of interconnected conductive networks that improve the strain sensitivity of the composite.

CB is an economical alternative for modifying the electrical conductivity of ERs. Although CB-ERs composites generally exhibit lower GF values (typically < 10) compared to CNT or GNP based composites, they are still widely used due to their ease of processing and cost-effectiveness [74]. CB based composites are particularly useful for applications where moderate strain sensitivity is sufficient.

Piezoresistive ERs incorporating carbon-based nanofillers have demonstrated significant potential for strain sensing applications Figure 1.12. Among the various fillers, CNTs exhibit the highest gauge factors, followed by CNFs and GNPs. Hybrid systems, such as CNT GNP composites, further enhance the piezoresistive performance, making them suitable for high-precision sensing applications. Future research

should focus on optimising nanofiller dispersion, improving processing techniques, and exploring hybrid nanofiller combinations to achieve even greater sensitivity and stability in piezoresistive ERs composites.

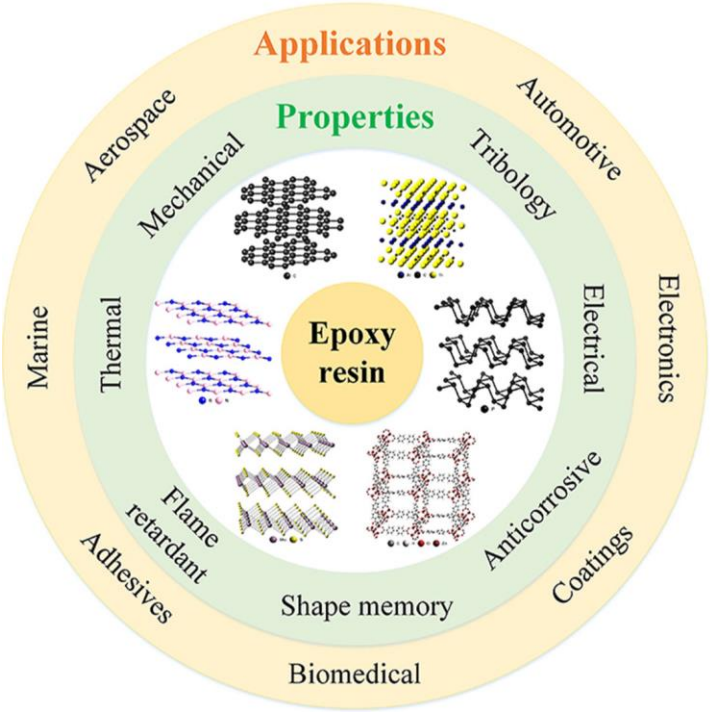


Figure 1.12 - Application areas of ERs matrix composites and the most relevant characteristics. Reproduced from [91].

1.5 Objectives and Methodology

The main objective of this research is to develop, understand and improve high-performance and printable materials based on ERs for sensor applications with excellent mechanical and adhesive properties. This will be achieved by using carbon-based nanomaterials to strengthen the ER structure.

The following methodology will be employed in pursuit of this objective:

1. Comprehensive evaluation of ERs to optimize processing and effective incorporation of nanofillers.
2. Evaluation of the main mechanical, adhesive, and physicochemical properties of the developed composite materials in view of the intended application.
3. Enhancing the performance and reproducibility of the functional piezoresistive and thermoresistive response.
4. Development and thorough testing of functional proofs of concept to demonstrate the potential of the added ERs as multifunctional sensors for a variety of applications.

1.6 Thesis Structure

The present thesis is divided into five chapters, three of which are based on published or submitted scientific manuscripts, thus presenting a clear and systematic narrative of the research advances achieved and explaining the methodologies employed. The following concise synopsis provides an overview of the material covered in each chapter.

Chapter 1 provides a comprehensive overview of the underlying motivations that guided the development of the thesis, along with a general introduction to all the important concepts for the following chapters. The primary objectives and structure of the thesis are also described. The subsequent chapters include a detailed state of the art in relation to key issues relevant to the chapter.

Chapters 2, 3 and 4 encompass the development and characterization of three distinct ERs that have been functionalised with varying carbonaceous nanofillers and processed by screen-printing.

In Chapter 2, a ERs with elastic properties is functionalised with MWCNTs. Despite the high reactivity of the ER, its viscosity posed a significant challenge, requiring the use of a solvent to effectively disperse the nanofiller. The chapter provides a comprehensive overview of the processing of the ER with the nanofiller in order to produce high quality functionalised materials with thermal and bending sensing capabilities for coatings or bond joints applications.

In Chapter 3, a more rigid ER and thixotropic is employed, which also exhibits high reactivity. The methodology employed in this section is similar to that of the first section. A cartridge system has been implemented to achieve improved results and facilitate greater multifunctional sensing for industrial applicability.

The fourth chapter employs a sustainable ER for the development and characterization of the functional nano composites. The cartridge system is utilised, enabling the incorporation of nanofillers MWCNTs, CB and G without the necessity for solvents.

Finally, Chapter 5 provides a summary of the main conclusions drawn from the research presented in this thesis and offers recommendations for future work and potential research directions in the field of advanced sensing ERs based polymer composites.

1.7 References

1. Fraga-Lamas, P., S. Lopes, and T. Fernández-Caramés, Green IoT and Edge AI as Key Technological Enablers for a Sustainable Digital Transition towards a Smart Circular Economy: An Industry 5.0 Use Case. Sensors, 2021. 21: p. 5745.
2. Barata, J. and I. Kayser, Industry 5.0 – Past, Present, and Near Future. Procedia Computer Science, 2023. 219: p. 778-788.
3. Wollschlaeger, M., T. Sauter, and J. Jasperneite, The Future of Industrial Communication: Automation Networks in the Era of the Internet of Things and Industry 4.0. IEEE Industrial Electronics Magazine, 2017. 11: p. 17-27.
4. Haque, M.S., Abstracts of Published Papers 2022, Vol. 17. 2024.
5. Mendonça, S., et al., The rise of 5G technologies and systems: A quantitative analysis of knowledge production. Telecommunications Policy, 2022. 46(4): p. 102327.
6. Martins, R., Materials as activator of future global science and technology challenges. Progress in Natural Science: Materials International, 2021. 31(6): p. 785-791.
7. Martins, P., V. Correia, and S. Lanceros-Mendez, Additive manufacturing of multifunctional materials, in Advanced Lightweight Multifunctional Materials. 2021, Elsevier. p. 25-42.
8. Holechek, J.L., et al., A global assessment: can renewable energy replace fossil fuels by 2050? Sustainability, 2022. 14(8): p. 4792.
9. Wang, S. and M.W. Urban, Redefining polymer science via multi-stimulus responsiveness. Chem, 2023. 9(6): p. 1362-1377.
10. Asyraf, M., et al., Filament-wound glass-fibre reinforced polymer composites: Potential applications for cross arm structure in transmission towers. Polymer Bulletin, 2023. 80(2): p. 1059-1084.
11. Rashid, M.A., et al., Review on intrinsically recyclable flame retardant thermosets enabled through covalent bonds. Journal of Applied Polymer Science, 2022. 139(27): p. e52493.
12. Lima, R., et al., Additive manufacturing of multifunctional epoxy adhesives with self-sensing piezoresistive and thermoresistive capabilities. Composites Part B: Engineering, 2025. 293: p. 112130.
13. Arana, G., F. Gamboa, and F. Avilés, Piezoresistive and thermoresistive responses of carbon nanotube-based strain gauges with different grid geometric parameters. Sensors and Actuators A: Physical, 2023. 359: p. 114477.
14. Higgins, C., et al., Epoxy resins. Kanerva's Occupational Dermatology, 2020: p. 757-788.

15. Szewczak, A. and M. Szelag. Modifications of Epoxy Resins and their Influence on their Viscosity. in IOP Conference Series: Materials Science and Engineering. 2019. IOP Publishing.
16. Ezeh, E.M., Advances in the development of polyester resin composites: a review. World Journal of Engineering, 2024.
17. Ramakrishnan, T., et al., Study of numerous resins used in polymer matrix composite materials. Advances in Materials Science and Engineering, 2022. 2022(1): p. 1088926.
18. Kinloch, A.J., Multiphase Thermosetting Polymers, in Polymer Blends and Mixtures, D.J. Walsh, J.S. Higgins, and A. Maconnachie, Editors. 1985, Springer Netherlands: Dordrecht. p. 393-412.
19. Weerasinghe, M.A.S.N., et al., Educational series: turning monomers into crosslinked polymer networks. Polymer Chemistry, 2023. 14(39): p. 4503-4514.
20. Liu, J., et al., Recent development on bio-based thermosetting resins. Journal of Polymer Science, 2021. 59(14): p. 1474-1490.
21. Derradji, M., et al., Sustainable and Ecofriendly Chemical Design of High Performance Bio-Based Thermosets for Advanced Applications. Frontiers in Chemistry, 2021. 9.
22. Feldman, D., Some considerations on thermosetting polymers as matrices for composites. Progress in Polymer Science, 1990. 15(4): p. 603-628.
23. Xie, H., L. Chenxuan, and Q. and Wang, Thermosetting Polymer Modified Asphalts: Current Status and Challenges. Polymer Reviews, 2024. 64(2): p. 690-759.
24. Liu, J., et al., Advances in sustainable thermosetting resins: From renewable feedstock to high performance and recyclability. Progress in Polymer Science, 2021. 113: p. 101353.
25. Teacă, C.-A., et al., Epoxidized Vegetable Oils for Thermosetting Resins and Their Potential Applications, in Functional Biopolymers, V.K. Thakur and M.K. Thakur, Editors. 2018, Springer International Publishing: Cham. p. 217-238.
26. Wang, B., et al., Upcycling of thermosetting polymers into high-value materials. Materials Horizons, 2023. 10(1): p. 41-51.
27. Gibson, G., Chapter 27 - Epoxy Resins, in Brydson's Plastics Materials (Eighth Edition), M. Gilbert, Editor. 2017, Butterworth-Heinemann. p. 773-797.
28. Shankar, A., S. Maloo, and A. Upadhyay, Synthesis And Applications of Bisphenol-A Epoxide Resins - A Review. Journal of Student Research, 2023. 12(4).
29. Gannon, J., Epoxy Resins, in Kirk-Othmer Encyclopedia of Chemical Technology.

30. Rashid, M.A., et al., A critical review of dynamic bonds containing curing agents for epoxy resin: Synthesis, challenges, and emerging applications. Polymer Degradation and Stability, 2024. 229: p. 110980.
31. Jin, F.-L., X. Li, and S.-J. Park, Synthesis and application of epoxy resins: A review. Journal of Industrial and Engineering Chemistry, 2015. 29: p. 1-11.
32. Kazemi, M., S.F. Kabir, and E. Fini, State of the art in recycling waste thermoplastics and thermosets and their applications in construction. Resources, Conservation and Recycling, 2021. 174: p. 105776.
33. Huang, J.-C., et al., Comparison of epoxy resins for applications in light-emitting diodes. Advances in Polymer Technology, 2004. 23(4): p. 298-306.
34. Park, S.-J. and F.-L. Jin, Epoxy Resins: Fluorine Systems, in Wiley Encyclopedia of Composites. p. 1-6.
35. Zhang, J., et al., Epoxy Resin Adhesives: Modification and Applications, in Epoxy-Based Composites, S.J.S. Chelladurai, R. Arthanari, and M. M.R, Editors. 2022, IntechOpen: Rijeka.
36. El-Hawary, M.M. and A. Abdul-Jaleel, Durability assessment of epoxy modified concrete. Construction and Building Materials, 2010. 24(8): p. 1523-1528.
37. Nordt, S., H. Pasch, and W. Radke, Method development for epoxy resin analysis. Microsystem Technologies, 2010. 16(8): p. 1347-1351.
38. Su, Y., et al., Printable, Highly Sensitive Flexible Temperature Sensors for Human Body Temperature Monitoring: A Review. Nanoscale Research Letters, 2020. 15(1): p. 200.
39. Noè, C., M. Hakkarainen, and M. Sangermano, Cationic UV-Curing of Epoxidized Biobased Resins. Polymers, 2021. 13(1): p. 89.
40. Kumar, S., et al., Recent Development of Biobased Epoxy Resins: A Review. Polymer-Plastics Technology and Engineering, 2018. 57(3): p. 133-155.
41. Olosho, A.I., et al. Recent Advances in the Synthesis of Biobased Epoxy Polymer: Replacing Bisphenol A with Sustainable Alternatives. in 2023 2nd International Conference on Multidisciplinary Engineering and Applied Science (ICMEAS). 2023.
42. Ding, C. and A.S. Matharu, Recent Developments on Biobased Curing Agents: A Review of Their Preparation and Use. ACS Sustainable Chemistry & Engineering, 2014. 2(10): p. 2217-2236.
43. Liu, G., et al., Preparation and properties of novel bio-based epoxy resin thermosets from lignin oligomers and cardanol. International Journal of Biological Macromolecules, 2021. 193: p. 1400-1408.

44. Wan, J., et al., Ultrastiff Biobased Epoxy Resin with High Tg and Low Permittivity: From Synthesis to Properties. ACS Sustainable Chemistry & Engineering, 2016. 4(5): p. 2869-2880.
45. Li, C., et al., Biobased Epoxy Resin with Low Electrical Permissivity and Flame Retardancy: From Environmental Friendly High-Throughput Synthesis to Properties. ACS Sustainable Chemistry & Engineering, 2018. 6(7): p. 8856-8867.
46. Gonçalves, F.A.M.M., et al., Advances in the development of biobased epoxy resins: insight into more sustainable materials and future applications. International Materials Reviews, 2022. 67(2): p. 119-149.
47. Boni, G., et al., Toward the Manufacturing of a Non-Toxic High-Performance Biobased Epoxy–Hemp Fibre Composite. Polymers, 2024. 16(14): p. 2010.
48. Deka, H., et al., Novel Biocomposites from Biobased Epoxy and Corn-Based Distillers Dried Grains (DDG). Journal of Polymers and the Environment, 2015. 23(4): p. 425-436.
49. Dal Pont, B., et al., Investigation of Novel Flax Fiber/Epoxy Composites with Increased Biobased Content. Polymers, 2023. 15(19): p. 4030.
50. Deng, Y., et al. Environmental Assessment of Printed Circuit Boards from Biobased Materials. in Glocalized Solutions for Sustainability in Manufacturing. 2011. Berlin, Heidelberg: Springer Berlin Heidelberg.
51. Chang, R., J. Qin, and J. Gao, RETRACTED ARTICLE: Fully biobased epoxy from isosorbidediglycidyl ether cured by biobased curing agents with enhanced properties. Journal of Polymer Research, 2014. 21(7): p. 501.
52. François, C., et al., Design and synthesis of biobased epoxy thermosets from biorenewable resources. Comptes Rendus. Chimie, 2017. 20(11-12): p. 1006-1016.
53. Novaković, D., et al., 15 - Screen Printing, in Printing on Polymers, J. Izdebska and S. Thomas, Editors. 2016, William Andrew Publishing. p. 247-261.
54. Frederichi, D., M.H.N.O. Scaliante, and R. Bergamasco, Structured photocatalytic systems: photocatalytic coatings on low-cost structures for treatment of water contaminated with micropollutants—a short review. Environmental Science and Pollution Research, 2021. 28(19): p. 23610-23633.
55. Paul, G., et al., An investigation into the durability of screen-printed conductive tracks on textiles. Measurement Science and Technology, 2014. 25(2): p. 025006.

56. Simon, J. and A. Langenscheidt, Curing behavior of a UV-curable inkjet ink: Distinction between surface-cure and deep-cure performance. Journal of Applied Polymer Science, 2020. 137(40): p. 49218.
57. Kołodziej, L., et al. The Influence of Screen-printingParameters on Properties of Conductive Layers for Application in Biomedical Electrodes. in Mechatronics 2019: Recent Advances Towards Industry 4.0. 2020. Cham: Springer International Publishing.
58. Xiao, G.G., et al. Screen printing RF antennas. in 2016 17th International Symposium on Antenna Technology and Applied Electromagnetics (ANTEM). 2016.
59. Suresh, R.R., et al., Fabrication of screen-printed electrodes: opportunities and challenges. Journal of Materials Science, 2021. 56(15): p. 8951-9006.
60. Zhang, Z., et al., Turning mechanism and optimisation design of automatic screen printing machine. International Journal of Wireless and Mobile Computing, 2018. 15(2): p. 151-156.
61. Somalu, M.R., et al., Screen-printinginks for the fabrication of solid oxide fuel cell films: A review. Renewable and Sustainable Energy Reviews, 2017. 75: p. 426-439.
62. Robin, M., et al., Epoxy Based Ink as Versatile Material for Inkjet-Printed Devices. ACS Applied Materials & Interfaces, 2015. 7(39): p. 21975-21984.
63. Mazela, W., P. Czub, and J. Pielichowski, Application of epoxy resins in electronics and optoelectronics. Part 1. Mechanical properties and thermal stability of epoxy resins used for encapsulation of electronic devices. Polimery, 2022. 49(4): p. 233-239.
64. Rademaker, M., Occupational epoxy resin allergic contact dermatitis. Australasian Journal of Dermatology, 2000. 41(4): p. 222-224.
65. Wacker, N. and H. Richter, Piezoresistive Effect in MOSFETS, in Ultra-thin Chip Technology and Applications, J. Burghartz, Editor. 2011, Springer New York: New York, NY. p. 233-243.
66. Dinh, T., et al., Thermoresistive Effect for Advanced Thermal Sensors: Fundamentals, Design Considerations, and Applications. Journal of Microelectromechanical Systems, 2017. 26(5): p. 966-986.
67. Lyapkosova, O.S. and N.G. Lebedev, Piezoresistive effect in single-walled carbon nanotubes. Physics of the Solid State, 2012. 54(7): p. 1501-1506.
68. Nguyen, T., et al., Advances in ultrasensitive piezoresistive sensors: from conventional to flexible and stretchable applications. Materials Horizons, 2021. 8(8): p. 2123-2150.
69. Elhenawy, S., et al., Recent Developments and Advancements in Graphene-Based Technologies for Oil Spill Cleanup and Oil–Water Separation Processes. Nanomaterials, 2022. 12(1): p. 87.

70. Shen, M.-Y., et al., Characteristics and Mechanical Properties of Graphene Nanoplatelets-Reinforced Epoxy Nanocomposites: Comparison of Different Dispersal Mechanisms. Sustainability, 2021. 13(4): p. 1788.
71. Ren, X. and G.D. and Seidel, Computational micromechanics modeling of piezoresistivity in carbon nanotube–polymer nanocomposites. Composite Interfaces, 2013. 20(9): p. 693-720.
72. Ferreira, A. and S. Lanceros-Mendez, Piezoresistive response of spray-printed carbon nanotube/poly(vinylidene fluoride) composites. Composites Part B: Engineering, 2016. 96: p. 242-247.
73. Cai, J., S. Chawla, and M. Naraghi, Piezoresistive effect of individual electrospun carbon nanofibers for strain sensing. Carbon, 2014. 77: p. 738-746.
74. Hernandez, J.A., et al., An experimental study on the piezoresistive and mechanical behavior of carbon nanocomposites subject to high-rate elastic loading. Composites Science and Technology, 2020. 198: p. 108285.
75. Ke, K., et al., Piezoresistive thermoplastic polyurethane nanocomposites with carbon nanostructures. Carbon, 2018. 139: p. 52-58.
76. Sanati, M., et al., Development of nanocomposite-based strain sensor with piezoelectric and piezoresistive properties. Sensors, 2018. 18(11): p. 3789.
77. Alamusi, et al., Piezoresistive strain sensors made from carbon nanotubes based polymer nanocomposites. Sensors, 2011. 11(11): p. 10691-10723.
78. Kanoun, O., et al., Review on conductive polymer/CNTs nanocomposites based flexible and stretchable strain and pressure sensors. Sensors, 2021. 21(2): p. 341.
79. Fiorillo, A.S., C.D. Critello, and S.A. Pullano, Theory, technology and applications of piezoresistive sensors: A review. Sensors and Actuators A: Physical, 2018. 281: p. 156-175.
80. Rao, R.K., S. Gautham, and S. Sasmal, A comprehensive review on carbon nanotubes based smart nanocomposites sensors for various novel sensing applications. Polymer Reviews, 2024. 64(2): p. 575-638.
81. Buga, C.S. and J.C. Viana, Development and characterization of flexible carbon temperature sensors: a study on different inks and sensor designs. Sensors and Actuators A: Physical, 2024. 378: p. 115823.
82. Cen-Puc, M., A.I. Oliva-Avilés, and F. Avilés, Thermoresistive mechanisms of carbon nanotube/polymer composites. Physica E: Low-dimensional Systems and Nanostructures, 2018. 95: p. 41-50.

83. Balam, A., et al., Influence of polymer matrix on the sensing capabilities of carbon nanotube polymeric thermistors. Smart Materials and Structures, 2020. 29(1): p. 015012.
84. Ke, K., et al., Boosting electrical and piezoresistive properties of polymer nanocomposites via hybrid carbon fillers: A review. Carbon, 2021. 173: p. 1020-1040.
85. Singh, N.P., V.K. Gupta, and A.P. Singh, Graphene and carbon nanotube reinforced epoxy nanocomposites: A review. Polymer, 2019. 180: p. 121724.
86. Aiyar, A.R., et al., An all-polymer airflow sensor using a piezoresistive composite elastomer. Smart Materials and Structures, 2009. 18(11): p. 115002.
87. Rafique, I., et al., Exploration of Epoxy Resins, Hardening Systems, and Epoxy/Carbon Nanotube Composite Designed for High Performance Materials: A Review. Polymer-Plastics Technology and Engineering, 2016. 55(3): p. 312-333.
88. Gonçalves, F.A., et al., Influence of fillers on epoxy resins properties: a review. Journal of materials science, 2022. 57(32): p. 15183-15212.
89. Ahmed, W., et al., A review: novel nanohybrids of epoxy/polyamide with carbon nanotube/nano-diamond. Polymer-Plastics Technology and Materials, 2021. 60(6): p. 579-600.
90. Gantayat, S., R. Dibyaranjan, and S.K. and Swain, Carbon Nanomaterial–Reinforced Epoxy Composites: A Review. Polymer-Plastics Technology and Engineering, 2018. 57(1): p. 1-16.
91. Dong, M., et al., Multifunctional epoxy nanocomposites reinforced by two-dimensional materials: A review. Carbon, 2021. 185: p. 57-81.
92. Grimaldi, C., et al., Piezoresistivity and conductance anisotropy of tunneling-percolating systems. Physical Review B, 2003. 67(1): p. 014205.
93. Gupta, N., et al., Temperature-dependent electron mobility in InAs nanowires. Nanotechnology, 2013. 24(22): p. 225202.
94. Blokhin, A., et al., Carbon nanofillers used in epoxy polymeric composites: a brief review. IOP Conference Series: Materials Science and Engineering, 2019. 693(1): p. 012015.
95. Wang, X., et al., Mechanical, Electrical, and Piezoresistive Sensing Characteristics of Epoxy-Based Composites Incorporating Hybridized Networks of Carbon Nanotubes, Graphene, Carbon Nanofibers, or Graphite Nanoplatelets. Sensors, 2020. 20(7): p. 2094.
96. Karnik, I.T. and T.N. Tallman, An experimental study on the effect of fatigue loading on electrical impedance in open-hole carbon nanofiber-modified glass fiber/epoxy composites. Composite Structures, 2021. 276: p. 114463.

97. Din, I.U., et al., Rate dependent piezoresistive characterization of smart aerospace sandwich structures embedded with reduced graphene oxide (rGO) coated fabric sensors. Composites Communications, 2022. 36: p. 101382.
98. Sanli, A., et al., Piezoresistive performance characterization of strain sensitive multi-walled carbon nanotube-epoxy nanocomposites. Sensors and Actuators A: Physical, 2017. 254: p. 61-68.
99. Hwang, M.-Y., D.-H. Han, and L.-H. Kang, Piezoresistive Multi-Walled Carbon Nanotube/Epoxy Strain Sensor with Pattern Design. Materials, 2019. 12(23): p. 3962.
100. Wang, Y., et al., Strain monitoring of concrete components using embedded carbon nanofibers/epoxy sensors. Construction and Building Materials, 2018. 186: p. 367-378.
101. Ferreira, A., et al., Effect of filler dispersion on the electromechanical response of epoxy/vapor-grown carbon nanofiber composites. Smart Materials and Structures, 2012. 21(7): p. 075008.

Chapter 2 - Additive manufacturing of multifunctional epoxy adhesives with self-sensing piezoresistive and thermoresistive capabilities

This chapter is based on the following publication: R. Lima, P. Costa, J. Nunes-Pereira, A.P. Silva, C. R. Tubio, S. Lanceros-Mendez, “Additive manufacturing of multifunctional epoxy adhesives with self-sensing piezoresistive and thermoresistive capabilities”, journal Composites Part B: Engineering with DOI https://doi.org/10.1016/j.compositesb.2025.112130

ERs composites are a class of materials that are widely used in various industries, including automotive, marine, and aerospace. They serve as adhesives to improve the mechanical strength of structures or to replace traditional joining methods.

This work evaluates the adhesive performance of a modified ERs, emphasizing its application for bonded joints with piezoresistive and thermoresistive sensing capabilities for real-time structural monitoring. A novel processing method has been developed that utilizes acetone to disperse conductive MWCNTs, thereby controlling the viscosity of the solution for screen-printing applications. This method enhances print definition and device design while maintaining the feasibility of large-area applications for industrial scale-up and minimizing waste during the process. The approach demonstrated high adhesion properties and the capability to detect bending deformation and temperature variations in screen-printed adhesive bonded joints, achieving sensitivities up to GF ≈ 30 and $S_{60\text{-}90} \approx -0.03$ (%.°C^{-1}) for piezoresistive and thermoresistive sensing, respectively. Finally, a successful proof-of-concept was developed using glass fibre adherents bonded with the functional adhesive, enabling real-time measurement of bending.

2.1 Introduction

Nowadays the use of thermosetting polymers (namely, ERs, discovered a century ago [1]) in critical structures is more than common due to their lightweight combined with excellent mechanical properties and simple processing, being by far the most used material in composites research and industrial structures development [1, 2]. The overall properties of ERs depend critically on the type of resin, curing agent, and processing method [1]. Most applications are as engineering adhesives, coatings, and host matrices to produce electronic components [1, 2]. High performance ERs with excellent mechanical properties and outstanding thermal and chemical stability have been tailored as composites or prototypes in the automotive [3], aerospace [4], and marine [5], industries due to their toughness and flexibility, recyclability, high temperature stability and electrical conductivity stability [2-5]. Academic and industrial development is strongly increasing, focusing on smart and multifunctional materials, enabling the implementation of Industry 4.0 and the IoT concepts, allowing interaction and control of processes in real time [6]. The overall mechanical properties of industrial resins have been extensively studied to improve their service performance, such as brittleness, poor crack resistance, and low impact strength [7]. To enhance the toughness of the resin and to obtain softer materials, strategies have been developed to make the resins compatible with thermoplastic polymers or with reinforced fillers [1]. Complementary, the reinforcement approaches allow to further tailoring and developing custom-by-design novel materials using ERs as a host matrix embedded with nano or microparticles, allowing the implementation of thermal

or piezoresistive sensing characteristics [1, 8, 9]. The most common fillers used to reinforce ERs composites are metal oxides, clays, and conductive carbonaceous nanomaterials such as G or MWCNTs [1, 10]. The wide range of combinations for specific applications depends critically on the choice of resin type, curing agent, and processing, together with the compatibilization of polymers, which determine the overall properties [1].

Lightweight and functional structures with adhesive properties can be engineered by incorporating various conductive nanofillers. Among these, MWCNTs are particularly advantageous due to their high aspect ratio, which enhances the mechanical properties and/or electrical conductivity of composites even at low filler concentrations [9]. When embedded in resin matrices, MWCNTs do not disrupt the resin's integrity due to their minimal volume, and they are characterized by their lightweight nature and cost-effectiveness in fabrication and application. Furthermore, MWCNTs exhibit exceptional mechanical and electrical properties, making them widely utilized in the development of sensing polymer composites. [9]. ERs embedded with MWCNTs exhibit a transition from insulator to conductor at low MWCNTs concentrations. In proximity to the percolation transition region, these composites demonstrate superior piezoresistive and thermoresistive responses while maintaining the essential mechanical and adhesive properties of the host resins. Near the percolation threshold, the piezoresistive and thermoresistive responses can be tailored to monitor the thermal and structural characteristics of the systems in which they are incorporated. These composites offer several advantages, including stable performance, easily and cost-effectively readable signals, low-cost processing, high durability, and endurance [11-13]. Piezoresistive materials are capable of detecting force and strain under tensile, compression and bending conditions across a range of deformations, while the thermoresistive response facilitates temperature detection from various sources, including the environment, the human body, or industrial applications [14-17]. Furthermore, these composites enable the tailoring of sensing responses with high precision and accuracy [6, 8, 9].

Additionally, multifunctional ERs composites can be developed in the form of an ink by controlling their viscosity and can be printed by diverse additive manufacturing methods with high-resolution and in large-scales for industrial applications [18]. Among the different 2-Dimensional (2D) additive manufacturing methods, screen-printing presents a high resolution (down to 100 μm) with good accuracy and a wide range of viscosity (100 to 50,000 mPa.s) [18]. The screen-printing technique can also be applied with multiple substrates and a throughput of up to 10 m^2/s [18], which is compatible with large area applications and therefore ideal for industrial scale-up processes.

This study reports on the development of multifunctional ERs composites reinforced with MWCNTs. Thus, together with the outstanding mechanical strength and adhesive performance of the ERs, advanced self-sensing capabilities have been induced in the adhesive by the presence of the MWCNTs, based on piezo- and thermo-resistive responses. Through the integration of adhesive properties with mechanical and thermal sensing multifunctionality, a proof of concept demonstrates the material's suitability for applications.

2.2 Experimental

2.2.1 Materials

Araldite AW 106 (30-50 Pa.s of viscosity) and hardener HV953-U (20-35 Pa.s of viscosity) were purchased at Huntsman. The ERs presents a glass transition temperature of 45 °C. The flexural strength and modulus are 60 and 1904 MPa, respectively. Acetone was purchased from Fisher with purity > 95 %. Multiwall carbon nanotubes MWCNTs were bought from Nanocyl (reference NC7000). They are characterized by a carbon purity of 90 %, an average diameter of 9.5 nm and a length of 1.5 µm, with an aspect ratio of ≈150. All materials were used as purchased, without further treatment.

2.3 Production of the ERs and composites adhesives

Adhesives composed of pristine ERs and corresponding MWCNTs-reinforced composites were prepared using two methods: doctor blade with controlled thickness and the screen-printing technique. To control the viscosity of the resin/hardener mixture, acetone was employed as a solvent and dispersion agent due to its low boiling temperature, compatibility with both resin and hardener, as well as with the MWCNTs, without chemical modification [19]. The resin/hardener ratio is 100/80 (parts per weight) for both resin and composites, as recommended by the supplier. The aforementioned conditions are the same for the two processing methods. The composites were reinforced with 1, 3, 5, 7, and 10 weight percentage (wt.%) of MWCNTs in relation to the ERs. The nomenclature for the samples will designate the resin for pristine sample and 1MWCNTs/RE or 3MWCNTs/RE (RE for resin) for composite with 1 and 3 wt.% MWCNTs, and so on for the remaining composites. In the preparation of the composites, for samples with 4 g of pristine ERs and 3.2 g of hardener, the acetone solvent volume was 5 ml, with 8, 10, 12, 14, and 16 ml for the composites with varying filler concentrations, respectively, to ensure adequate dispersion of the MWCNTs. To enhance processing efficiency, the resin and hardener were prepared separately. The MWCNTs and acetone were placed into two separate containers, each of them either for the resin or the hardener, thereby preventing the premature curing of the samples. In the first step, the

appropriated quantities of acetone and MWCNTs were added into both containers (one for the resin (100 parts per weight) and one for the hardener (80 parts per weight)). These mixtures were then subjected to ultrasonic bath (Fisherbrand with model FB-15056) for 2 hours at a temperature between 25-35 °C to deagglomerate the MWCNTs clusters (Figure 2.1A). In the second step, the respective content of ERs and hardener were added in the ratio of 100/80 parts per weight. Then, the acetone/MWCNTs with both the resin and hardener were homogeneously mixed in separate containers using a mechanical mixer Heidolph RZR 1 (Figure 2.1B) for 15 min at 2200 rpm. To achieve a uniform and controlled viscosity of the samples, sealing film and aluminium foil were employed to prevent the solvent evaporation. Additionally, pristine resin samples were dissolved in acetone to maintain similar properties as viscosity and adhesion compared to the composites. Following the dissolution of both solutions, they were placed in a sealed chamber connected to a vacuum pump (GAST model 0523-V191Q-G588DX) for 15 min (Figure 2.1C) to eliminate air bubbles generated during the dispersion process. Once the air was removed from the solutions, the mixtures were combined to produce both pristine ERs and composite samples for further characterization. This methodology was consistently applied across all materials and each developed solution used in the doctor blade (Figure 2.1D) and screen-printing (Figure 2.1E) methods.

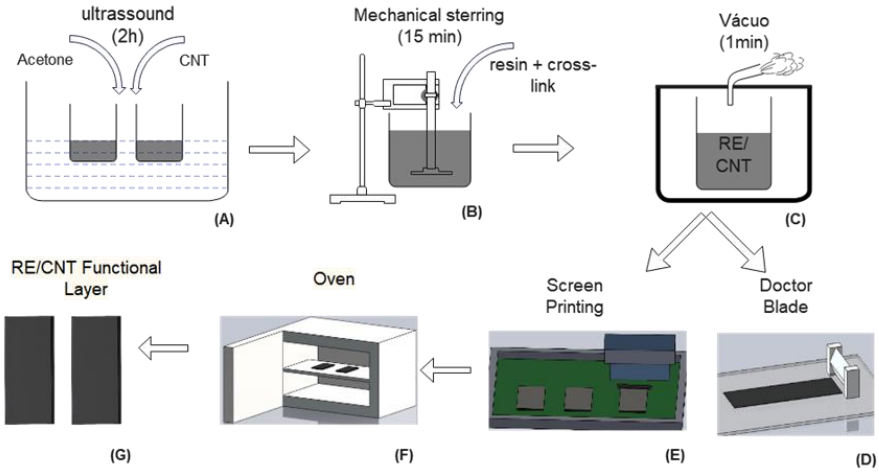


Figure 2.1 - Schematic illustration of the samples manufacturing procedure by the doctor blade and screen-printing techniques.

In the doctor blade processing technique, a cardboard mold with an area of 100×200 mm2 with a thickness near 600-700 μm. To facilitate demolding post-curing, a commercial Teflon® sheet was placed at the top and bottom of the mold. Two glasses were used to sandwich the film and Teflon sheets. This assembly was subsequently within a vacuum bag with a valve and connected to the vacuum pump for

15 min to eliminate any residual bubbles and then cured in a hot press at 90 °C and 100 N/m2 for 30 min. During this cure process, the acetone evaporates through the valve.

The screen-printed samples were fabricated using a custom-built screen-printing apparatus in conjunction with pre-prepared solution mixtures. The printing mesh utilized had a density of 24 wires/cm and an emulsion used to generate a specific pattern with 10 μm depth to increase both the resolution and thickness of the printed samples, with about 1 cm distance between the mesh and the commercial Teflon sheet used as substrate. Each sample consisted of 3 printing layers per sample, resulting in an average thickness between 110 and 400 μm. To ensure complete solvent evaporation and curing of the printed samples, they were placed in an oven (Figure 1F- Binder E, model 28) at 60 °C for 30 min to obtain the functional films (Figure 2.1G).

2.4 Fabrication of adhesively bonded joints with sensing capabilities

The resin and MWCNTs composites were employed as adhesives to fabricate bonded joints exhibiting both piezoresistive and thermoresistive functionalities (Figure 2.2 A) using aluminium, carbon fibre, and glass fibre composites served as adherends in this study. Adherend strips with 1 mm of thickness present a bonded active area of 30×10 mm^2 using either the pristine resin or the 5MWCNTs/RE composite in a shear lap configuration. The adhesive was applied to one strip via screen-printing, while the other strip was pressed against the first using a commercial spring clamp (about 20 N/m^2 of force) with an area of 10×10 mm^2. The bonded adherends were cured in an oven at 90 °C for 30 min.

In the evaluation of the piezoresistive sensor, bonded joints utilizing the 5MWCNTs/RE composite adhesive were employed, consistent with prior 4-point-bending methodologies. The adherents were exclusively composed of glass fibre composites, selected for their electrically insulating properties. Additionally, the thermoresistive sensors were fabricated using a printed composite material sandwiched between aluminium strips, which were chosen for their superior thermal and electrical conductivity.

2.5 Characterization techniques and procedures

2.5.1 Physical-chemical characterization

Morphological evaluation of the ERs and composites was performed by scanning electron microscopy (SEM) using a Hitachi S-4800 with an accelerating voltage of 10 kV. The samples were coated with a thin gold layer using a Polaron SC502 sputtering.

Fourier transform infrared (FTIR) spectroscopy was carried out in the attenuated total reflectance (ATR) mode using a Jasco FT/IR-4100 instrument. Analyses were performed from 4000 to 600 cm^{-1} after 32 scans with a resolution of 4 cm^{-1}.

The thermal behaviour of the samples was evaluated by differential scanning calorimetry (DSC) using a model DSC200 F3 Maia (NETZSCH) under a dry nitrogen atmosphere at temperatures ranging from 30 to 250 °C at a heating rate of 20 °C/min. Measurements were carried out in aluminium pans with a sample mass of less than 20 mg.

Surface contact angles were measured using a Dataphysics OCA 15EC optical system from Neurtek Instrument. Water droplets of 2 μL of 5 mg/L As(V) standard solution were dropped on each sample. Three measurements were obtained in different sample zones using the SCA20 software. The values provided correspond to the average of the tests.

The mechanical properties of the samples were determined by uniaxial stress-strain tests using a Shimadzu AG-IS with a 500 N load cell. The tests were performed at a rate of 3 mm/min rate until specimen rupture using samples with an area of 20×4 mm^2 and a thickness varying from 100 to 400 μm. Three tests were performed on each material. The modulus of elasticity was calculated by applying Hooke's law to the initial linear elastic curve strength versus strain.

The electrical sheet resistance (Rs) of the samples was obtained by four-probe measurements using a Keithley 2400 source meter by applying voltages (V) in the range from -10 V to + 10 V, while measuring the current (I). Each sample was evaluated twice at three different locations and the sheet resistance was determined using Equation 2.1:

$$R_s = \frac{\pi}{\ln 2} \times \frac{\Delta V}{I} \quad (2.1)$$

where $\frac{\pi}{\ln 2}$ is the geometric factor for a semi-infinite thin film.

2.5.2 Functional response characterization.

Adhesion tests were performed on the bonded joints using a Shimadzu AGS-X universal testing machine equipped with a 50 kN load cell and appropriate grips, and the data was processed using the Trapezium X software. Shear tests were performed at a loading rate of 1.3 mm/min in accordance with ASTM D3165. Both carbon fibre composite and aluminium bonded joints were used in these tests. The lap shear strength (τ) of the joint was determined using Equation 2.2:

$$\tau = \frac{P}{A_0} \tag{2.2}$$

where P represents the cell load and A_0 is the overlap area of the bonded joint. The tensile strain (ε_t) was determined by the Equation 2.3:

$$\varepsilon_t = \frac{\Delta L}{L_0} = \frac{L_t - L_0}{L_0} \tag{2.3}$$

where L_0 is the original distance between the gage marks, L_t is the distance at any given moment, and ΔL is the gage marks distance increase.

Piezoresistive tests were carried out in four-point-bending mode using a Shimadzu model AG-IS universal testing machine with a 500 N load cell. The electrical resistance variation under mechanical deformation was obtained using a multimeter model Agilent 34401A. The four-point-bending setup, shown in Figure 2.2A, was applied to the 5MWCNTs/RE sample with an area of 30×10 mm^2 processed by doctor blade (≈ 600 μm of thickness) and screen-printing (≈ 120-400 μm of thickness). The blade composite was bonded (transparent double-sided adhesive tape from Tesa®) to a flexible polypropylene (PP) substrate with a thickness of 1 mm, and the screen-printed composite was applied for bonded glass fibre composites (insulator substrates in Figure 2.2A), similar to the adhesion tests. The electrodes on the composite surface were printed with silver ink (Agar Scientific, AGG3790) with a spacing of 20 mm and a length of 10 mm. The piezoresistive response was evaluated for 1, 3, and 5 mm of displacement/strain bending at a speed of 3 mm/min. The piezoresistive response or gauge factor (GF), a measure of the sensitivity of the samples, was determined using Equation 2.4 [20]:

$$GF = \frac{\Delta R/R_0}{\Delta l/l_0} = \frac{\partial \rho/\rho_0}{\varepsilon} + (1 + 2\upsilon) \tag{2.4}$$

where ΔR is the electrical resistance variation, R_0 is the initial resistance, $\Delta l/l_0 = \varepsilon$ is the strain, and υ is the Poisson's coefficient ($\upsilon \approx 0.3$ for ERs [7]) and (ρ) is the electrical resistivity. For the four-point bending mode, the strain (ε) was calculated from the pure bending theory valid between the inner loading points given by Equation 2.5 [16]:

$$\varepsilon = \frac{3}{5}\frac{dz}{a^2} \tag{2.5}$$

where d is the thickness of sample, z is the vertical displacement and a is the distance between bending points (a = 25 mm), as shown in Figure 2.2A.

The piezoresistive response (Equation 2.4) is composed by two contributions: the geometrical effect (1 + 2υ ≈ 1.6) and the intrinsic component, which depends on the electrical conductivity variation due to the network rearrangements of nanofillers [5].

The thermoresistive response was measured for the 5MWCNTs/RE composites using an Agilent 34401A digital multimeter synchronized with a temperature control equipment Linkam THMSE 600. Measurements were carried out in the surface mode with an area of 20×20 mm2 for the composite. Commercial silver ink was used to pattern the conductive electrodes on the samples, and the contact to the multimeter was achieved with copper wire. The thermoresistive sensitivity (S) is defined by Equation 2.6:

$$S = \frac{\Delta R/R_0}{\Delta T} \times 100 \tag{2.6}$$

where ΔT is the temperature variation (in °C).

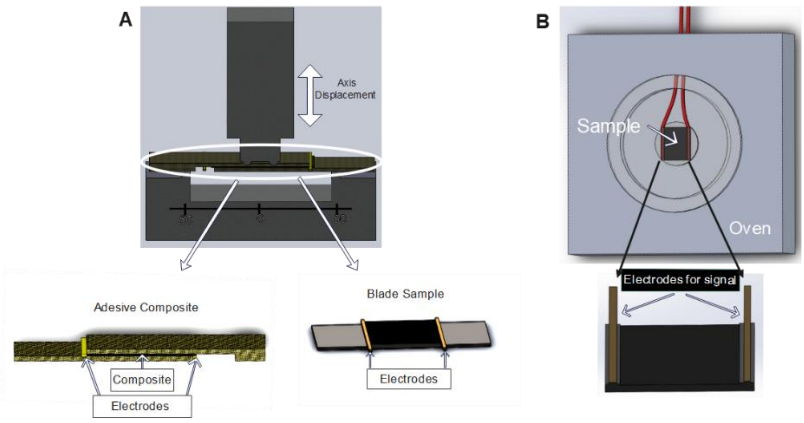


Figure 2.2 Schematic illustration of the evaluation of the functional sensing response of the samples: A) four-point-bend piezoresistive and B) thermoresistive measurements.

To validate the adhesive properties of the resin and the functionality of the composites as sensing materials, single lap joints were developed using glass and carbon fibres, and aluminium adherends of 50×15×1 mm3 (length, width, and thickness, respectively). These joints were bonded by screen-printing method using 3 layers of the 5MWCNTs/RE composite, with a thickness of the active material in the range of 500-600 μm (a shim was utilized to control the thickness of the adherent film) and a bonded/active area of 20×15 mm2 (as shown in Figure 2.10). A square piece of each material was bonded to the end of each adherend strip as an end tab to ensure uniform volume throughout the joint.

Table 2.1 - Samples nomenclature and compositions

Nomenclature	ERs (g) + Hardener (g)	Acetone (ml)	MWCNTs (wt.%)
Resin ERs		5	-
1MWCNTs/RE	4	8	1
3MWCNTs/RE	+	10	3
5MWCNTs/RE	3.2	12	5
7MWCNTs/RE		14	7
10MWCNTS/RE		16	10

2.6 Results and Discussion

2.6.1 Physical-chemical properties of resin and composites

The morphology of pristine resin and composites reinforced with varying contents of MWCNTs is illustrated in the representative SEM images of the screen-printed materials, which consist of three printed layers, as presented in Figure 2.3. The thickness of the samples can be obtained from the lower magnification images, ranges from 390 ± 35 μm for the pristine ERs to 150 ± 20, 110 ± 20 and 380 ± 40 μm, respectively for the composites with 3, 5, and 10 wt.% MWCNTs content, respectively. The individual screen-printed layers exhibit thicknesses ranging from 40 to 130 μm for all materials. Consequently, the thickness of the composites increases with higher MWCNTs content, particularly at elevated filler concentrations. The incorporation of acetone and MWCNTs affects the rheological properties of the ink, thereby influencing the thickness of the screen-printed materials. The SEM images (Figure 2.3D, F, and H) reveal a uniform dispersion of individual MWCNTs within the resin matrix, with no significant agglomerates observed, although they increase with increasing filler concentration. Both the pristine resin and composite samples exhibit a compact structure devoid of voids or cracks. Nonetheless, some cracks are noted in the composite with the highest filler content (10MWCNTs/RE, Figure G and H), with influence in the mechanical properties (as discussed later). The employed fabrication method proves to be effective, allowing for the production of samples via the screen-printing technique without compromising structural integrity when compared to samples prepared using the doctor blade or other coating methods documented in the literature [21, 22].

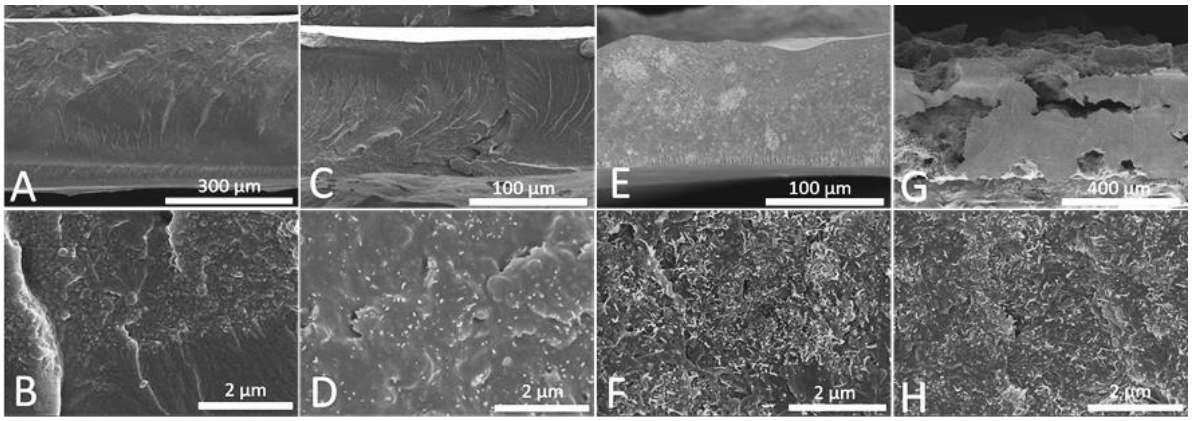


Figure 2.3 - Cross-section SEM micrographs of 3-layer screen-printed samples: resin (A and B), 3MWCNTs/RE (C and D), 5MWCNTs/RE (E and F) and 10MWCNTs/RE (G and H) composites. Magnifications from 130x to 20,000×.

The FTIR-ATR characteristic absorption bands of the ERs and its composites are shown in Figure 2.4A. The absorption bands observed at 1506 and 1606 cm^{-1} are related to C=C stretching of benzene rings [23]. Additionally, the bands at 821 and 1026 cm^{-1} are attributed to Ar–O–C bonds and ether group, respectively [23]. A broad band in the range of 3100-3400 cm^{-1} is assigned to the stretching vibrations of O–H bonds. The stretching vibrations of the C–C bonds, the aromatic component of the Ar–O–C bonds, and C–N bonds are related to the absorption peaks at 1292, 1228, 1176 cm^{-1}, respectively [23]. Lastly, the peaks at 2847 and 2916 cm^{-1} correspond to the stretching vibration group (C-H) in the CH2 and CH3 absorption bands, respectively [23]. It is noteworthy that the characteristic peaks of the ERs are attenuated in the composites, with a more pronounced attenuation observed in the composite with the highest filler content.

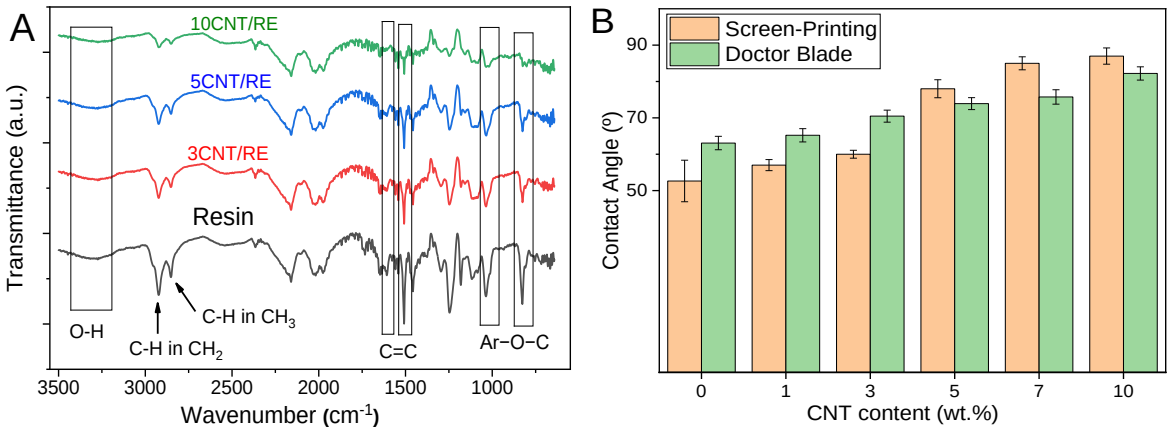


Ilustração 2.4 - A) FTIR spectra and B) contact angle of resin and corresponding composites prepared by screen-printing and doctor blade.

The contact angle of the resin is about 53° and 63° for those prepared using the screen-printing and doctor blade methods Figure 2.4B. This angle increases with the addition of MWCNTs in both composites, reaching values of 82° and 87° for the 10MWCNTs/RE composite, respectively. Samples processed via the doctor blade method exhibit slightly higher contact angle values compared to screen-printed samples for resin and composites with 1 and 3 wt.% MWCNTs content. Conversely, this trend is reversed for the remaining composites. In both processing methods, the contact angle increases with the incorporation of a greater amount of MWCNTs in the composites, with all observed differences primarily attributed to the variations in the rugosity of the materials. Overall, both the resin and the composites show hydrophilic behaviour, consistent with findings reported in the literature [24, 25].

The mechanical properties of the materials were evaluated in uniaxial tensile stress-strain conducted until failure, with representative data in Figures 2.5A and B for both resin and composite samples. The strain at rupture, as illustrated in Figure 2.5D, is approximately 6% for printed resin samples and 10% for those prepared using the doctor blade method. In contrast, composites with low filler content exhibit and increase in strain at rupture, reaching nearly 11% of strain. However, this strain decreases abruptly for composites containing 10 wt.% MWCNTs, for both methods. The observed increase in strain at rupture in polymers occurs even at room temperature and under low-stress conditions, attributed to molecular motion within the polymer backbone due to viscous flow and elastic deformation. Consequently, the addition of a relatively low content of MWCNTs restricts the mobility of the ERs matrix polymer chains, thereby inhibiting disentanglement and slippage. This phenomenon is attributed to the establishment of a strong interfacial strength between the MWCNTs and the matrix, where the MWCNTs particles act as obstruction sites, and their high aspect ratio of the MWCNTs enhances the contact surface area for effective load transfer. However, increasing the weight content of MWCNTs may resulting in agglomeration issues and a deterioration of particle-ERs adhesion [26].

The maximum stress exhibited by the composites is influenced by the filler content, demonstrating similar trends across both processing methods. As illustrated in Figure 2.5C, the stress at break diminishes with increasing MWCNTs content, decreasing from approximately 13 MPa for the resin to between 4 and 5 MPa for the composites with the highest filler content. The use of acetone as a solvent, along with the incorporation of MWCNTs, results in a reduction of the maximum stress in the composites while simultaneously enhancing the elongation at break, particularly in screen-printed composites. Notably, the overall mechanical properties of the composites decline significantly when the MWCNTs content exceeds 7 wt.%. Furthermore, materials produced via the screen-printing process exhibit lower strain and greater

mechanical strength at rupture. This phenomenon can be attributed to the preferential alignment of MWCNTs along the printing direction during the sample preparation process [27].

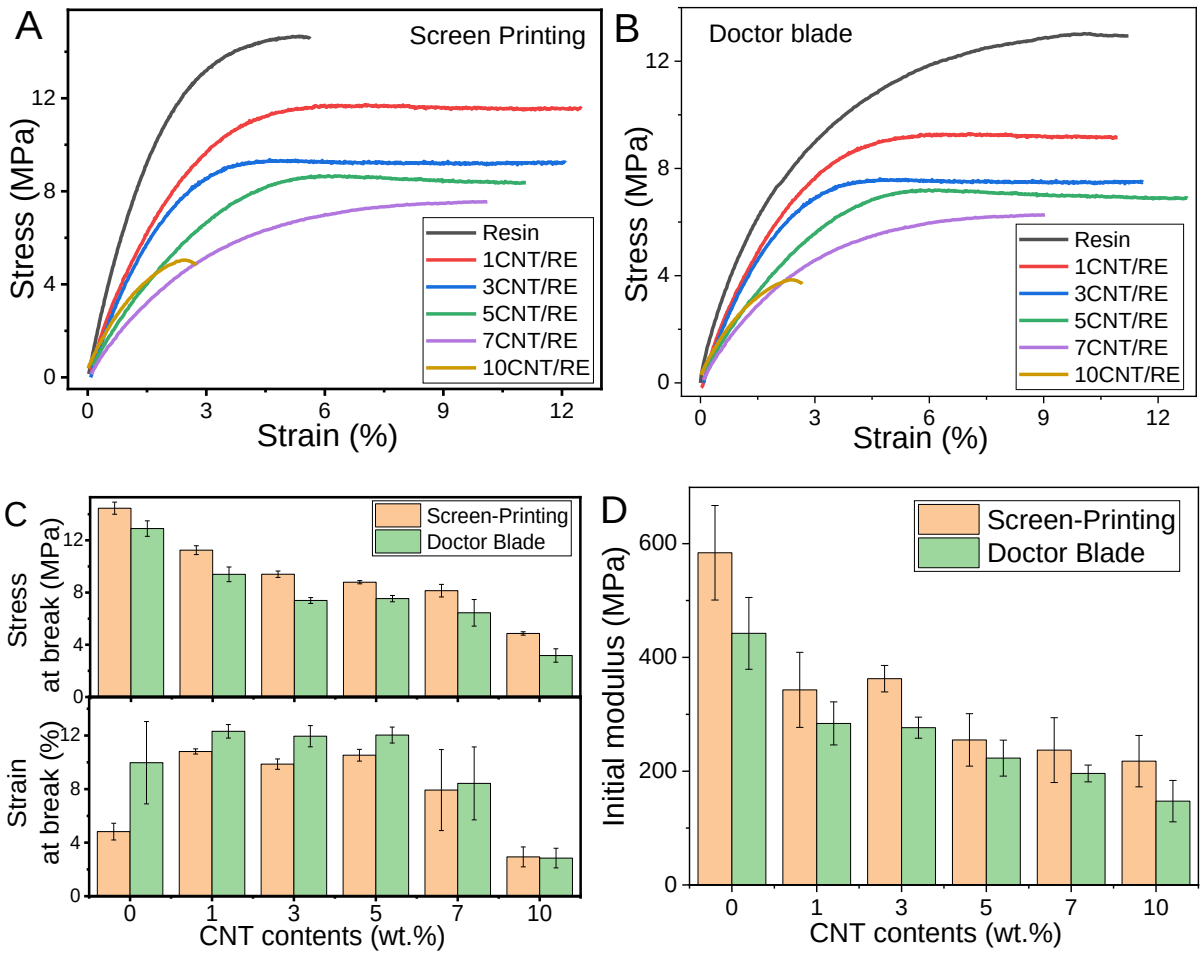


Figure 2.5 - Representative tensile stress-strain measurements showing the elongation at break for A) screen-printing and B) doctor blade prepared samples. C) stress and strain at break and D) Initial elastic modulus measured up to 1% for all samples.

The initial elastic modulus is shown in Figure 2.5D. The combination of the solvent effect on the ERs and composites processing resulted in screen-printed materials exhibiting plastic behaviour compared with the doctor blade method (Figure 2.5D). The initial modulus values are approximately 590 and 430 MPa for the resin and 220 and 180 MPa for the largest filled screen-printed and doctor blade processed composites, respectively.

The surface electrical resistance of the materials was evaluated using the four-point method. ERs is an insulator material exhibiting a resistance of nearly 1010 Ω/sq Figure 2.6. Notably, the electrical sheet resistance decreases with an increase in the content of conductive MWCNTs within the composites. Specifically, the sheet resistance decreased by nearly 8 orders of magnitude from the pristine resin to the

7MWCNTs/RE composite, reaching nearly 100 Ω/sq, with some stabilization observed at higher MWCNTs concentrations. The electrical percolation threshold is near 3-4 wt. % MWCNTs content in the composite. Despite the high viscosity of the materials (30-45 Pays), the employed processing methods facilitate the production of composites with a relatively low percolation threshold, which also indicates effective filler dispersion. The use of solvent to disperse the MWCNTs before mixing with the resin and hardener enhances the electrical properties of the composites to values comparable with those reported in literature [28], while also showing suitable mechanical properties.

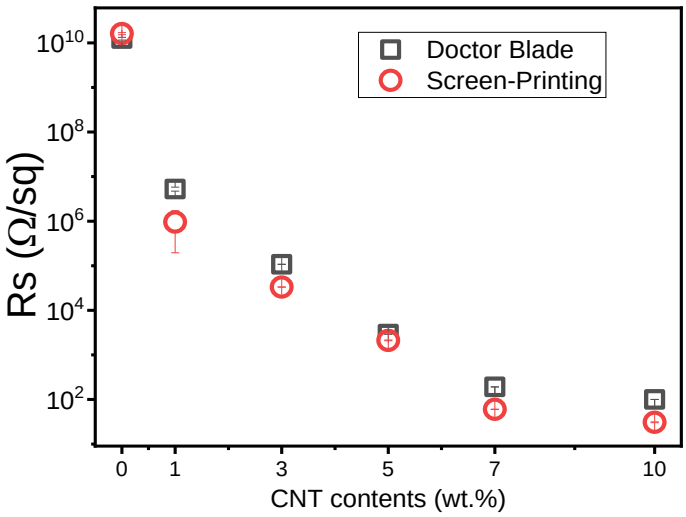


Figure 2.6 - Electrical sheet resistance for pristine resin and polymer composites up to 10 wt.% MWCNTs content. Films are processed both by screen-printing and doctor blade.

2.7 Piezoresistive and thermoresistive functional response

Composite films prepared through both screen-printing and doctor blade methods exhibit similar mechanical and electrical properties. Screen-printing facilitates the customization of device designs while offering advantages such as rapid processing, minimal material waste, and scalability for industrial applications. Consequently, the evaluation will focus on the functional sensing response of the screen-printed composites.

The piezoresistive sensitivity was measured as a function of filler content in composites containing 3, 5 and 10 wt. % MWCNTs, near and after the percolation threshold, for 10 loading-unloading cycles in bending mode, with maximum vertical displacement ranging from 0.1 to 5 mm of (Figure 2.7). The representative piezoresistive measurements for the 3MWCNTs/RE, 5MWCNTs/RE, and 10MWCNTs/RE composites under a maximum bending of 3 mm are represented in Figures 2.7A-C. It is observed that

the electrical resistance changes in response to the applied mechanical stimulus for all composites, the electrical resistivity increases with increasing bending deformation and decreases upon the release of the bending stimulus. A slight increase in resistance was noted over repeated cycling for the various composites, attributed to the elastic-to-plastic transition in the ERs and irreversible variations within MWCNTs network [29, 30], as similarly reported in commercial strain gauges [30]. However, the absolute value of the relative change in resistance for each cycle remained nearly constant throughout the tests. Subsequently, 100 cycles were performed at a displacement of 1 mm to evaluate the cyclability of the composites (Figure 2.7D). A slight increase in overall resistance was again observed over the cycling process, yet the stability of the piezoresistive response for each cycle was maintained.

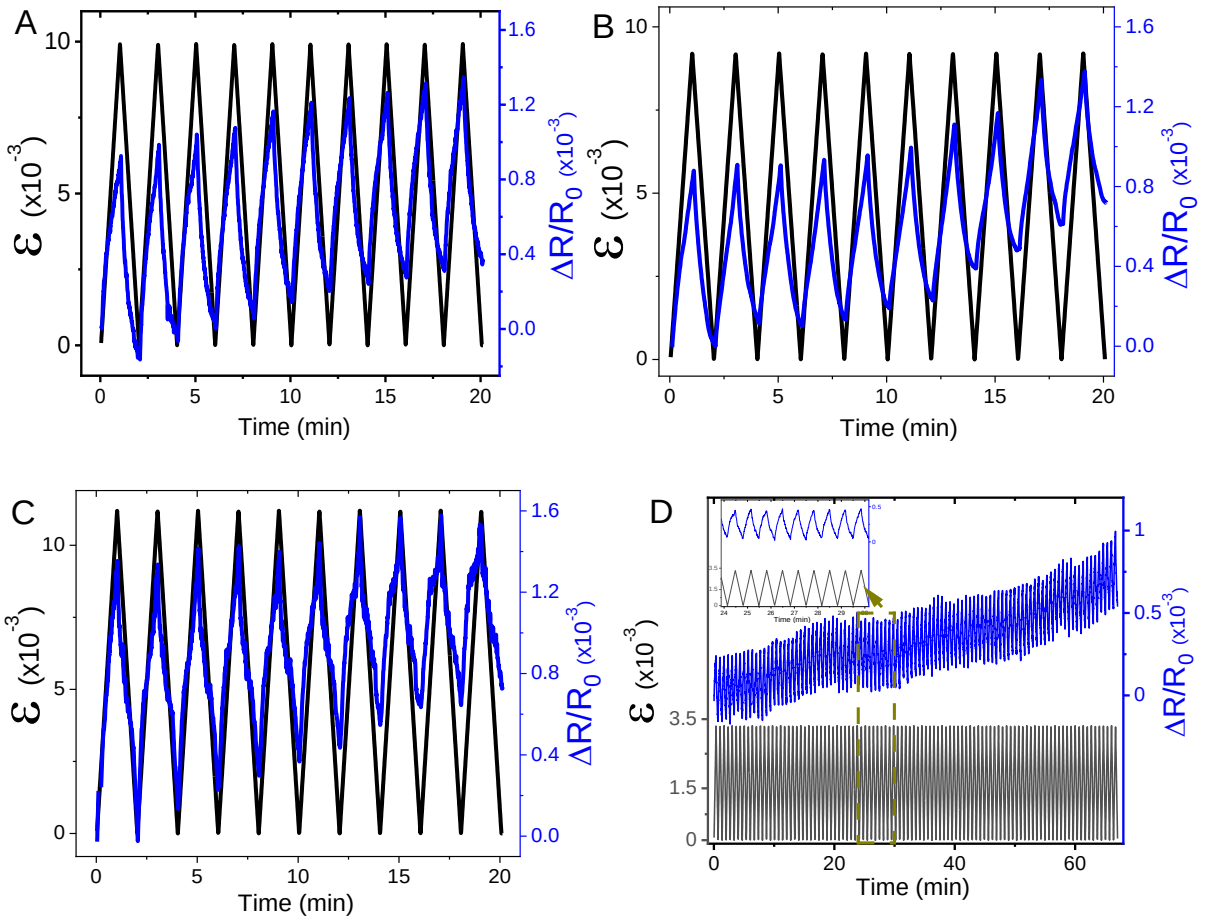


Figure 2.7 - Representative piezoresistive response under cyclic bending tests at 3 mm maximum displacement for A) 3MWCNTs/RE, B) 5MWCNTs/RE and C) 10MWCNTs/RE composites. D) Repeated bending tests for 100 cycles at maximum vertical deformation of 1 mm for the 5MWCNTs/RE composite.

The piezoresistive sensitivity or GF calculated using Equation 2.4 is shown in Figure 2.8. For the different MWCNTs contents and applied bending, the GF< 0.4 is always within the geometric effect, owing to the

stiffness of the ERs and consequent small changes in the MWCNTs network during the loading-unloading bending tests. The ERs reinforced with MWCNTs exhibits piezoresistive values near GF ≈ 0.43 for uniaxial stress and 0.05 <GF< 0.6 in flexural stress [31, 32]. The piezoresistive sensitivity of resin ERs composites usually does not change as much with filler content as that of thermoplastic composites [33] even for materials near the electrical percolation threshold [33], owing to the rigid polymer network. Piezoresistive measurements demonstrated the ability of the composites to work as functional materials with suitable mechanical performance for structural applications. Therefore, the functional composites can be applied as bending sensors capable of detecting low to large strains.

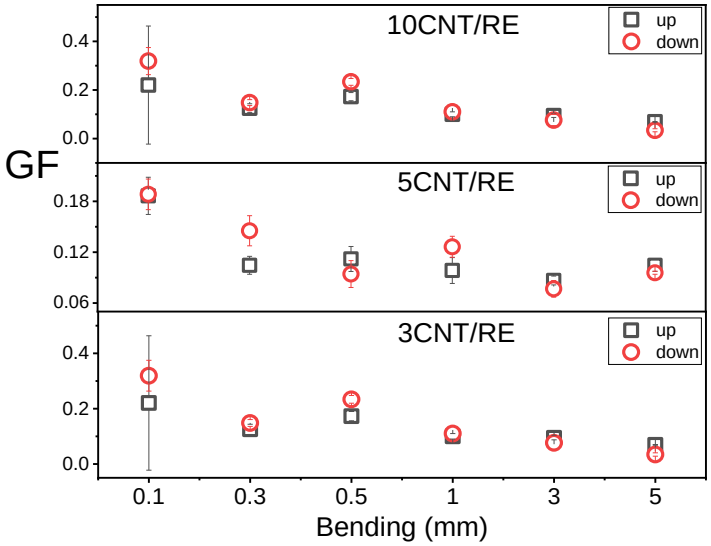


Figure 2.8 - Piezoresistive gauge factors of composites with 3, 5 and 10 wt.% MWCNTs content for maximum bending strains from 0.1 to 5 mm at 3 mm/min.

Furthermore, polymer composites with a MWCNTs conductive network can exhibit thermoresistive response, which is suitable for temperature sensing applications [15]. The thermoresistive sensitivity (S) in Figure 2.9, of the 5MWCNTs/RE composite was evaluated for applications in two different temperature ranges: for human body temperature sensing, from 32 to 40 °C, and for higher temperature applications, from 60 to 90 °C. The 5MWCNTs/RE composite presents thermoresistive sensitivities of $S_{32\text{-}40} \approx -0.004$ (%.°C^{-1}) and $S_{60\text{-}90} \approx -0.07$ (%.°C^{-1}). The slower rate and small temperature changes demonstrate much lower resistance variation, as reported in the literature for similar samples [34]. Thermal sensitivity critically depends on the MWCNTs content [35], which is one order of magnitude lower than that of thermoplastic composites [36], but increases for higher temperature ranges, with excellent linearity between temperature and electrical resistance variations. The composites present negative thermal coefficient, attributed to the dominant effect of the intrinsic thermoresistivity of the MWCNTs in composites above

the percolation threshold [36] as well as their thermally activated tunnelling effect in the thermoresistive response of the composite [36, 37]. Thus, the multifunctionality of the developed composites for deformation and temperature variation applications was demonstrated.

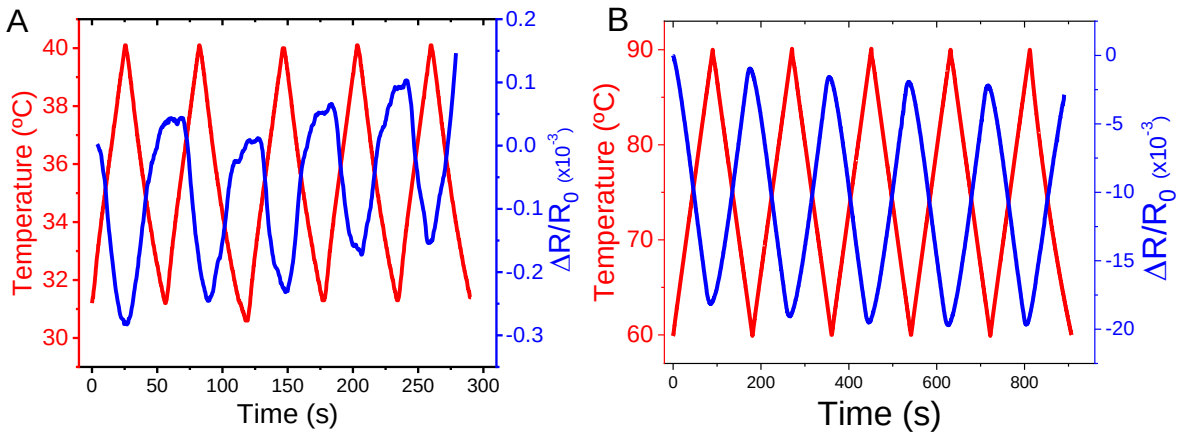


Figure 2.9 - Thermoresistive response of the 5MWCNTs/RE composite for temperature variations in the A) human body regime (32 to 40 °C) and B) higher temperatures (60 to 90 °C).

2.8 Multifunctional adhesively bonded joints

One of the main functions of the resins is to be used as a mechanical adhesive on joints. This was evaluated in the present study using uniaxial shear tests (Figure 2.10A). The shear strength at break (Figure 2.10B) was evaluated using two types of adherends (carbon fibres reinforced polymers- CFRP- and aluminium) and it was observed that the shear strength is larger for aluminium (27 and 15 MPa for resin and 5MWCNTs/RE composite, respectively) than for CFRP (7-9 MPa). Compared to the resin, functional 5MWCNTs/RE composite shows lower shear strength (15 MPa in aluminium and 7 MPa in CFRP) but can work as adhesive with sensing properties. The differences between shear strength in CFRP and aluminium adherends are related to the specific surface characteristics of each sample, namely the rugosity [38] and chemical composition, and is in accordance with the manufacturer's data, where aluminium has the highest shear strength [39]. In addition, bonded joints with aluminium adherends exhibited a combination of adhesive and cohesive failure. However, the CFRP bonded joints predominantly show fibre tear failure in addition to adhesive and cohesive failure modes, which can be attributed to a lower interlaminar shear stress of the adherent when compared to bonded joints. Shear strengths approaching 30 MPa have been reported for single lap aluminium joints using Araldite AW106 ERs adhesives, both MWCNTs-reinforced and unreinforced [40], and up to 12 MPa for composite adherends [41].

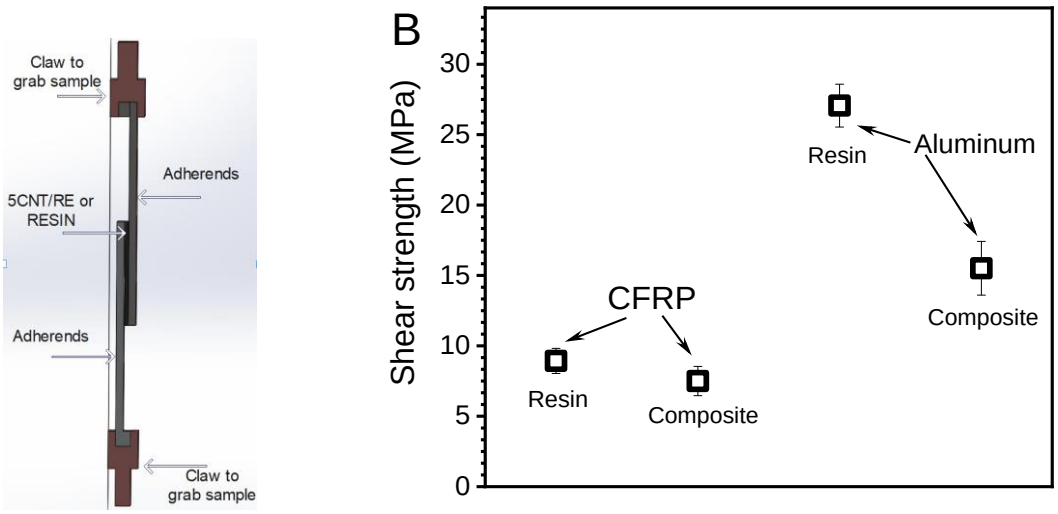


Figure 2.10 - A) Schematic illustration of the bonded joint with uniaxial shear test setup. B) Shear strength of CFRP and aluminum bonded joints.

The piezoresistive evaluation of the bonded joints was evaluated for 10 cycles of for 0.1, 0.3, and 0.5 mm maximum bending deformation (Figure 2.11A) and for 1, 3 and 5 maximum bending (Figure 2.11B), respectively. Further, long-term cycling evaluation was performed for 500 cycles at a maximum deformation of 1 mm (Figure 2.11C). The piezoresistive response of the multifunctional joint (i.e., self-sensing adhesives) is similar to that of the bulk printed film (Figure 2.7), but with larger sensitivity values owing to the larger compression forces between the fibre glass during bending cycles, and the resistance variation over cycling is linear and follows the applied strain, increasing with increasing bending and decreasing when bending is released (Figure 2.11A and B). Under long-term cycling, a decrease in the overall resistance of the system is observed, being larger for the first 50-100 cycles comparing the minimum and maximum values of electrical resistance (Figure 2.11C), with a stabilization trend thereafter. This effect is common in polymer-based piezoresistive sensors, due to irreversible variations and breakup-rebuilding of the conductive network [42, 43], as well as the creep behaviour of the resin [43]; however it trends to stabilize over cycling. It should be noted that since the maximum and minimum resistance variations undergo similar changes, the resistance variation for each cycle remains consistent; therefore, the piezoresistive sensitivity is stable over cycling resistance variation per cycle. The GF as a function of maximum deformation is represented in Figure 2.11D, showing an increasing sensitivity with increasing deformation, from close to GF ≈10 for 0.1 mm of maximum bending strain to between 20 to 30 for 1 and 3 mm of maximum bending strain. For the largest applied strain (5 mm of bending), the two glass fibre structures bonded with the 5MWCNTs/RE composite showed difficulties following the mechanical stimuli, leading to a decrease in sensitivity (GF ≈ 5), as observed by the resistance behaviour

with cycles near non-deformation of the cantilever. The GF over repeated cycling is near GF ≈12 ± 4 for all tested cycles. Thus, the developed composite is suitable as a self-sensing adhesive for bending applications, presenting stability over cycling.

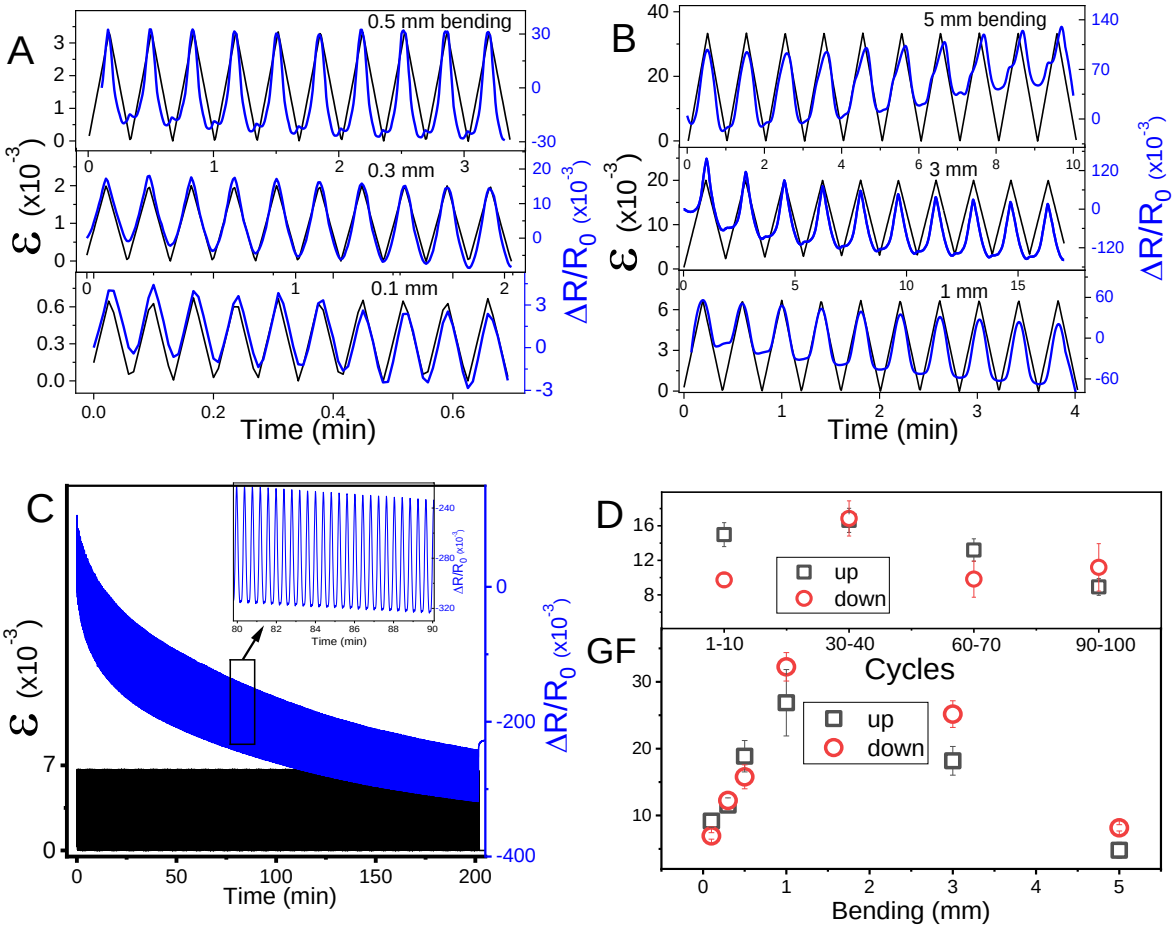


Figure 2.11 - Piezoresistive response of a bonded joint with 5MWCNTs/RE during 10 loading-unloading bending cycles for A) maximum bending of 0.1, 0.3, 0.5 mm; B) and 1, 3, and 5 mm. C) 500 cycles at 1 mm bending; D) corresponding GF for maximum bending displacements.

The thermoresistive response of the multifunctional bonded joints was determined for 5 cycles between 32 and 50 °C and from 60 to 90 °C, as shown in Figure 2.12. The electrical resistance decreases with increasing temperature and vice versa, as previously observed for the 5MWCNTs/RE composite, and the temperature sensitivity is near $S_{32\text{-}50} \approx -0.02$ (%.°C^{-1}) and $S_{60\text{-}90} \approx -0.03$ (%.°C^{-1}). Increasing the temperature range increased the resistance variation, as shown in the literature [34]. The thermoresistive sensitivity values are in agreement with those reported in the literature [34, 36].

This thermoresistive response demonstrates that filled resin materials can act mechanically as adhesives and exhibit piezo- and thermoresistive properties, which is interesting for the development of self-sensing

adhesives in a variety of Industry 4.0 related applications, allowing the monitoring of structural devices in real time.

With response to possible crosstalk between both effects, it is to notice that the resistance variation of the composite for sensing applications is quite different for piezo- and thermoresistive in terms of the response time, slower for temperature than for mechanical stimuli. The thermoresistive response in the low temperature range was an order of magnitude lower than in the mechanical bending mode, the response time for resistance variations was also lower for temperature changes than for mechanical variations. Thus, both signals can be appropriately addressed using specific electronic interfaces.

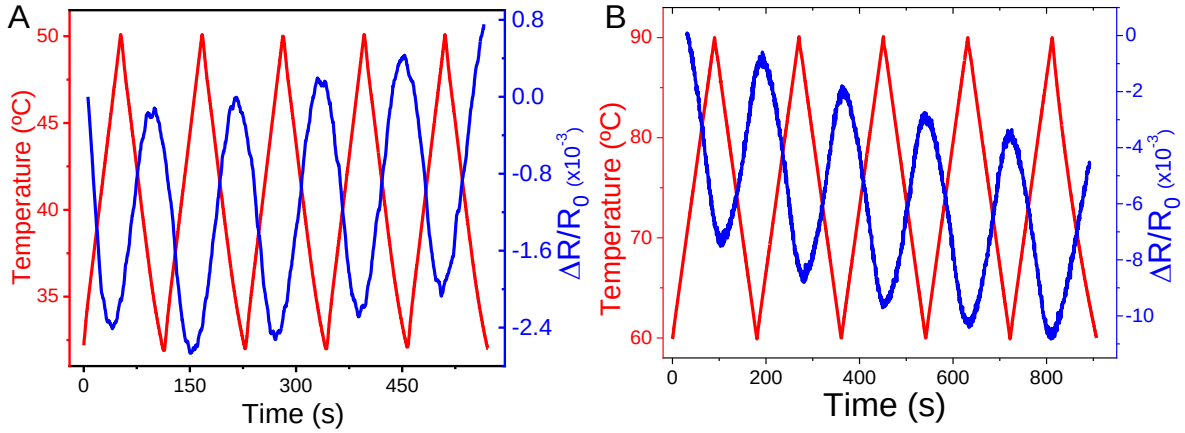


Figure 2.12 - Thermoresistive response of a 5MWCNTs/RE composite bonded joint between A) 32 to 50 °C and B) 60 to 90 °C for 5 cycles.

In summary, the mechanical and functional properties (electromechanical and thermoresistive) of the ERs composite with 5 wt.% of MWCNTs demonstrate excellent adhesive properties and linear piezo- and thermoresistive responses. The piezoresistive and thermoresistive responses of 5 wt.% of MWCNTs composite is similar with other resin ERs composites in literature [44], being thermoplastic or elastomers composites more appropriated for larger strains and presenting larger sensitivities. Nevertheless, ERs shows excellent adhesive characteristics to bond materials and, simultaneously, suitable multifunctional sensing properties.

2.9 Piezoresistive prototype for cantilever applications

A prototype was developed using a cantilever system with a bonded joint of two glass fibre adherents (insulators fibres) of 80 × 23 mm^2 each and with the 5MWCNTs/RE composite as functional adhesive with an area of 25 × 23 mm^2, as illustrated in Figure 2.13A. Shear forces demonstrate that the cantilever system supports up to 5 mm of bending displacement (about 4°) without compromising structural

characteristics, corresponding to a force of about 2 N (≈ 3.5 kappa) during multiple cycles. The piezoresistive bending analysis of the cantilever system is presented in Figures 2.13B and C, up to 5 mm of maximum bending displacement without and with a dwell time of 60 s in unloaded position, respectively. It can be observed that, after the first cycle, the relative resistance variation over repeated bending presents a stable behaviour for 1, 3, and 5 mm of maximum bending displacement (Figure 2.13B). The piezoresistive sensitivity of the prototype presents a similar response when compared to the films (Figure 2.7). With the introduction of a dwell time of 60 s to evaluate the stabilization of the signal at the unloading point, the electrical resistance decreases slightly with a tendency to stabilize, showing a rapid detection of the bending movement of each test.

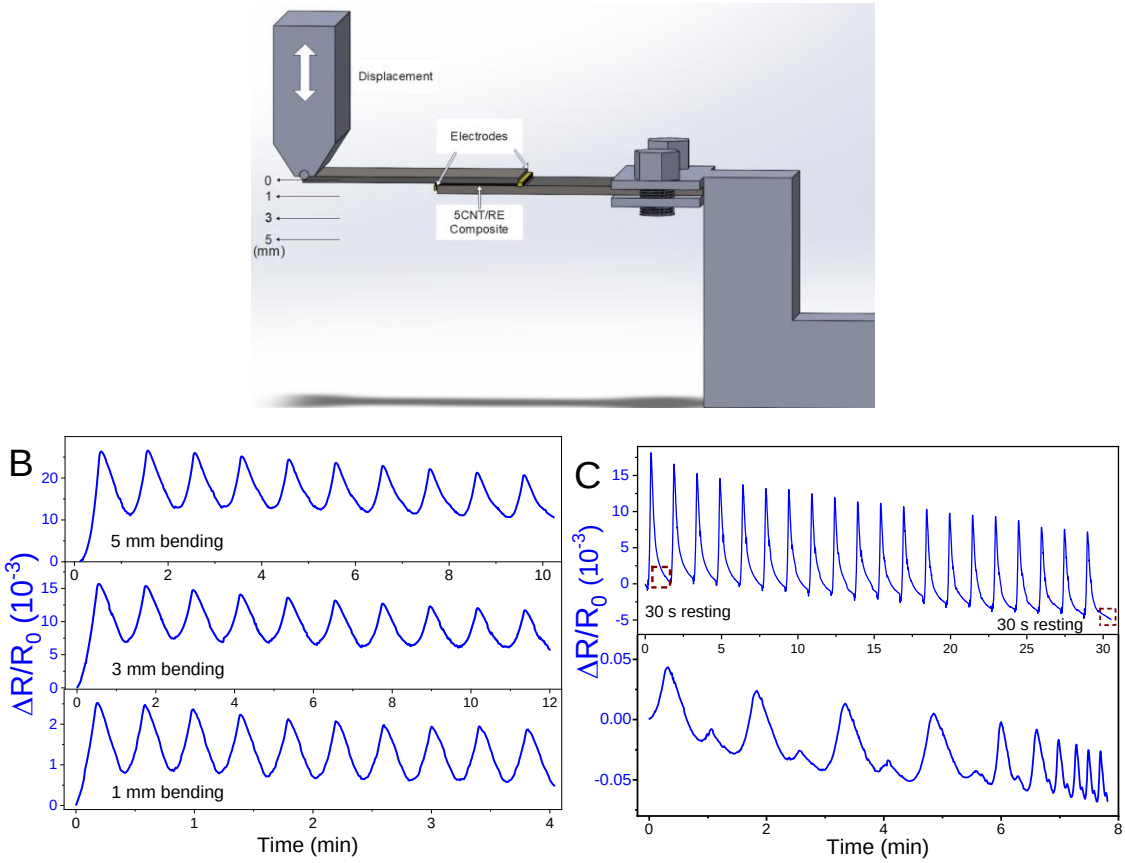


Figure 2.13 - A) Schematic representation of the prototype to evaluate the ERs composite as a self-sensing adhesive in a cantilever structure. Piezoresistive response of the 5MWCNTs/RE composite as a cantilever bending sensor for B) 1, 3, and 5 mm maximum displacement.

2.10 Conclusions

ERs matrices present adhesive properties and can be manipulated to function as effective sensing materials. Bonded joints utilizing these matrices are prevalent in the marine, aerospace, and automotive industries. Furthermore, these matrices can be filled with MWCNTs without compromising their intrinsic

properties, thereby serving as multifunctional adhesives with both piezoresistive and thermoresistive sensing capabilities. In the present study, ERs nanocomposites containing MWCNTs were prepared with filler contents of up to 10% wt. both by screen-printing and doctor blade methods. The results indicate that the initial elastic modulus and stress at break decrease as the concentration of MWCNTs in the composites increases. Additionally, the electrical sheet resistance decreases from 10^{-10} to 10^{-2} Ω/sq with increasing the filler content. Screen-printed films of the 5MWCNTs/RE composite exhibited linear piezoresistive and thermoresistive properties in response to applied bending and temperature variations, with GF< 0.4 and S< 0.07 (%.°C^{-1}). When employed in bonded joints with CFRP and aluminium adherents, the shear strength is greater than 27 and 8 MPa, respectively. The sensing properties for both piezoresistive and thermoresistive responses enable effective monitoring of deformation and temperature fluctuations within the joints.

A cantilever structural application has been developed to measure the bending stimulus applied to a glass fibre joint bonded with a 5% wt. MWCNTs composite as a function of cyclic bending. This application demonstrates a rapid detection of bending displacement, thereby indicating the appropriateness of the developed materials for self-sensing adhesive applications.

2.11 References

[1] Jin F-L, Li X, Park S-J. Synthesis and application of epoxy resins: A review. Journal of Industrial and Engineering Chemistry. 2015;29:1-11.

[2] Capricho JC, Fox B, Hameed N. Multifunctionality in Epoxy Resins. Polymer Reviews. 2020;60(1):1-41.

[3] Sarfraz MS, Hong H, Kim SS. Recent developments in the manufacturing technologies of composite components and their cost-effectiveness in the automotive industry: A review study. Composite Structures. 2021;266:113864.

[4] Li Y, Xiao Y, Yu L, Ji K, Li D. A review on the tooling technologies for composites manufacturing of aerospace structures: materials, structures and processes. Composites Part A: Applied Science and Manufacturing. 2022;154:106762.

[5] Barsotti B, Gaiotti M, Rizzo CM. Recent Industrial Developments of Marine Composites Limit States and Design Approaches on Strength. Journal of Marine Science and Application. 2020;19(4):553-66.

[6] Mendes-Felipe C, Costa P, Roppolo I, Sangermano M, Lanceros-Mendez S. Bio-Based Piezo- and Thermoresistive Photocurable Sensing Materials from Acrylated Epoxidized Soybean Oil. Macromolecular Materials and Engineering. 2022;307(7):2100934.

[7] Kumar Singh S, Gunwant D, Vedrtnam A, Kumar A, Jain A. Synthesis, characterization, and modelling the behavior of in-situ ZrO2 nanoparticles dispersed epoxy nanocomposite. Engineering Fracture Mechanics. 2022;263:108300.

[8] Irfan MS, Ali MA, Khan T, Anwer S, Liao K, Umer R. MXene and graphene coated multifunctional fiber reinforced aerospace composites with sensing and EMI shielding abilities. Composites Part A: Applied Science and Manufacturing. 2023;165:107351.

[9] del Río JS, Ridruejo Á, Martínez V, Jiménez JL, Ramos C, Vilatela JJ, et al. CNTs monitoring sensors for resin infusion optimization. Sensors and Actuators A: Physical. 2023;364:114852.

[10] Atif R, Shyha I, Inam F. Mechanical, Thermal, and Electrical Properties of Graphene-Epoxy Nanocomposites-A Review. Polymers. 2016;8(8).

[11] Lin Q, Zhang F, Xu X, Yang H, Mao Q, Xian D, et al. A Flexible Pressure Sensor Based on Graphene/Epoxy Resin Composite Film and screen-printing Process. Nanomaterials. 2023;13(19):2630.

[12] Vicente J, Costa P, Lanceros-Mendez S, Abete JM, Iturrospe A. Electromechanical Properties of PVDF-Based Polymers Reinforced with Nanocarbonaceous Fillers for Pressure Sensing Applications. Materials. 2019;12(21):3545.

[13] Dios JR, García-Astrain C, Costa P, Viana JC, Lanceros-Méndez S. Carbonaceous Filler Type and Content Dependence of the Physical-Chemical and Electromechanical Properties of Thermoplastic Elastomer Polymer Composites. Materials. 2019;12(9):1405.

[14] Franco M, Alves R, Perinka N, Tubio C, Costa P, Lanceros-Mendéz S. Water-Based Graphene Inks for All-Printed Temperature and Deformation Sensors. ACS Applied Electronic Materials. 2020;2(9):2857-67.

[15] Avilés F. Thermoresistivity of Carbon Nanostructures and their Polymeric Nanocomposites. Advanced Materials Interfaces. 2023;10(31):2300218.

[16] Arboleda L, Ares A, Abad MJ, Ferreira A, Costa P, Lanceros-Mendez S. Piezoresistive response of carbon nanotubes-polyamides composites processed by extrusion. Journal of Polymer Research. 2013;20(12):326.

[17] Ferreira RG, Silva AP, Nunes-Pereira J. Current On-Skin Flexible Sensors, Materials, Manufacturing Approaches, and Study Trends for Health Monitoring: A Review. ACS Sensors. 2024;9(3):1104-33.

[18] Rodrigues-Marinho T, Perinka N, Costa P, Lanceros-Mendez S. Printable lightweight polymer-based energy harvesting systems: materials, processes, and applications. Materials Today Sustainability. 2023;21:100292.

[19] Zainuddin S, Fahim A, Arifin T, Hosur MV, Rahman MM, Tyson JD, et al. Optimization of mechanical and thermo-mechanical properties of epoxy and E-glass/epoxy composites using NH2-MWCNTs, acetone solvent and combined dispersion methods. Composite Structures. 2014;110:39-50.

[20] Mendes-Felipe C, Oliveira J, Costa P, Ruiz-Rubio L, Iregui A, González A, et al. Stimuli responsive UV cured polyurethane acrylated/carbon nanotube composites for piezoresistive sensing. European Polymer Journal. 2019;120:109226.

[21] Joseph EJ, Panneerselvam K. Manufacturing and Characterization of Tungsten Particulate-Reinforced AW106 Epoxy Resin Composites. Transactions of the Indian Institute of Metals. 2021;74(4):817-25.

[22] Mittal V, Sinha S. Effect of alkali treatment on the thermal properties of wheat straw fiber reinforced epoxy composites. Journal of Composite Materials. 2016;51(3):323-31.

[23] Abdi E, Khabaz-Aghdam A, Hasan-nezhad H, Behjat B, Marques EAS, Yang Y, et al. The effect of graphene and graphene oxide on defective single lap adhesively bonded joints. Journal of Composite Materials. 2022;56(17):2665-75.

[24] Atmakuri A, Palevicius A, Vilkauskas A, Janusas G. Numerical and Experimental Analysis of Mechanical Properties of Natural-Fiber-Reinforced Hybrid Polymer Composites and the Effect on Matrix Material. Polymers. 2022;14(13):2612.

[25] Goyat M, Jaglan V, Tomar V, Louchaert G, Kumar A, Kumar K, et al. Superior thermomechanical and wetting properties of ultrasonic dual mode mixing assisted epoxy-CNT nanocomposites. High Performance Polymers. 2019;31(1):32-42.

[26] Santos P, Silva AP, Reis PNB. The Effect of Carbon Nanofibers on the Mechanical Performance of Epoxy-Based Composites: A Review. Polymers. 2024;16(15):2152.

[27] Moyano JJ, Gómez-Gómez A, Pérez-Coll D, Belmonte M, Miranzo P, Osendi MI. Filament printing of graphene-based inks into self-supported 3D architectures. Carbon. 2019;151:94-102.

[28] Imran KA, Shivakumar KN. Graphene-modified carbon/epoxy nanocomposites: Electrical, thermal and mechanical properties. Journal of Composite Materials. 2019;53(1):93-106.

[29] Vertuccio L, Guadagno L, Spinelli G, Lamberti P, Tucci V, Russo S. Piezoresistive properties of resin reinforced with carbon nanotubes for health-monitoring of aircraft primary structures. Composites Part B: Engineering. 2016;107:192-202.

[30] Sanli A, Benchirouf A, Müller C, Kanoun O. Piezoresistive performance characterization of strain sensitive multi-walled carbon nanotube-epoxy nanocomposites. Sensors and Actuators A: Physical. 2017;254:61-8.

[31] Spinelli G, Lamberti P, Tucci V, Vertuccio L, Guadagno L. Experimental and theoretical study on piezoresistive properties of a structural resin reinforced with carbon nanotubes for strain sensing and damage monitoring. Composites Part B: Engineering. 2018;145:90-9.

[32] Rodríguez-González JA, Rubio-González C, Soto-Cajiga JA. Piezoresistive Response of Spray-coated Multiwalled Carbon Nanotube/Glass Fiber/Epoxy Composites under Flexural Loading. Fibers and Polymers. 2019;20(8):1673-83.

[33] Avilés F, Oliva-Avilés AI, Cen-Puc M. Piezoresistivity, Strain, and Damage Self-Sensing of Polymer Composites Filled with Carbon Nanostructures. Advanced Engineering Materials. 2018;20(7):1701159.

[34] Cen-Puc M, Pool G, Oliva-Avilés AI, May-Pat A, Avilés F. Experimental investigation of the thermoresistive response of multiwall carbon nanotube/polysulfone composites under heating-cooling cycles. Composites Science and Technology. 2017;151:34-43.

[35] Dai H, Thostenson ET, Schumacher T. Comparative study of the thermoresistive behavior of carbon nanotube-based nanocomposites and multiscale hybrid composites. Composites Part B: Engineering. 2021;222:109068.

[36] Cen-Puc M, Oliva-Avilés AI, Avilés F. Thermoresistive mechanisms of carbon nanotube/polymer composites. Physica E: Low-dimensional Systems and Nanostructures. 2018;95:41-50.

[37] Mecklenburg M, Mizushima D, Ohtake N, Bauhofer W, Fiedler B, Schulte K. On the manufacturing and electrical and mechanical properties of ultra-high wt.% fraction aligned MWCNT and randomly oriented CNT epoxy composites. Carbon. 2015;91:275-90.

[38] Cardoso JV, Gamboa PV, Silva AP. Effect of surface pre-treatment on the behaviour of adhesively-bonded CFRP T-joints. Engineering Failure Analysis. 2019;104:1188-202.

[39] Huntsman. Advanced Materials; Araldite AW 106 / Hardener HV 953U Structural Adhesives. 2010.

[40] Londhe VH, Misal ND. Influence of Multiwall Carbon Nanotubes on Shearstrength of Single Lap Joint. International Journal of Scientific Research and Management (IJSRM). 2015;3(11):3769-74.

[41] B R, Chinnathambi S, E N, R H. Mechanical Characterization of Adhesive in Lap Joint Under Tensile Load. Journal of Polymer & Composites. 2024;11:S96-S103.

[42] Costa P, Maceiras A, San Sebastián M, García-Astrain C, Vilas JL, Lanceros-Mendez S. On the use of surfactants for improving nanofiller dispersion and piezoresistive response in stretchable polymer composites. Journal of Materials Chemistry C. 2018;6(39):10580-8.

[43] Deka BK, Hazarika A, Kim J, Jeong HE, Park Y-B, Park HW. Fabrication of the piezoresistive sensor using the continuous laser-induced nanostructure growth for structural health monitoring. Carbon. 2019;152:376-87.

[44] Arana G, Gamboa F, Avilés F. Piezoresistive and thermoresistive responses of carbon nanotube-based strain gauges with different grid geometric parameters. Sensors and Actuators A: Physical. 2023;359:114477.

Chapter 3 - Develop of thermo- and piezoresistive responses in epoxy resins-based adhesives

This chapter is based on the following publication: Ricardo Lima, Luís Amorim, João Nunes-Pereira, Carmen Rial Tubio, Senentxu Lanceros-Mendez1, Pedro Costa, “Development of thermo- and piezoresistive responses in epoxy resin-based adhesives”, journal Wiley Polymer Composites with DOI https://doi.org/10.1016/j.compositesb.2025.112130

ERs composites produced by additive manufacturing have been developed for their use as adhesive materials with sensing functionalities as multifunctional piezoresistive and thermoresistive materials.

The processing of the composites involves acetone as a solvent to tune the viscosity and achieve a homogeneous dispersion of the MWCNTs, resulting in a solution with suitable characteristics for application by additive manufacturing. Doctor blade and screen-printing films have been prepared with a low electrical resistivity of approximately 100 Ω/sq for composites with 10 wt.% of MWCNTs. The largest piezoresistive sensitivity, determined by a Gauge Factor of approximately 15 under 5 mm bending, has been obtained, with suitable stability over cycling solicitation. Furthermore, the thermoresistive response exhibited a sensitivity of 0.05 $\%.C^{-1}$. Self-sensing bonded structures have been obtained with excellent adhesive forces (approximately 20 MPa in glass fibre joints) in shear lap tests. In addition, the bonded structure demonstrated a linear response to loading-unloading up to 5 mm of bending in the cantilever mode, with cycle stability. Overall, a scalable methodology to obtain high-performance self-sending adhesive materials processable by additive manufacturing is presented, which shows excellent bonding characteristics, together with mechanical and thermal sensing properties.

3.1 Introduction

Thermosetting polymers cure irreversibly by forming a crosslinked molecular network through heating and chemical reactions involving a prepolymer (resin), which is typically in a liquid, viscous, or soft solid state [1]. The degree of crosslinking can be controlled by adapting the curing process parameters, such as the type of agent, time, and temperature, with critical influences on performance of mechanical and thermal properties, providing versatility based on the requirements of the final application [2]. Once cured, thermoset resins are suitable candidates for structural and semi-structural applications, including coatings, adhesives, composite matrices, and electronic encapsulation [3]. The most common thermoset resins include polyester, vinyl ester, and polyurethane, with ERs representing one of the most accepted materials in the market due to their versatility and performance [4].

The discovery of ERs comes back to the beginning of the XIX century and they have achieve significant implementation in industrial applications in harsh and highly demanding service environments in the form of adhesives, coatings, and advanced structural composites [5], due to their exceptional adhesion and mechanical properties, excellent chemical and environmental resistance, and low shrinkage and moisture absorption.

ERs are typically made by mixing a prepolymer resin (monomer block with functional groups) and a curing agent (so-called initiator or hardener) which, upon reaction, forms a three-dimensional and irreversible

crosslinked network [6]. The curing agent induces and controls the cure kinetics, determining the Tg (glass-transition temperature) and, consequently the mechanical properties [7]. Low crosslinking density results in low Tg, leading to modest stiffness and strength, but good impact and fatigue properties. On the contrary, high crosslinking densities result in high-performance epoxies with high stiffness and chemical resistance [8].

Among their wide range of application areas, ERs are often used as adhesives in structural bonded joints. Their exceptional adhesion properties to a wide range of dissimilar adherends, high bond strength, corrosion resistance, and lightweight make them natural candidates to replace traditional mechanical joints (welded, riveted, or bolted) [9]. In addition, their ease of application allows for faster assembly processes, which is extremely attractive for a broad range of industries, including automotive and aerospace [8, 10]. Nevertheless, highly crosslinked epoxies are typically brittle and highly susceptible to cracking at low strains, raising safety concerns. The incorporation of second-phase thermoplastic copolymers, rubbers, and inorganic and carbonaceous nanoparticles (e.g., CB MWCNTs, and G) has been successfully explored to increase toughness and fracture resistance [11, 12]. Despite the reported enhancements in fracture toughness [12], the integration of thermoplastics and rubbers can yield an increase in viscosity and a reduction in Tg, compromising processability and mechanical properties [13]. On the other hand, the dispersion of inorganic and carbonaceous nanoparticles allows to enhance the mechanical properties (stiffness and strength) and fracture resistance of ERs by deflecting the crack path, with small impact on the rheologic properties, slightly increase on viscosity, due to their small aspect ratio [14]. Nevertheless, the dispersion of such nanofillers has been the major processing challenge to take full advantage of these materials [15]. A good and homogeneous dispersion can provide a large interfacial area and, consequently, an effective and multi-mechanism energy dissipation system [16]. In particular, carbon-based nanoparticles, such as MWCNTs and G, possess high thermal, electrical, and mechanical properties, making them suitable not only for toughening, but also to provide multifunctionality [17, 18].

Due to their highly specific and tailorable characteristics, multifunctional polymer-based materials are being strongly investigated, finding applications in a wide range of technological fields as sensors and actuators [19]. Deeply rooted in the industry for a long time and with excellent compatibilization properties, ERs are at the top of the list of tunable polymers for multifunctional applications, opening up a wide range of opportunities in the ongoing industrial digitalization [20]. For instance, the inclusion of MWCNTs or G can convert ERs into electrically conductive materials [10, 21], providing sensitive features that can offer valuable information about structural integrity and thermal environment without compromising weight and overall mechanical performance [22, 23]. These multifunctional nano

composites can exhibit piezoresistive [24] and thermoresistive [25] behaviour, allowing simple and real-time monitoring [26]. Recent studies have demonstrated the enhanced piezoresistive and thermoresistive properties of MWCNT screen-printing polymer composites for strain and temperature sensing applications [27]. Polymer-based piezoresistive sensors can distinguish force, strain and bending from low to high deformation [23]. Furthermore, the viscosity of multifunctional epoxies can be adjusted, enabling easy printing with high-resolution, scalable and cost-effective, additive manufacturing processes such as screen- and spray-printing [10, 24, 28].

Considering the critical role of adhesives and bonded joints in the structural integrity of many devices and systems, it is paramount to developing a new class of multifunctional adhesives that integrate self-sensing capabilities while maintaining strong mechanical properties. This work presents a scalable methodology for fabricating MWCNTs-reinforced ERs adhesives using doctor blade and screen-printing techniques that enable real-time monitoring of mechanical and thermal stresses in bonded structures. This approach bridges the gap between traditional adhesives and smart sensing materials, providing a novel solution for structural health monitoring applications in the aerospace, automotive, and industrial sectors.

3.2 Experimental

3.2.1 Materials

The adhesive ERs and hardener with commercial references Araldite AV 4076-1 (thixotropic) and HY 4076 (viscosity of 1.0-2.0 Pa.s), respectively, were acquired from Huntsman. According to the purchaser, depending on the curing time and temperature, the resin can present a glass transition temperature (Tg) between 64 to 78 °C, and a lap shear strength of 30 N/mm^2 in steel bonds and about 5 N/mm^2 for polymers bonds. Multiwall carbon nanotubes MWCNTs from Nanocyl (NC7000), with 90% carbon purity, 9.5 nm of external diameter and 1.5 μm of length, that gives an aspect ratio near of 158 were employed as a conductive filler.

The dispersion of MWCNTs into the adhesive was improved by tuning the viscosity using acetone with purity >95%, purchased from Fisher Scientific.

3.3 ERs and composites process

ERs as matrix and composites reinforced with MWCNTs were prepared in the form of thick and thin films using doctor blade and screen-printing methods, respectively.

The first processing step was to disperse the MWCNTs and obtain a printable solution of pristine resin ERs and respective composites for both processes, by tuning the resin/hardener viscosity. Therefore, acetone in different concentrations was used to improve MWCNTs dispersion and reduce pristine resin and composites viscosity. The choice of acetone mostly relied on its low boiling point, simple use [29] and environmental friendliness.

First, MWCNTs were disposed in acetone for 2 hours at room temperature to facilitate deagglomeration using an ultrasound bath (ATU, model ATM-3LCD with 40 kHz of frequency and 200 W of power) (Step 1 Figure 3.1) [29]. Then, an evenly content of this solution was added to the resin and hardener individually. Both mixtures were then stirred mechanically for 10 min at 2200 rpm and room temperature using a Heidolph RZR 1 (Step 2 Figure 3.1). During those two steps, containers were kept closed using parafilm to avoid acetone evaporation. Afterwards, the final mixture was degassed in vacuum with the aim of removing air bubbles introduced during the stirring step and acetone (Step 3 Figure 3.1). Finally, resin and hardener solution were mixed using a commercial mixing cartridge for good homogenization and then dispersed in a film form by doctor blade or screen-printing (Steps 4 and 5 Figure 3.1). All printable adhesives were produced using a 1:0.5 ratio between resin and hardener, a volume of 5 ml of acetone for the pristine resin printing solution and 9, 11, 13, and 15 ml for composites with a final MWCNTs content of 3, 5, 7 and 10 weight percentage (wt.%), respectively. Table 3.1 shows detailed information about each sample.

Table 3.1 - Nomenclature and main processing characteristics of the samples.

Samples	ERs:Hardener ratio	MWCNTs content (wt.%)	Acetone volume (ml)
Pristine resin	1:0.5	-	5
3MWCNTs/ER		3	9
5MWCNTs/ER		5	11
7MWCNTs/ER		7	13
10MWCNTs/ER		10	15

Doctor blade prepared adhesive samples were spread over a 25×15 cm glass flat substrate covered with a Teflon film. The sample geometry was controlled by a blade device with a rectangular shape of 15×10 cm and a thickness of 200 μm. Screen-printed samples were produced in two film deposition steps over a Teflon film using a screen frame mesh with 48 wires/cm with approximately thickness of 100 μm. The two-layer approach ensures to obtain a completely uniform film without imperfections, voids or holes. Between each deposition, the residual acetone was evaporated within an oven at 60 °C for 1 min.

The final curing for the samples (doctor bladed and screen-printed) was carried out at 60 °C for 30 min in an oven (Step 6 Figure 3.1). The final samples thickness prepared by doctor blade or screen-printed were in a range of 150 -180 μm and 85 - 140 μm, respectively.

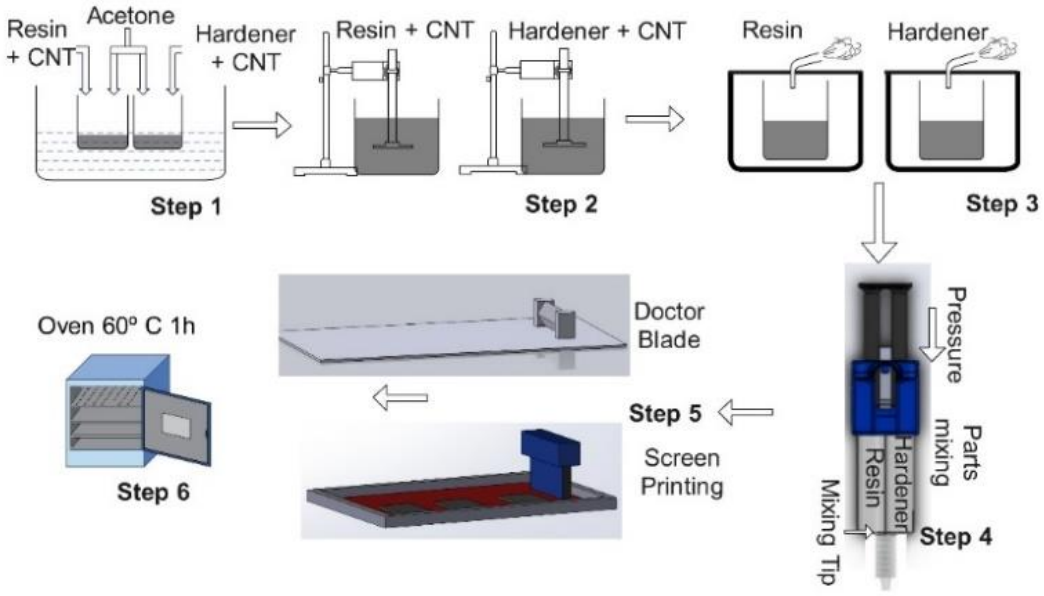


Figure 3.1 - Representation of the ERs and respective composites preparation by doctor blade and screen-printing methods.

3.4 Production of adhesively bonded joints for functional applications

Screen-printing was used to produce adhesively bonded samples in different commercial substrates, namely, aluminium, and glass and carbon fibres reinforced polymer (GFRP and CFRP) composites. For adhesion tests, two stripes of each substrate of approximately 100 × 10 × 1 mm were bonded together with pristine resin and 3MWCNTs/ER composite using screen-printing to apply one layer in each stripe and then placed in contact by means of a commercial and plastic spring clamp (compression force of 20 N) with a bonding area of 10 × 10 mm (Figure 3.2). The bonded stripes samples were placed inside an oven to cure at 60 °C during 30 min before testing.

3.5 Samples Characterization

The characterization was carried out in samples produced by screen-printing for resin and respective composite samples. The morphological characterization was done using the scanning electron microscopy (SEM) with a Hitachi S-4800 system with 10 kV of accelerating voltage. Samples were analysed in surface and cross-section mode after being layered with conductive gold using a Polaron SC502 sputtering.

Fourier transformed infrared spectroscopy (FTIR) in the attenuated total reflectance (ATR) mode was evaluated with a Jasco FTIR-4100 instrument. Tests were carried out between 600 and 4000 cm^{-1} through 32 scans with a 4 cm^{-1} of resolution.

The measurements of the contact angle were complete using an optical system Dataphysics OCA 15EC Neurtek. Water drops of 2 μL were used on every sample. Measurements were taken at three different positions on the samples using the SCA20 software.

The uniaxial stress-strain mechanical properties of the pristine ERs and respective composites were evaluated with a universal test equipment Shimadzu AG-IS using a load cell of 500 N. The mechanical tests were evaluated at a rate of 5 mm/min to specimen break using rectangular specimens (according to ASTM D882 and ISO 527-3 for thin films) with an area of 5 × 20 mm^2 and a thickness (d) varying between 85 and 140 μm. Five tests were evaluated for each sample.

The electrical resistance was evaluated using the four-point probe method, which measures the sheet resistance (Rs) on the sample surface. The electrodes were applied with commercial silver ink to ensure good electrical contact. The van der Pauw method was chosen due to the thin nature of the samples where volumetric measurements would be less representative. This method allows accurate resistivity evaluation in thin films without the need for defined sample dimensions.

The resistivity (ρ) was evaluated as surface resistivity (sheet resistance, Rs), following the four-point probe method with a Keithley 2400 source meter with an applied voltage ranging from -10 V to +10 V. The resistivity was determined using equation 3.1:

$$\rho = R_S \times \frac{\pi}{\ln 2} \times t \tag{3.1}$$

where t is the film thickness.

The sensing performance was evaluated for the sample prepared by doctor blade and screen-printing (bulk adhesives) and for the bonded joints. Piezoresistive tests were performed using the mode denominated as 4-point bending (Figure 3.2A) in same Shimadzu equipment, with simultaneous electrical resistance measurements using a multimeter from Agilent with reference 34401A. The 4-point-bending cyclical tests were carried out for 0.1, 0.3, 0.5, 1, 3, and 5 mm of bending using 5 mm/min rate for 3MWCNTs/ER, 5MWCNTs/ER, or 10MWCNTs/ER composites, with a total area of 30×10 mm^2. The screen-printed composite sample was bonded (double-side tape from Tesa) to a polyethylene terephthalate (PET) flexible substrate with 1 mm of thickness as a support for bending tests.

The piezoresistive tests in bonded joints were performed in the 3MWCNTs/ER composites using glass fibre adherends as insulator substrate, as shown in Figure 3.2A. The piezoresistive sensitivity was then calculated using the gauge factor, GF, in Equation 3.2, determined through the 4-point bending test [30]:

$$GF = \frac{\Delta R/R_0}{\varepsilon} = \frac{\partial \rho/\rho_0}{\varepsilon} + 1 + 2\upsilon \quad (3.2)$$

where $\Delta R/R_0$ is the relative change in electrical resistance, ε is the strain, ρ is the electrical resistivity and υ is the Poisson's ratio of the samples. The term $1 + 2\upsilon$ accounts for the geometrical effect on resistance variation, but in nanocomposite systems, the electrical response is also influenced by changes in the conductive network structure. Therefore, while this equation provides a general estimation, the actual GF may differ from the purely geometrical assumptions due to strain-induced MWCNTs reorganization [31].

The mechanical strain during 4-point bending is given by Equation 3.3 [18, 31]:

$$\varepsilon = \frac{3dz}{5a^2} \quad (3.3)$$

where the sample thickness d is near 80 μm (piezoresistive sample and support), vertical displacement is z and a= 25 mm is the bending points distance as illustrated in Figure 3.2A.

The thermoresistive response was measured using a multimeter Agilent with reference 34401A digital synchronized with a Linkam THMSE 600 temperature oven. The measurements were performed in surface method in an area of 20×20 mm^2 for the 3MWCNTs/ER screen-printed composites, using a commercial silver ink from Agar Scientific (reference AGG3790) for the conductive contact electrodes figure 3.2. Tests were performed between 35 to 40 °C and between 60 to 90 °C at a rate of 20 °C/min to resemble human conditions and industrial applications, respectively. For the bonded joints, the 3MWCNTs/ER composite was also used with two rectangular aluminium adherends with a bond area of 20×20 mm^2. For bonded joint preparation, one side of each strip was screen-printed and then placed face-to-face and cured. Silver ink electrodes (Agar Scientific) were placed at the longitudinal ends of the bonding layer on both adherend surfaces, enabling volumetric measurement throughout the mechanical loading process. The curing process and contact with the multimeter were also carried out similarly to the piezoresistive sensors, as shown in Figure 3.2B.

The thermoresistive sensitivity (S) was calculated according to equation 3.4 [25]:

$$S = \frac{\Delta R/R_0}{\Delta T} \times 100 \quad (3.4)$$

where the temperature variation is ΔT (in °C).

Stress-strain tests up to failure were evaluated in the bonded structures using a universal mechanical equipment (Zwick Z005) using a 10 kN load cell at a strain rate of 1.3 mm/min. Adhesives piezoresistive sensitivity was evaluated under dynamic bending tests, while the thermal sensitivity was assessed by static thermoresistive tests (Figure 3.2), similar to previously described for bulk composites.

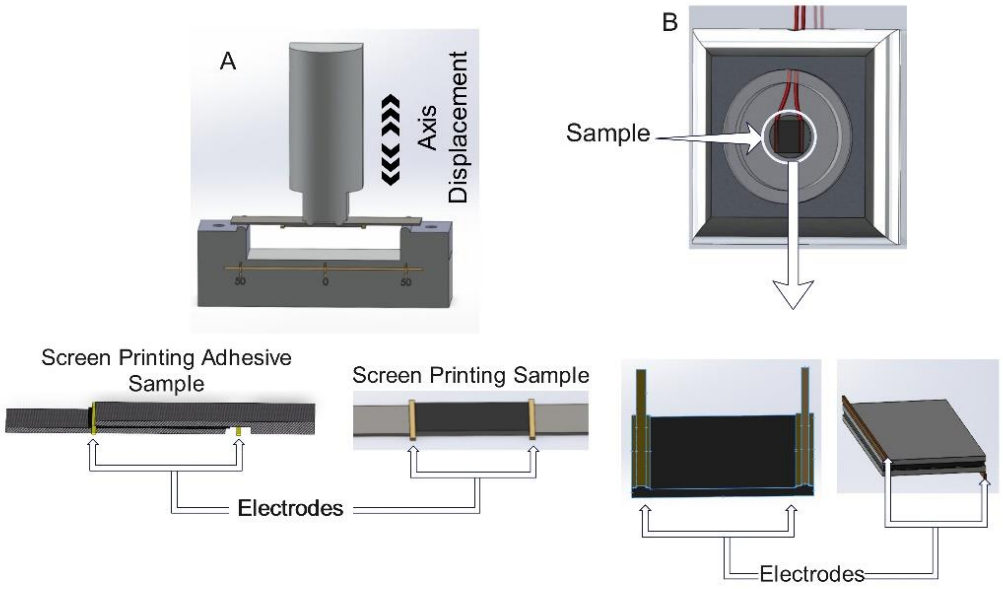


Figure 3.2 - Representation of the A) piezoresistive (0.1 to 5 mm of bending) and B) thermoresistive tests. The lower row shows the placement of the electrodes in the samples for the corresponding tests.

3.6 Results and Discussion

3.6.1 Morphology, chemical structure, and contact angle properties

The morphological structure of the screen-printed ERs and Composites reinforced with 3, 5, and 10 wt.% MWCNTs content is displayed in Figure 3.3, in cross-sectional mode. From the lower magnification images (Figure 3.3A for ERs; C, E, and G for composites), the thickness of each sample was determined, which varies from 150 ± 25 μm for ERs and for composites changes between 150 ± 20 μm, 130 ± 25 μm and 110 ± 30 μm for 3, 5, and 10 wt.% filler content samples, respectively. The use of solvents and fillers has a critical effect on the viscosity and rheology of the adhesive solution and consequently on the thickness of the two-layer screen-printed materials. A compact structure of the ERs was obtained in all cases, although some cracks appeared in the composites due to the higher viscosity or occasional voids

of resin in films or between printed layers and possibly due to acetone evaporation during processing, since rapid solvents removal can induce residual stresses that affect the microstructure [32]. In addition, the presence of pores in the cross-sectional SEM images can also be attributed to rapid acetone removal inducing microvoid formation, a common effect in solvent-based nanocomposite processing.

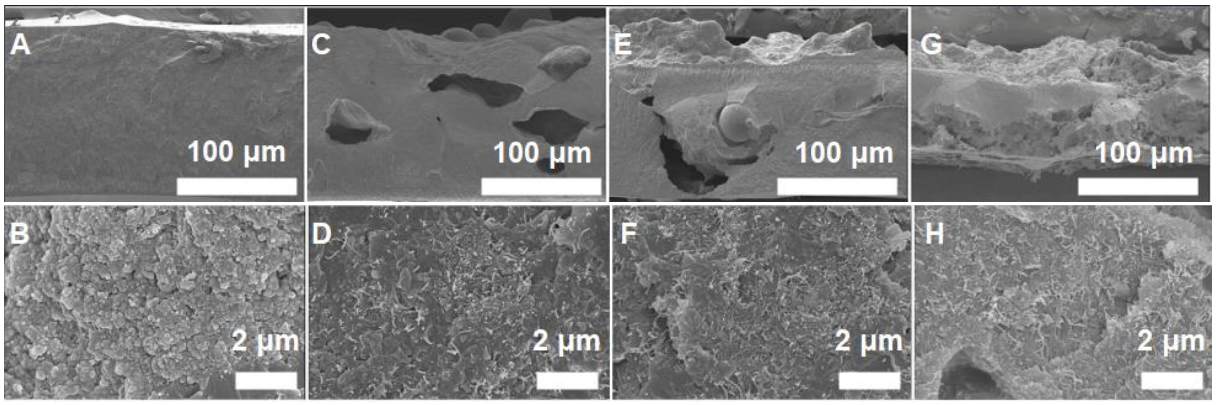


Figure 3.3 - Cross section (above) and surface (below) SEM images of the screen-printed ERs (A and B) and composites with 3 wt.% (C and D), 5 wt.% (E and F), and 10 wt.% (G and H) MWCNTs content.

Regarding the surface of the samples (Figure 3.3 B, D, F, and H), can be observed a flawless surface on the ERs and a homogeneous and efficient distribution of the MWCNTs within the matrix in the corresponding composites. The surface of the samples shows higher filler contents with increasing MWCNTs in the composites, but no large MWCNTs agglomerates are found, even for the larger filler concentrations. Literature reports that ERs composites prepared using solution methods achieve homogeneous dispersion, as observed in Figure 3.3, exhibiting superior filler dispersion than other methods. [33].

The FTIR vibrational spectra (Figure 3.4A) of ERs and composites show the typical absorption bands of the resin. The bands stretching of benzene rings are related to C=C at 1506 and 1606 cm^{-1}, and the ones at 820 and 1025 cm^{-1} are related to Ar–O–C bonds and ether group [34]. A pronounced band at about 3150-3400 cm^{-1} is due the stretching vibration of O–H bonds. The observed peaks at 2848 and 2915 cm^{-1} are related to the stretching vibration of C-H, respectively, in the CH_2 and CH_3 characteristic bands [34]. It can be noticed that the typical bands of the matrix are reduced to different composites, mainly for the highest filled composite.

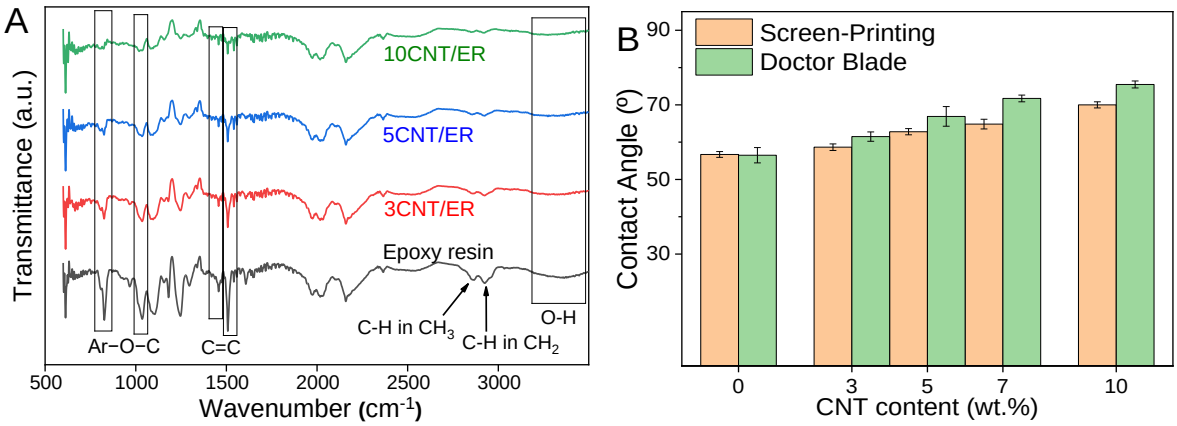


Figure 3.4 - Representative FTIR spectra A) and contact angle B) for ERs matrix and composites with different MWCNTs contents.

The wettability of the samples processed by screen-printing and doctor blade (Figure 3.4B) is around 56° for ERs and increases to 70° and 75° for the composites at 10 wt.% filler content prepared by doctor blade and screen-printing, respectively, showing therefore hydrophilic behaviour [35]. The addition of MWCNTs reduces the wettability mainly by increasing the rugosity of the composites. Further, the samples prepared by doctor blade show lower wettability compared to the screen-printed samples, mainly for the largest filled composites, which may be also attributed to differences in samples surface morphology.

3.7 Mechanical and electrical measurements

The uniaxial stress-strain properties of the ERs and composites were characterized and their typical behaviour is shown in Figures 3.5A and B for both prepared materials, presenting similar behaviour with literature [33]. The fracture strain and stress for the ERs prepared by doctor blade and screen-printing are close to 2% and 4%, and approximately 30 and 25 MPa, respectively. Slightly higher stress and strain at facture are obtained for the samples processed by doctor blade. The fracture strain increases to nearly 5% for the composites, except for the largest filled one, which remains similar to the one of the pristine ERs. The stress at fracture tends to decrease with increasing filler content in the composites, being nearly 8 MPa for the 10MWCNTs/ER sample. While there is a slight reduction in mechanical properties due to MWCNTs inclusion, the composites retain sufficient strength for structural applications. This balance between mechanical integrity and electrical functionality is critical, as the incorporation of MWCNTs not only affects stiffness and strength but also improves electrical conductivity and sensing performance. The following section explores how these materials leverage their electrical properties for real-time mechanical and thermal sensing. This method enables customization and the creation of innovative geometries during the scale-up process, as observed with related resins and techniques [36].

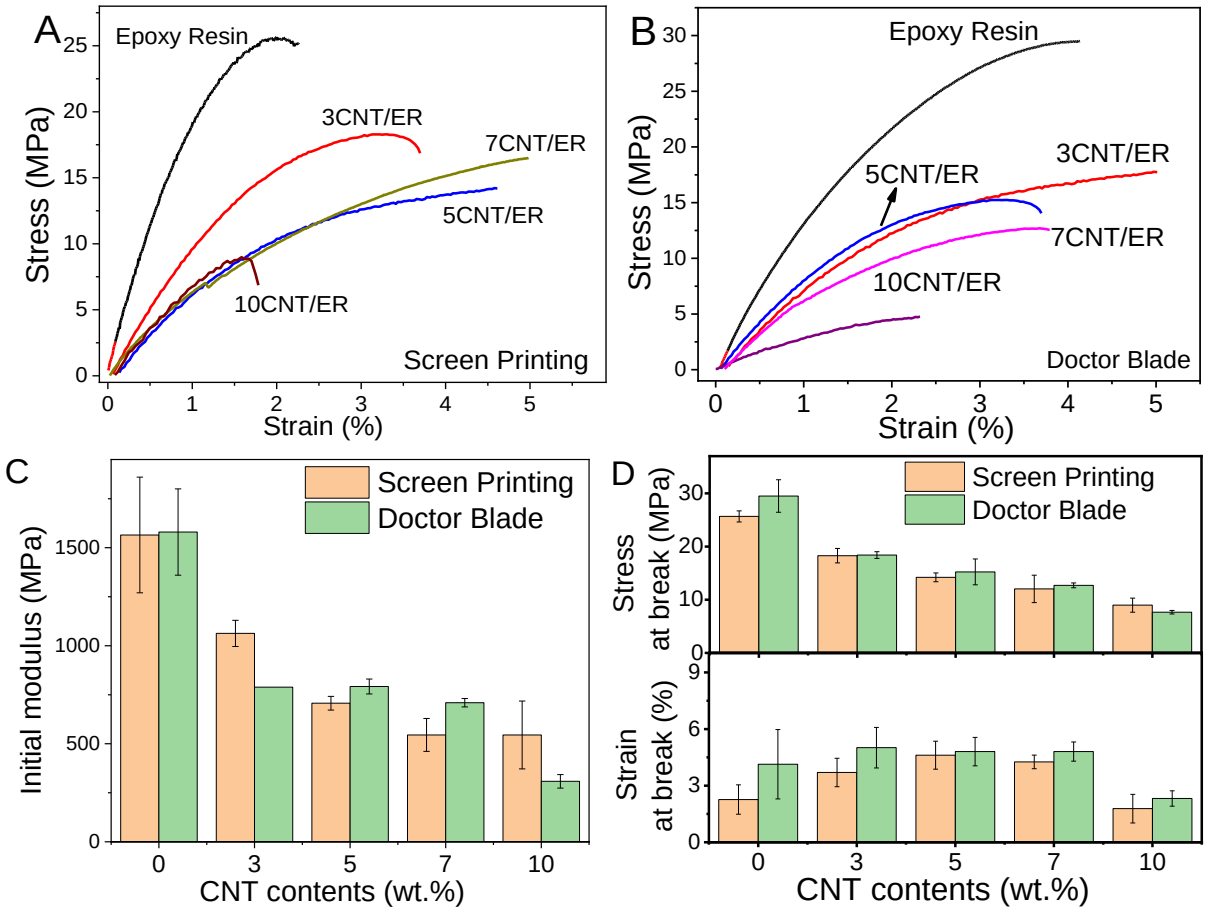


Figure 3.5 - Representative uniaxial stress-strain curves for screen-printed A) and doctor blade B) samples. C) Performance of initial modulus calculated up to 1% for all samples and D) stress and strain at fracture.

The initial modulus, and stress-strain at fracture are shown in Figures 3.5C and D, where the general trend with increasing MWCNTs content is similar for the samples prepared with both processing methods. The resin shows an initial modulus around 1.5 GPa for both samples, and as the filler content in the composites increases, the initial modulus decreases to about 0.6 and 0.3 GPa for the samples prepared by screen-printing and doctor blade methods, respectively. The stress at fracture decreases with increasing filler content in the composites, as shown in Figure 3.5D, exhibiting similar behaviour to the initial modulus, decreasing from 25 and 30 MPa, for doctor blade and screen-printing processing, respectively, to less than 10 MPa for both composites at 10 wt.% MWCNTs content. This reduction in mechanical properties is attributed to MWCNTs agglomeration and incomplete stress transfer between nanofillers and to plasticizing effects due to residual acetone used during processing. Acetone can act as a plasticizer and slightly reduce the stiffness and strength of the ERs matrix [37]. Previous studies have reported similar effects of solvent-induced plasticization in polymer-based composites [38]. The strain at fracture of the materials changes from about 2% to 5%, increasing from pure ERs to composites, except

for the largest filled samples (Figure 3.5D). Despite their stiffness, the resins and composites exhibit enough flexibility for applications in the sensing field, as reported [33].

The electrical resistance of the samples measured in surface was characterized in 4-point mode, as shown in Figure 3.6. The matrix is an insulator material, showing a sheet resistance near Rs ≈ 9.2×10^{8} Ω/sq, which decreases abruptly by 3 and 5 wt.% MWCNTs (about 4 and 5 orders of magnitude), with a tendency to stabilize at larger filler contents, with a low electrical resistivity value of nearly 100 Ω/sq. This percolative behaviour is typical for ERs composites using nanocarbon reinforcing fillers [39, 40]. The electrical percolation threshold for composites is estimated to be less than 3 wt.%, based on the sharp drop in sheet resistance observed in Figure 3.6. While this behaviour is consistent with literature reports showing that the percolation threshold can range from 0.1 to 15 wt.% depending on the resin, filler type, or processing conditions [39, 41], a more accurate experimental determination would require a finer range of filler concentrations and additional conductivity measurements. Typically, the rigid thermosetting materials present lower threshold than soft thermoplastic composites [41].

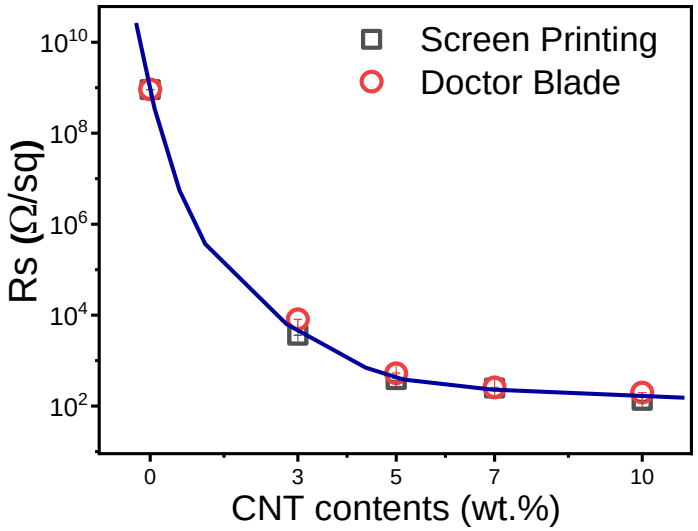
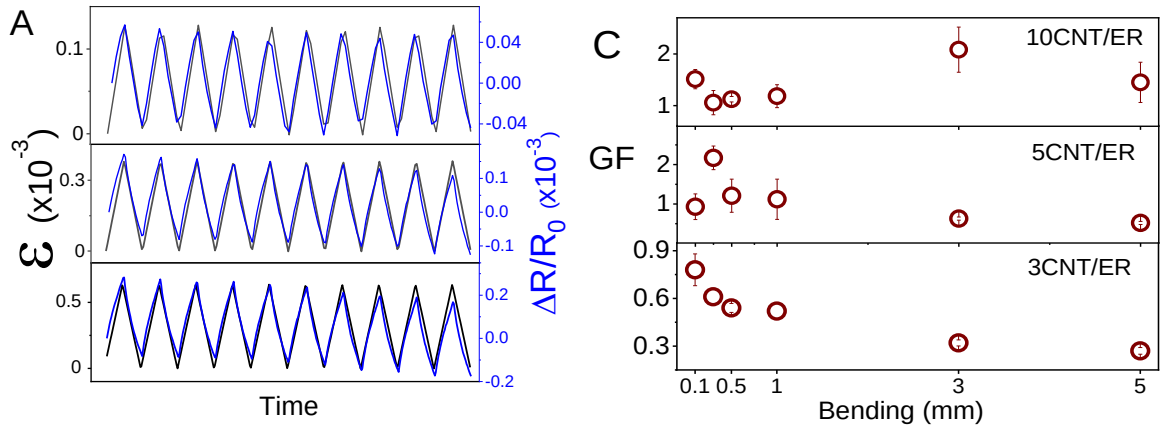


Figure 3.6 - Electrical sheet resistance as a function of MWCNTs filler concentration for samples prepared by doctor blade and screen-printing methods. The line is for guiding the eyes.

3.8 Functional composites: piezoresistive and thermoresistive sensing

The piezoresistive behaviour of the samples has been evaluated over 10 bending cycles (Figures 3.7A and B) and the corresponding sensitivity, quantified by GF, is presented in Figure 3.7C. The piezoresistive response was evaluated as a function of bending strain (0.1, 0.3, 0.5, 1, 3 and 5 mm) and filler content (3, 5 and 10 wt.% MWCNTs). Piezoresistive tests were carried out for composites near and after the percolation threshold to assess the variation in sensitivity as a function of the number of conductive

network paths created by the MWCNTs within the composite. Figure 3.7A and B show the data for the 3MWCNTs/ER sample, being also representative for the 5 and 10 wt.% composite samples. For all samples, the electrical resistance response to mechanical stimulus is governed by strain-induced changes in the percolative MWCNTs network. Under bending, the MWCNTs contacts are modified by tunnelling resistance and microstructural rearrangements, leading to a measurable increase in resistance. Upon unloading, the network partially recovers, restoring the initial resistance value. Similarly, thermoresistance effect is attributed to electron scattering and tunnelling effects between the MWCNTs, where increasing temperature causes an increase in electron mobility and a corresponding decrease in resistance [25]. These mechanisms ensure that the developed MWCNTS-ERs composites exhibit reliable and reversible resistive behaviour, making them suitable for real-time sensing applications. As observed in the measurements in Figures 3.7A and B, the linearity of the resistance change with applied stimuli is more consistent for smaller bending (Figure 3.7A) than for larger bending (Figure 3.7B). Larger bending deformation led to deviations from linear behaviour, mainly for unloading cycles. This is attributed to increased variation in the MWCNTs conductive network, leading to larger hysteresis components both in the mechanical and the electrical responses [42]. Similar to the linearity of the piezoresistive response, stability over cycling also decreases for larger bending, showing a slight decrease of the minimum and maximum resistance values with increasing of cycles.



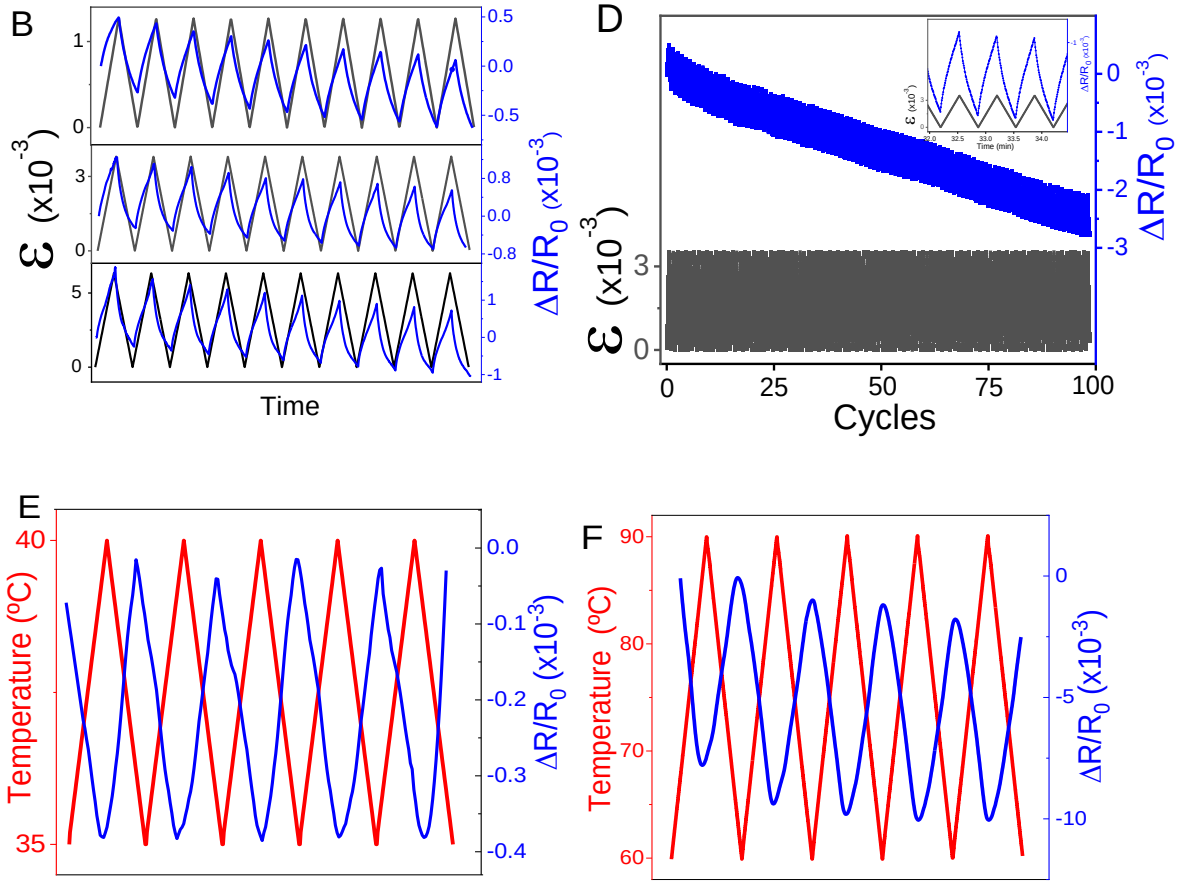


Figure 3.7 - Piezoresistive response of the ERs composites (3MWCNTs/ER) under 10 cyclic 4-point bending tests for small bending (0.1, 0.3, and 0.5 mm) A) and larger bending deformations of 1, 3, and 5 mm in B). C) Gauge Factor of the 3MWCNTs/ER, 5MWCNTs/ER, and 10 MWCNTs/ER composites as a function of bending deformation. D) Piezoresistive response of the 3MWCNTs/ER composite under cyclic bending up to a maximum bending of 1 mm for 100 cycles. Thermoresistive response of the screen-printed 3MWCNTs/ER composites to temperature ranges close to the human body (35 to 40 °C) E) and for industrial applications (60 to 90 °C) in F).

The sensitivity of the composites was determined by the GF (equations 3.2 and 3.3) for small and large bending and for all composites for different MWCNTs content: 3, 5 and 10 wt.%. Greater resistance variations observed during the bending tests indicate a higher sensitivity of the composite materials. The piezoresistive sensitivity of the different Composites as a function of the bending tests (Figure 3.7C) shows that it decreases with increasing applied bending in lowest filled composites, being stable for 5 and 10 wt.% MWCNTs composites. Variations in the GF< 0.8 for the 3MWCNTs/ER sample to 1 <GF< 2 for other composites demonstrate that the ERs composites present a slightly larger sensitivity for specimens above the percolation threshold. It is also relevant that their performance for loading and unloading cycles is

similar. The piezoresistive sensitivity of typical thermosetting-based sensing materials is in the range in 0.5 <GF< 3 [41, 43], although it can reach values up to 15-20 near the percolation threshold under uniaxial strain [41, 43]. Under flexural stress, the electrical resistivity variations depend on both compressive and stress forces, depending on the curvature of the samples under bending [44].

The stable cyclability of the piezoresistive response upon repeated cyclic bending up to 100 cycles at 1 mm maximum bending was evaluated for the 3MWCNTs/ER composite (Figure 3.7D) showing a decrease at the maximum and minimum values of the electrical resistance changes, although their piezoresistive sensitivity is equivalent along the 100 cycles, as observed in the inset for the intermediate test cycles, showing a stable sensing stability. In addition, the observed decreasing trend in resistance variation is attributed to changes in the electrical network and changes in tunnelling resistance due to rearrangements and possible degradation of electrode/sample contact interfaces over prolonged cycling [44].

The multifunctionality of the composites is further complemented by the thermoresistive response, evaluated for the screen-printed 3MWCNTs/ER composite between 35 and 40 °C and between 60 and 90 °C for human health and industrial applications, respectively (Figures 3.7E and F). The thermoresistive response, relative resistance variation with temperature, shows a linear variation with a negative temperature correlation, which has been proposed to be dominated by tunnelling effect within the conductive network [45], though it is not a well-established mechanism[25]. The composite presents thermal sensitivities close to $S_{35\text{-}40} \approx 0.01$ (%.°C^{-1}) and $S_{60\text{-}90} \approx 0.03$ (%.°C^{-1}) for the two different temperature variation ranges. The thermal response is within the typical values for MWCNTs films [25], which crucially depends on the reinforcement filler type and content [45].

In this way, the developed materials can be applied in industry as bonding materials with piezoresistive and thermoresistive characteristics.

3.9 Adhesion and sensing properties

The main goal of the developed ERs is their use as mechanical adhesives on material joints, replacing the traditional use of solder or screws, with self-sensing capabilities. Thus, the ERs and the 3MWCNTs/ER composites were evaluated as adhesive under stress-strain uniaxial shear lap tests (Figure 3.8A) using aluminium and carbon fibre reinforced polymer (CFRP) adherends. A thin layer of resin or 3MWCNTs/ER composite was printed by screen-printing on each adherent material to bond both stripes and later cured, as shown in Figure 3.8A. Figure 3.8B shows that the shear strength of the CFRP bonded materials is larger than that of the aluminium joints and that the pure ERs presents larger strength than the composites. Comparing both materials, the functional 3MWCNTs/ER composite presents a slightly lower

shear strength (16 MPa for CFRP and 6 MPa for aluminium compared to 22 and 16 MPa for ERs, respectively, in all samples with an active square area of 10×10 cm^2), but the bonding value is suitable for adhesive applications. This reduction is attributed to the presence of MWCNTs agglomerates, which act as stress concentrators, and the reduced continuity of the polymer matrix. In addition, variations in adhesive thickness affect the shear strength, as increased thickness can lead to changes in the stress distribution at the bonded interface. The difference between aluminium and carbon fibre is consistent with the supplier data, where CFRP presents the highest shear strength. Similar reports show that CFRP joints with ERs and composites with MWCNTs exhibit around 30 MPa [46], or up to 14 MPa in the case of aerospace substrates [47]. Shear strength also increases with area and thickness of the bonded joints [48].

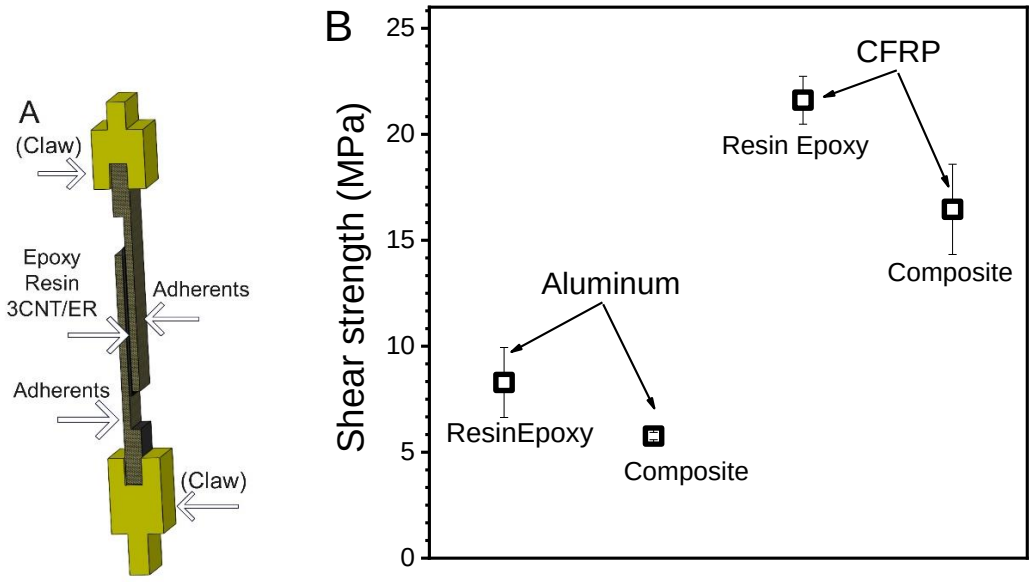
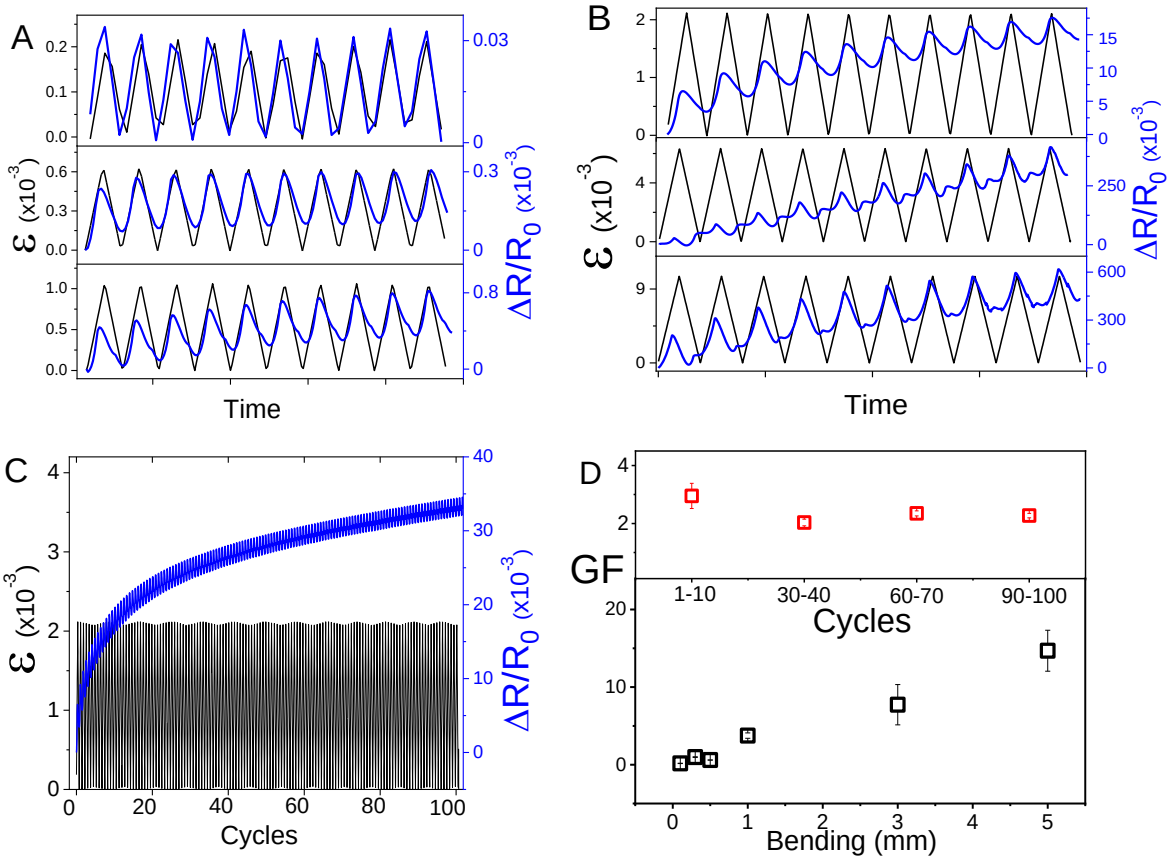


Figure 3.8 - Illustration of the uniaxial shear lap tests. B) Shear strength of bonded carbon fibre and aluminum adhesive joints for ERs and 3MWCNTs/ER composite.

The piezoresistive behaviour of the 3MWCNTs/ER composite as an adhesive self-sensing functional material was evaluated under 4-point bending solicitation from 0.1 to 5 mm for 10 loading-unloading bending cycles and the results are presented in Figure 3.9A and B for 10 cycles and in Figure 3.9C for over 100 cycles to evaluate the endurance stability. The cyclic behaviour of the adhesive film is different to that of the printed film tested on PET substrates (Figure 3.7), as the resistance increases over cycling, mainly for the initial cycles and larger bending stimuli. Nevertheless, the relative change in resistance follows the applied stimuli from small to large bending, showing excellent sensing properties. In addition, the resistance of the samples tends to increase with increasing number of cycles, which is more obvious

for larger bending deformations. However, the variation in resistance is similar for all cycles of each test, leading to a constant piezoresistive response over cycling. The rigid structure with bonded adherents with the sensing resin composite demonstrates some difficulty in recovering from applied bending, and the electrical resistance does not fully recover after 0.5 mm of bending, as shown from Figure 3.9A to B. The piezoresistive sensitivity of the bonded structure increases with strain, showing a non-constant GF< 1 for 0.1, 0.3, and 0.5 mm of bending to GF ≈ 4 for 1 mm, GF ≈ 8 for 3 mm, and GF ≈ 15 for 5 mm of bending. This behaviour suggests a strain-dependent response, influenced by changes in the embedded MWCNTs percolation network. The differences observed with respect to the films (Figure 3.7), in particular for the larger bending deformations, are related to the larger thickness of the bonded structure [49]. In addition, the sandwiched sensor film between adherents under bending tests are under compressive and tensile stress, leading to the curvature of the structure [44], increasing the resistance variations under bending. The geometrical factor predominantly influences the piezoresistive response at smaller bending, contrary to larger bending where the intrinsic resistivity changes are dominant, exhibiting larger piezoresistive sensitivity [44]. The cycling stability analysis (Figure 3.9C) reveals that resistance changes stabilize after approximately 20-40 cycles, indicating a consistent response over repeated cycling, and remaining stable throughout the testing process. The piezoresistivity response of the adhesive structure, tested over 100 cycles, shows a GF ≈ 2 (at 1 mm bending) across all cycles.



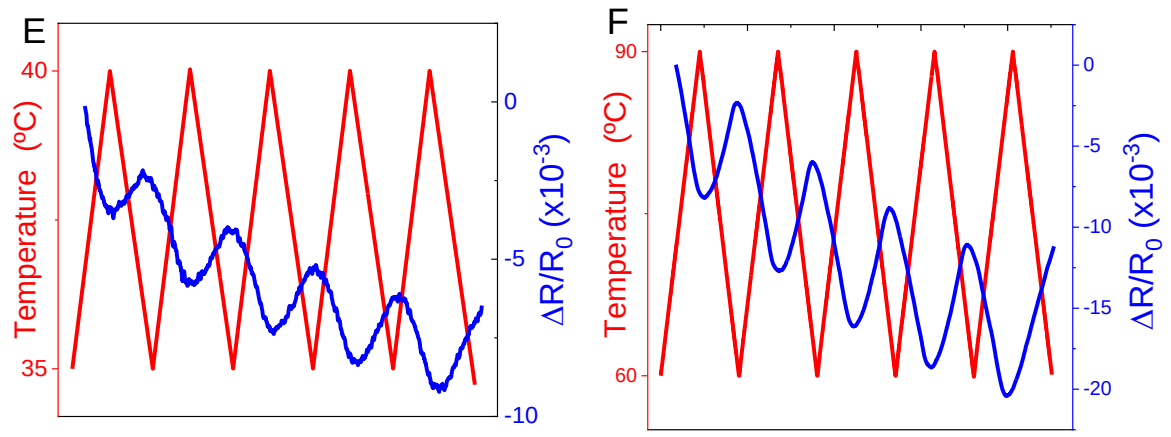


Figure 3.9 - Piezoresistive response of screen-printed bonded adherent systems with 3MWCNTs/ER for low displacement 0.1, 0.3 and 0.5 mm A) and for 1, 3 and 5 mm B). Piezoresistive response at 1 mm maximum bending displacement C) and Piezoresistive gauge factors D). Thermoresistive response of screen-printed 3MWCNTs/ER composite as bonding for aluminum stripes between 35 to 40 °C E) and 60 to 90 °C F).

The thermoresistive behaviour of the aluminium joints with 3MWCNTs/ER adhesive composites was evaluated for 5 cycles of temperature variation between 35 and 40 °C and between 60 to 90 °C, as shown in Figure 3.9. Aluminium adherents work as electrodes and low-filled composites were selected as adhesives. The device exhibits a negative temperature correlation where the behaviour of the electrical resistance linearly decreases with increasing temperature and increases with decreasing temperature, as previously observed in the film composites. The linear correlation between resistance and temperature changes is excellent but, contrary to film tests, the resistance shows a decreasing value with increasing number of cycles. The distinct thermal conductivity of the aluminium and composite can cause the resistance not to recover to the initial point at the temperature rate, especially for small temperature changes. The bonded joint exhibits a thermoresistive sensitivity of $S_{35\text{-}40} \approx 0.05$ (%.°C^{-1}) and $S_{60\text{-}90} \approx 0.04$ (%.°C^{-1}) which is similar to the bulk adhesive composite in terms of behaviour and sensitivity. This performance reveals that filled ERs samples can act mechanically as an adhesive with both self-sensing piezoresistive and thermoresistive properties, which is suitable for the implementation of the Industry 4.0 paradigm of real-time monitoring of structural devices.

3.10 Self-sensing piezoresistive adhesive for cantilever applications

The sensing properties of the 3MWCNTs/ER composite for mechanical bending and temperature variation, together with its adhesive properties, make this material suitable for the implementation of bonded joints with real-time sensing monitoring in aerospace and automotive industries, among others.

A prototype was therefore developed employing glass fibre (an insulator widely used in industry) adherends with an area of 100 × 15 mm2. The structure was bonded using a 3MWCNTs/ER composite screen-printed on each of the layers to be bonded. The electrodes were placed at each extreme of the bonded structure- as shown in Figure 3.10A. The structure was cured at 60 ˚C for 30 min using a clamp with 20 N/m^2 of force. The piezoresistive response was evaluated in the cantilever mode in function of displacement (in zz axis) to differentiate from the 4-point bending mode previously presented, at a rate of 10 mm/min.

The piezoresistive tests for glass fibre as adherents bonded using the piezoresistive 3MWCNTs/ER composite show similar behaviour to the ones presented by the shear lap samples (Figure 3.8). Their good linearity for loading-unloading cycles is superior for low bending than for larger stimulus- slightly decreasing for larger ones, due to mechanical hysteresis of the cantilever (Figure 3.10B). Thus, it is shown that the displacement of the cantilever can be detected in real-time. The cycles stabilization due to the slight increase of maximum and minimum values of the resistance starts to occur between 20 and 40 cycles, tending to standardize after a larger number of cycles (Figure 3.10C). Indeed, similar piezoresistive values are observed with similar relative resistance changes per cycle after these 20-40 cycles. The functional prototype using a ERs composite with sensing properties shows its suitability for applications.

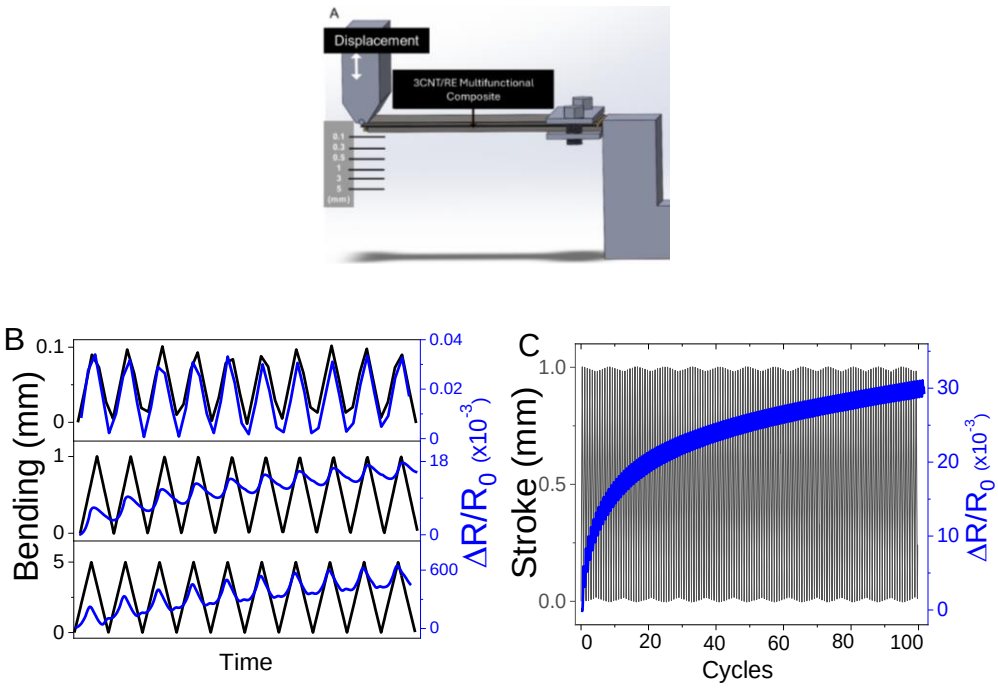


Figure 3.10 - A) Schematic of the structure developed for monitoring bending in cantilever mode using a 3MWCNTs/ER composite to bond together two glass fibres as adherents. Piezoresistive response for bending of 0.1, 0.3 and 0.5 mm B), and cycling stability for 100 cycles at 1 mm of bending C).

The results of this study demonstrate the feasibility of MWCNTs-reinforced ERs adhesives with integrated sensing capabilities. Research and focus on optimizing MWCNTs dispersion techniques to further improve mechanical properties, as well as exploring alternative solvents or solvent-free processing methods to eliminate potential plasticization effects can enlarge the range of applications for these functional materials. The development of hybrid MWCNTs-G systems could also improve sensitivity and durability for long-term sensing applications. Further investigation of alternative adhesive joints designs, and electrode configurations could improve measurement accuracy and enable volumetric resistance assessments. Finally, real-world fatigue and durability testing under operational conditions will be critical to validate the long-term performance of these self-sensing adhesives.

3.11 Conclusions

Thermosetting materials are extensively applied because of their exceptional mechanical and adhesive properties, turning them remarkably appropriated for bonded structures. Rigid ERs, enhanced with MWCNTs, can be designed to meet the functional requirements of structural health monitoring (SHM) applications.

To ensure effective processing, acetone was employed as a solvent to control resin/hardener viscosity, while conductive MWCNTs were incorporated as reinforcement fillers. This methodology enabled the fabrication of composites using doctor blade and screen-printing techniques. As result, composites with 1, 3, 5, 7, and 10 wt.% MWCNTs present homogeneous MWCNTs dispersion and low-size agglomerates, with electrical resistivity approximately 100 Ω/sq for composites having 10 wt.% MWCNTs, processed by both techniques. Piezoresistive response was obtained under cyclic bending for composites with 3, 5, and 10 wt.% MWCNTs, being suitable for SHM applications. The piezoresistive sensitivity for bending deformations up to 5 mm was characterized by a GF< 2, within the geometrical piezoresistive response of the materials. A notable decrease in initial mechanical modulus, strain, and stress at break was observed with increasing MWCNTs content, particularly at higher filler concentrations, an effect attributed to challenges in MWCNTs dispersion and interfacial stress transfer affecting load distribution within the matrix. Despite this decrease, the mechanical performance remains within acceptable limits for adhesive applications, especially considering the added sensing functionalities. Bonded structures with aluminium and CFRP strips, using both ERs and 3MWCNTs/ER composites, achieved shear lap strengths exceeding 20 MPa for CFRP assemblies. Composites combining strong adhesion with piezoresistive sensitivity over a bending range of 0.1 to 5 mm, achieved a gauge factor close to 15 for bonded structure under larger strains. This piezoresistive sensitivity remained constant over endurance cycles after initial stabilization.

Additionally, the 3MWCNTs/ER composite shows thermoresistive capabilities across a wide range of temperatures, with a sensitivity of $S_{60\text{-}90} \approx 0.05\ \%.°C^{-1}$. As a proof of concept, a bonded cantilever structure was developed using CFRP strips to demonstrate the composite's sensing properties under deformation forces, highlighting the potential of the developed material as smart sensing adhesives for structural monitoring in aerospace, automotive and related areas.

3.12 References

[1] S. Ma, D. C. Webster, Progress in Polymer Science 2018, 76, 65.

[2] Y. Zaokari, A. Persaud, A. Ibrahim, Engineered Regeneration 2020, 1, 51.

[3] Y. Liu, Z. Yu, B. Wang, P. Li, J. Zhu, S. Ma, Green Chemistry 2022, 24, 5691; Y. Yang, Y. Xu, Y. Ji, Y. Wei, Progress in Materials Science 2021, 120, 100710; C. Tosto, L. Saitta, A. Barouni, F. Sarasini, J. Tirilló, I. Bavasso, G. Ziegmann, Polymer Composites 2024, 45, 15649.

[4] A. Kandelbauer, G. Tondi, O. C. Zaske, S. H. Goodman, in Handbook of Thermoset Plastics (Fourth Edition), (Ed: H. Dodiuk), William Andrew Publishing, Boston 2022, 97.

[5] S. G. Prolongo, G. del Rosario, A. Ureña, International Journal of Adhesion and Adhesives 2006, 26, 125; M. M. Y. Zaghloul, M. M. Y. Zaghloul, M. Fuseini, Polymers for Advanced Technologies 2023, 34, 3438.

[6] A. Shundo, S. Yamamoto, K. Tanaka, JACS Au 2022, 2, 1522.

[7] F.-L. Jin, X. Li, S.-J. Park, Journal of Industrial and Engineering Chemistry 2015, 29, 1.

[8] P. Jojibabu, Y. X. Zhang, B. G. Prusty, International Journal of Adhesion and Adhesives 2020, 96, 102454.

[9] C. L. Yip, S. Sugiman, D. Chin, H. Ahmad, Case Studies in Construction Materials 2024, 20, e02790; G. S. Baş, E. Sancaktar, ChemEngineering 2020, 4, 38; G. C. G. Serra, J. A. M. Ferreira, P. N. B. Reis, in Processes, Vol. 11, 2023; R. Ciardiello, Materials 2021, 14, 6351.

[10] M. Peerzada, S. Abbasi, K. T. Lau, N. Hameed, Industrial & Engineering Chemistry Research 2020, 59, 6375.

[11] X.-F. Liu, X. Luo, B.-W. Liu, H.-Y. Zhong, D.-M. Guo, R. Yang, L. Chen, Y.-Z. Wang, ACS Applied Polymer Materials 2019, 1, 2291; B. Du, X. Zhou, Q. Li, J. Liu, Y. Liu, X. Zeng, X. Cheng, H. Hu, ACS Omega 2023, 8, 39984; Y. Wang, K. Wang, Z. Ma, T. Meng, R. Cao, N. Jiang, Polymer Composites 2024, 45, 11635.

[12] L. Ravindran, S. M. S., A. Kumar S., S. Thomas, Polymer Composites 2022, 43, 8602.

[13] C. Yun, F. Chu, B. Cui, X. Wang, G. Liu, J. Sun, Materials Letters 2020, 266, 127461.

[14] P. Jojibabu, M. Jagannatham, P. Haridoss, G. D. Janaki Ram, A. P. Desfhpande, S. R. Bakshi, Composites Part A: Applied Science and Manufacturing 2016, 82, 53.

[15] C. M. C. Pereira, P. Nóvoa, M. Martins, S. Forero, F. Hepp, L. Pambaguian, Composite Structures 2010, 92, 2252.

[16] H. Chi, G. Zhang, N. Wang, Y. Wang, T. Li, F. Wang, C. Ye, Nanoscale Advances 2022, 4, 1151.

[17] X. Wang, J. Wang, S. Biswas, H. Kim, I. Nam, in Sensors, Vol. 20, 2020; X. Xin, M. Liang, Z. Yao, L. Su, J. Zhang, P. Li, C. Sun, H. Jiang, Construction and Building Materials 2020, 257, 119404.

[18] P. Costa, J. Silva, A. Ansón-Casaos, M. T. Martinez, M. J. Abad, J. Viana, S. Lanceros-Mendez, Composites Part B: Engineering 2014, 61, 136.

[19] P. Zheng, H. Zhao, J. Li, Q. Liu, H. Ai, R. Yang, W. Xing, Journal of Safety Science and Resilience 2024, 5, 179; T. Khan, M. A. Ali, M. S. Irfan, K. A. Khan, K. Liao, R. Umer, Polymer Composites 2022, 43, 2924.

[20] L. Luo, F. Zhang, J. Leng, Research 2022, 2022.

[21] J. S. del Río, Á. Ridruejo, V. Martínez, J. L. Jiménez, C. Ramos, J. J. Vilatela, C. D. González, Sensors and Actuators A: Physical 2023, 364, 114852.

[22] A. K. Upadhyay, M. S. Goyat, A. Kumar, Journal of Materials Science 2022, 57, 13202.

[23] S. Hassani, M. Mousavi, A. H. Gandomi, Sensors 2022, 22, 153.

[24] S. Nauman, Eng 2021, 2, 197; M. S. Irfan, T. Khan, T. Hussain, K. Liao, R. Umer, Composites Part A: Applied Science and Manufacturing 2021, 141, 106236.

[25] F. Avilés, Advanced Materials Interfaces 2023, 10, 2300218.

[26] D. Yuan, H. Guo, K. Ke, I. Manas-Zloczower, Composites Part A: Applied Science and Manufacturing 2020, 132, 105837.

[27] W.-B. Zhu, Y.-Y. Wang, T. Fan, Y. Zhu, Z.-H. Tang, P. Huang, Y.-Q. Li, S.-Y. Fu, Langmuir 2024, 40, 8170; D.-Y. Wang, Z.-H. Tang, P. Huang, Y.-Q. Li, S.-Y. Fu, Carbon 2023, 201, 910; Z.-H. Tang, Y.-Q. Li, P. Huang, H. Wang, N. Hu, S.-Y. Fu, Composites Science and Technology 2021, 208, 108761; R. Lima, P. Costa, J. Nunes-Pereira, A. P. Silva, C. R. Tubio, S. Lanceros-Mendez, Composites Part B: Engineering 2025, 293, 112130.

[28] T. Rodrigues-Marinho, N. Perinka, P. Costa, S. Lanceros-Mendez, Materials Today Sustainability 2023, 21, 100292; M. Franco, A. Motealleh, C. M. Costa, N. Perinka, C. Ribeiro, C. R. Tubio, S. A. C. Carabineiro, P. Costa, S. Lanceros-Méndez, ACS Applied Polymer Materials 2023, 5, 7144.

[29] C. Peng, H. Wu, X. Jiang, IEEE Nanotechnology Magazine 2023, 17, 4.

[30] J. N. Pereira, P. Vieira, A. Ferreira, A. J. Paleo, J. G. Rocha, S. Lanceros-Méndez, Journal of Polymer Research 2012, 19, 9815.

[31] L. Arboleda, A. Ares, M. J. Abad, A. Ferreira, P. Costa, S. Lanceros-Mendez, Journal of Polymer Research 2013, 20, 326.

[32] J. Li, M. H. P. de Heer Kloots, G. van Ewijk, D. J. van Dijken, W. M. de Vos, J. van der Gucht, Langmuir 2024, 40, 2531.

[33] A. S. Wajid, H. S. T. Ahmed, S. Das, F. Irin, A. F. Jankowski, M. J. Green, Macromolecular Materials and Engineering 2013, 298, 339.

[34] E. Abdi, A. Khabaz-Aghdam, H. Hasan-nezhad, B. Behjat, E. A. S. Marques, Y. Yang, L. F. M. da Silva, Journal of Composite Materials 2022, 56, 2665.

[35] A. Atmakuri, A. Palevicius, A. Vilkauskas, G. Janusas, Polymers 2022, 14, 2612; M. Sabu, Y. J. V. Ruban, M. S. Ginil, Materials Today: Proceedings 2021, 41, 549.

[36] Q. Lin, F. Zhang, X. Xu, H. Yang, Q. Mao, D. Xian, K. Yao, Q. Meng, Nanomaterials 2023, 13, 2630.

[37] C. M. Becker, A. D. Gabbardo, F. Wypych, S. C. Amico, Composites Part A: Applied Science and Manufacturing 2011, 42, 196.

[38] M. R. Loos, L. A. F. Coelho, S. H. Pezzin, S. C. Amico, Polímeros 2008, 18, 76; F. U. Buehler, J. C. Seferis, Composites Part A: Applied Science and Manufacturing 2000, 31, 741.

[39] D. H. Andreghetto, G. d. C. Fuzari, Polymer Bulletin 2020, 77, 3725.

[40] K. A. Imran, K. N. Shivakumar, Journal of Composite Materials 2019, 53, 93.

[41] R. K. Rao, S. Gautham, S. Sasmal, Polymer Reviews, 1.

[42] S. Stassi, V. Cauda, G. Canavese, C. F. Pirri, Sensors 2014, 14, 5296.

[43] A. Sanli, C. Müller, O. Kanoun, C. Elibol, M. F. X. Wagner, Composites Science and Technology 2016, 122, 18.

[44] G. Spinelli, P. Lamberti, V. Tucci, L. Vertuccio, L. Guadagno, Composites Part B: Engineering 2018, 145, 90.

[45] H. Dai, E. T. Thostenson, T. Schumacher, Composites Part B: Engineering 2021, 222, 109068.

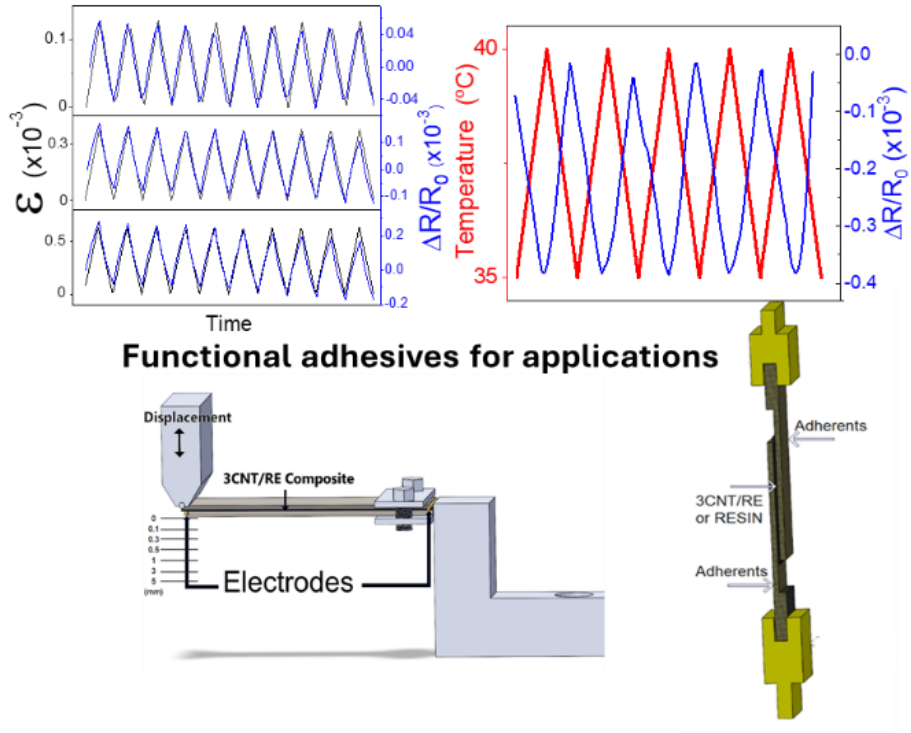
[46] V. H. Londhe, N. D. Misal, International Journal of Scientific Research and Management (IJSRM) 2015, 3, 3769.

[47] R. B, S. Chinnathambi, N. E, H. R, Journal of Polymer & Composites 2024, 11, S96.

[48] L. Mercy, Senguttuvan, International Journal of applied engineering research 2015, 10, 16535.

[49] G. Yang, Q. OuYang, J. Ye, L. Liu, Composites Part A: Applied Science and Manufacturing 2022, 152, 106712; J.-W. Zha, B. Zhang, R. K. Y. Li, Z.-M. Dang, Composites Science and Technology 2016, 123, 32.

3.13 Graphical Abstract



Chapter 4 - Effect of carbonaceous filler type content on the piezo- and thermoresistive response of screen-printing sustainable adhesive epoxy composites

This chapter is based on the article that was submitted for review: R. Lima, J. Serra, C.M. Costa, C.R. Tubio, J. Nunes-Pereira, S. Lanceros-Mendez, P. Costa, “Effect of carbonaceous filler type and content on the piezo- and thermoresistive response of screen-printed sustainable adhesive epoxy composites”.

Thermoset materials offer outstanding mechanical and adhesive properties, making them essential for high-performance applications. Nowadays, environmentally friendly ERs exhibit comparable properties to petroleum-based alternatives, allowing them to be engineered into multifunctional materials with sensing capabilities while maintaining strong adhesion and reducing environmental impact.

Bioresins reinforced with nanocarbonaceous such as CB or MWCNTs or G show great potential as piezoresistive and thermoresistive sensors, enabling functional sensing in bonded joints through cost-effective processing techniques such as doctor blade and screen-printing. This work reports on a bioresins (B-ERs) modified with these nanofillers and on its piezoresistive and thermoresistive sensing characteristics. It was found that with increasing filler content, the electrical resistivity decreases from 1013 Ω/sq for resin to about 100 Ω/sq for 7MWCNTs/ER composite, with a percolation threshold around 3MWCNTs/ER. The tensile strength and elongation of the bioresin (≈ 40 MPa and 3%) decreases with increasing filler content, as does the shear strength in the bonded joints, except for 3MWCNTs/ER (≈ 150 MPa). The adhesive composites also exhibit sensing properties, with GF ≈ 5 for 5CB/ER and S ≈ 0.61 %·°C^{-1} for 15G/ER. Piezoresistive bending increases the sensitivity in bonded structures, with GF exceeding 15 for 15G/ER composites. These findings highlight that sustainable B-ERs composites are suitable for functional adhesives with self-sensing capabilities, making them appropriate for industrial applications with reduced environmental impact.

4.1 Introduction

As sustainability becomes a driving force in materials science, research into B-ERs is emerging as a promising alternative to petroleum-based thermoset materials [1]. Derived from renewable or biodegradable resources, these bioresins can offer significant environmental benefits by reducing dependence on fossil fuels, minimising waste and improving the recycling process [1, 2]. This is critical to reduce environmental impacts related to the increasing production prospects in the overall plastics market, which have been implemented in all areas of industry with enormous benefits, such as reducing the weight of structures [3]. However, despite their environmental benefits, bioresins often lack the mechanical strength, thermal stability and electrical conductivity required for advanced technological applications [1, 4]. To overcome these limitations, novel formulations with comparable overall properties have been developed [4, 5] many of them based on the incorporation of different fillers such as conductive carbonaceous, dielectric ceramic or natural fibre-based materials [6], allowing to tune materials functional characteristics. These composite ERs-based resins are known for their remarkable properties, including enhanced mechanical strength, high electrical conductivity and thermal stability, which can significantly

improve the overall performance of B-ERs [6-8]. In terms of fillers for composite development, conductive fillers such as MWCNTs, CB and G have been extensively studied for their reinforcing properties as well as for their electrical properties, allowing sensing and electronic applications [6, 9-11].

The incorporation of conductive nanocarbons, in addition to mechanical reinforcement and improved electrical and thermal conductivity [12], has been explored for multifunctional composite development [13-15]. Thus, ERs-based resins with conductive fillers allow adhesives with sensor functionalities to be incorporated into structural devices for automotive, aerospace and human health monitoring [13, 14, 16]. The reinforcing fillers used in polymer-based conducting composites for sensing applications are typically different forms of nanocarbonaceous [14, 17, 18]. The distinct carbon nanostructures present higher conductivity (thermal and electrical) with several orders of magnitude greater than ERs, and higher modulus of elasticity (hundreds of GPa) with lower density and less than 100 nm in one of their dimensions [18]. The appropriate type and content of carbon nanofillers in the ERs, combined with the processing method, allow to obtain tailor-made composites with tuned functional response [14, 18]. To achieve the exceptional overall properties of these composites, it is necessary to the efficient dispersion of the nanofillers within the ERs. The mechanical and electrical properties are critically dependent on the filler dispersion, as well as the filler properties or content, and the deagglomeration of the carbon nanofillers must be achieved to obtain a three-dimensional network of fillers in the Composites, minimising the filler-filler interfaces [3, 14]. The remarkable ease of processing of ERs can be maintained by mechanically mixing the fillers in the ERs and controlling the viscosity of the solution for additive manufacturing processes, such as screen-printing [19]. Screen-printing is a versatile, fast and cost-effective method of producing high-quality and high-resolution printed patterns [19]. This printing method also reduces material waste by reusing or recycling the additional material, reduces energy consumption, and is an industrially scalable approach [20].

In this study, sustainable ERs composite adhesives have been developed by incorporating MWCNTs, G and CB into a bio-based (58% biomaterial) ERs matrix. The adhesive Composites were processed by dispersing the fillers in an ultrasonic bath followed by mechanical stirring to ensure that the fillers were uniformly distributed throughout the resin. Screen-printing was used to achieve uniform thickness and layering, allowing precise control of material deposition. This two-step process ensured optimum filler distribution, a patterned design and an industrially scalable approach. The mechanical and electrical properties of the composites enable multifunctional thermal and mechanical sensing capabilities, while maintaining excellent adhesive properties in bonded joints.

4.2 Experimental details

4.2.1 Materials

ERs from Sicomin (Surf Clear EVO) with 58% bio-based carbon content and a viscosity of 30 MPa.s was purchased from Rebelco. The nanocarbon-based materials multiwall carbon nanotubes (MWCNTs) from Nanocyl (NC7000) with 90% carbon purity, a diameter of 9.5 nm and a length of 1.5 μm; carbon Black (CB) from Nanografi (C-nergy SuperC45) with >96% carbon content and a BET specific surface area of 45 m^2/g; and graphene (G) from Graphenest with a thickness of less than 10 nm, 2-140 layers and a majority particle size <7 μm.

4.2.2 Production of the ERs and composite adhesives

Adhesives based on pristine bio-ERs and MWCNTs, CB and G reinforced composites were produced by screen-printing. Different weight percentages of fillers were incorporated: 1, 3, 5, 7 wt.% MWCNTs; 3, 5, 7, 10, 12 wt.% CB; and 7, 10, 12, 15, 20 wt.% G, as shown in Table 1. The samples are designated as "ER" for pristine ERs and "1MWCNTs/ER", "3CB/ER" and "7G/ER" for the respective composites, indicating the fillers and their concentrations. A resin/hardener ratio of 1/0.37 wt.% was used in accordance with the technical data sheet.

Table 4.1 - Sample nomenclature as a function of filler type and content in the ERs.

Filler content (wt.%)	Nomenclature		
0	ER	ER	ER
1	1MWCNTs/ER		
3	3MWCNTs/ER	3CB/ER	
5	5MWCNTs/ER	5CB/ER	
7	7MWCNTs/ER	7 CB/ER	7G/ER
10		10 CB/ER	10G/ER
12		12CB/ER	12G/ER
15			15G/ER
20			20G/ER

To simplify sample handling during preparation, the ERs and hardener were prepared separately to prevent premature curing. Fillers were added individually to the resin and hardener at concentrations of 1 wt.% for the resin and 0.37 wt.% for the hardener, maintaining the resin-to-hardener ratio recommended by the supplier. Each was subjected to sonication in a Fisherbrand bath ultrasonic (40 kHz of frequency and 200 W of power) at 25-35 °C for 2 hours to deagglomerate the filler materials. This was followed by mechanical mixing at 2200 rpm for 15 minutes using a Heidolph RZR 1 mixer (Figure 4.1A). Both

solutions were then placed in a vacuum chamber for 15 minutes to eliminate air bubbles [21]. The pristine ERs underwent similar steps except for the addition of filler and ultrasonic treatment [22].

Once the solutions were ready, the components were combined using a commercial screen-printing cartridge with a screen mesh of 24 wires/cm and an emulsion thickness of 40 μm, applying two printed-layers [13]. The samples were cured in an oven at 23 °C for 24 hours followed by a post-cure at 40 °C for 24 hours. The resulting thickness averaged close to 100 μm for ER and between 50 and 100 μm for the composites. This method was consistent across all materials, facilitating screen-printing applications.

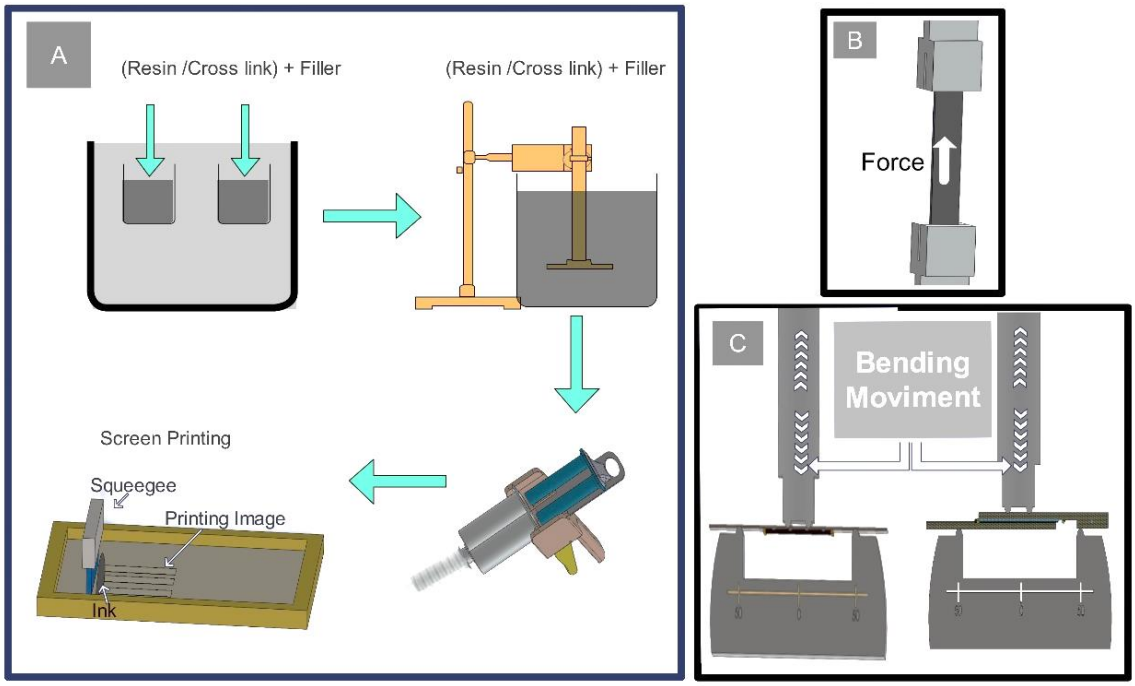


Figure 4.1 - Schematic representation of: A) functionalization of ERs by incorporation of nanocarbons and preparation of samples by screen-printing; B) tensile stress-strain test; C) piezoresistive bending tests.

4.3 Fabrication of adhesively bonded joints and coatings with sensing capabilities

To evaluate the adhesion, piezoresistive and thermoresistive properties of the bonded joints, commercial aluminium, carbon fibre and glass fibre based adherends of 30×10 mm² (bonded area of ≈ 10×10 mm² by ≈ 500 μm thick) were bonded with bio-ERs and composite adhesives (3MWCNTs/ER and 5MWCNTs/ER; 5CB/ER and 7CB/ER; 12G/ER and 15G/ER). The bonding process involved screen-printing a single layer onto both adherends, which were then pressed using a commercial spring clamp at a force of ≈ 20 N over an area of ≈ 100 mm². To ensure uniform elongation and vertical alignment during the shear tests, a square shim (of the same material as the adherends) was glued to each

adherend strip as a final tab. The bonded joints were cured in an oven at 23 °C for 24 hours and post-cured at 40 °C for 24 hours, as recommended in the datasheet.

Similar processing were applied to coatings- evaluated by microindentation technique- over three different substrates (commercial aluminium, glass and glass fibre materials) using screen-printing technique with a screen mesh of 24 wires/cm and an emulsion thickness of 40 μm, with 2 layers and cured as mentioned above. The samples present an area of 50×100 mm^2.

4.4 Characterization procedures

The morphological evaluation of the resin and its composites was carried out by scanning electron microscopy (SEM) using a Hitachi S-4800 at 10 kV on samples previously coated with a thin gold layer using a Polaron SC502 sputter coater.

Chemical bonding and functional groups were assessed by Fourier transform infrared spectroscopy (FTIR) analysis performed in attenuated-total-reflectance (ATR) mode using a Jasco FT/IR-4100 over a wavenumber range of 600 to 4000 cm^{-1}, with 32 scans at 4 cm^{-1} resolution.

The thermal properties of the bio-ERs and composites were evaluated by differential scanning calorimetry (DSC) using a NETZSCH DSC200 F3 Maia under dry nitrogen from 30 to 250 °C at 20 °C/min.

Surface wettability was assessed by contact angle measurements using a Dataphysics OCA 15EC analysing water droplets at different surface locations. Three measurements in two different locations were performed for each sample and the value is provided as average of the results.

Mechanical properties were investigated by uniaxial stress-strain tests using a Shimadzu AG-IS tensile system at 5 mm/min up to samples failure. Samples measuring ≈ 4×20 mm^2 and 50 to 100 μm thick were subjected to three to five tests each.

The electrical sheet resistance of the samples was measured by the four-point-probe technique with a Keighley 2400 source. Each sample was positioned in a meter to apply a voltage in the range -10 V to +10 V, while the resulting current (I) was measured and the resistance ($R = \Delta V/I$) calculated. To ensure reliable results, each sample was tested twice at three different surface locations to reduce variability and provide a robust data set for calculating the sheet resistance (Rs) using Equation 4.1 [23]:

$$R_s = \frac{\rho}{t} = \frac{\pi}{\ln 2} \times \frac{\Delta V}{I} \tag{4.1}$$

Where $\frac{\pi}{\ln 2}$ is the geometric factor for a semi-infinite thin film, ρ is the resistivity and t is the thickness.

Indentation tests were performed on screen-printing materials over glass, aluminium and glass fibre using a Micro Materials NanoTest with a diamond indentation tip. The tests were conducted in displacement control mode with an indentation depth of 500.0 mN and an indentation tip displacement rate of 10 mN/s. The hardness (H) was determined by Equation 4.2:

$$H = P_{max}/A \tag{4.2}$$

Where P_{max} is the maximum load and A is the area.

Piezoresistive tests were performed using a four-point-bending method on composites near the percolation threshold using a Shimadzu AG-IS universal testing machine. During the tests, changes in electrical resistance (R) were monitored in real time during samples deformation using an Agilent 34401A multimeter. The printed samples measured 30×10 mm², with silver-painted electrodes spaced 20 mm apart. For the thin film tests, the samples were bonded to flexible polypropylene using double-sided tape from Tesa, with the electrodes fabricated to the same parameters as the bonded joints.

The piezoresistive response was evaluated at maximum bending displacements of 0.1, 0.3, 0.5, 1, 3 and 5 mm applied at a constant speed of 5 mm/min. The gauge factor (GF), which is used to quantify the piezoresistive sensitivity, was calculated using Equation 4.3 [24]:

$$GF = \frac{\Delta R/R_0}{\Delta l/l_0} = \frac{\partial \rho/\rho_0}{\varepsilon} + (1 + 2\upsilon) \tag{4.3}$$

Where the electrical resistance variation (ΔR), the initial resistance (R_0), the strain ($\varepsilon = \Delta l/l_0$) and the Poisson's coefficient of the ERs ($\nu \approx 0.35$) [25], allow to determine the sensitivity of the materials. The first term in the equation accounts for the intrinsic resistivity changes with strain, while the second term accounts for the geometrical effect. For the four-point bending mode, the strain is calculated from pure bending theory, valid between the inner loading points, and is given by Equation 4.4 [26]:

$$\varepsilon = 3dz/5a^2 \tag{4.4}$$

Where the thickness of the sample is close to 1.1 mm, z is the vertical displacement and a=25 mm is the span.

The thermoresistive response was evaluated using an Agilent 34401A digital multimeter synchronised with a Linkam THMSE 600 temperature oven. Measurements were performed in volume mode on 20×20 mm² by 50-100 μm thick samples, in samples 3MWCNTs/ER, 5CB/ER and 15G/ER, due to their superior electrical conductivity, screen-printed with conductive commercial silver ink contacts, connected to aluminium adherends. The temperature range for the measurements was 30 to 50 °C and 60 to 90

°C, both at a rate of 20 °C/min, targeting human health related measurements and industrial applications. The samples, which were approximately 100 μm thick, had conductive electrodes connected to copper wires for signal collection. The thermoresistive sensitivity (S) is defined by Equation 4.5, which quantifies the change in resistance with respect to temperature variation (ΔT):

$$S = \frac{\Delta R/R_0}{\Delta T} \times 100 \quad (4.5)$$

The adhesion of the bonded joints was also evaluated by lap shear tests using a Shimadzu AGS-X universal testing machine equipped with a 50 kN load cell and suitable grips. Data was collected using Trapezium X software. Tests were performed in accordance with ASTM D3165 at a loading rate of 1.3 mm/min and included both carbon fibre and aluminium joints. Shear strength (τ) was determined by Equation 4.6:

$$\tau = \frac{P}{A_0} \quad (4.6)$$

Where P is the cell load and A_0 is the overlap area of the bonded joint.

4.5 Results and Discussion

4.5.1 Physicochemical properties of bio-resin and composite adhesives

The morphology of the samples and the dispersion of the nanofillers were evaluated by SEM images as shown in Figure 4.2. For the pristine ERs with two screen-printed layers, shown in Figure 4.2A and 4.2B as resin cross section and surface images, respectively, a smooth surface without holes or defects is observed, with a thickness close to 80 μm (≈ 40 μm per printed layer). It should be noted that the interface between the layers is not observed due to the well achieved compact structure of the sample. For composites with different fillers, the thickness varies from 40 to 100 μm, with MWCNTs reinforced composites being the thickest samples due to the characteristic expansion of MWCNTs during the deagglomeration process. Regardless of the filler content, MWCNTS and CB fillers do not affect the compact morphology of the samples, whereas G composites lead to a less compact structure. Agglomerates of the reinforcing fillers are observed in the composites, increasing with increasing filler content (data not shown). MWCNTS and CB composites present agglomerates of less than 10 μm, whereas G presents a better dispersion of individual particles in the respective composites, with some voids in the G-ERs interfaces.

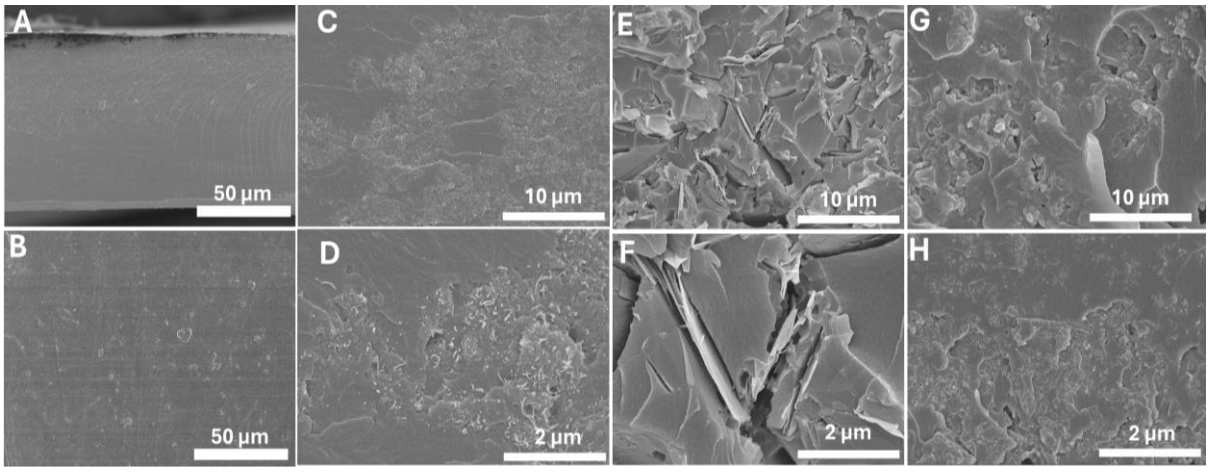


Figure 4.2 - SEM images of screen-printed samples with two layers, for resin (A in cross section and B in surface modes), 3MWCNTs/ER (C and D), 10G/ER (E and F), 3CB/ER (G and H), composites in cross section mode.

Based on the FTIR-ATR spectra presented Figure 4.3A, the absorption bands of the ERs are identified and the effect of the fillers in these bands is evaluated [27-29]. The vibrational bands of the ERs are detected at 821 and 1026 cm^{-1}, related to the C-O-C stretching of the oxirane group and ethers, respectively [27-29]. The aromatic C-C and C=C rings at 1512 and 1612 cm^{-1} and the stretching vibration group (C-H) in the CH2 and CH3 absorption bands are represented by the vibration peaks observed at 2847 and 2916 cm^{-1} respectively [27-29]. The O-H stretching appears as a broad peak at 3200-3600 cm^{-1} [27-29]. It is to notice that the presence of the fillers does not induce new vibration bands or energy shits in the bends of the ERs, demonstrating lack of strong chemical interactions between fillers and polymer.

The influence of the filler type and content in the composites on the surface wettability was measured by the contact angle as shown in Figure 4.3B. In general, the screen-printed samples are hydrophilic. The smooth surface of the screen-printed samples increases their wettability compared to the literature [18, 30, 31]. The wettability increases for all composites from 52.7 ± 2.0 ° for ERs to a maximum value of 77.3 ± 1.0 ° for 10CB/ER, the water contact angle increasing with increasing filler content in a similar way for all filler types.

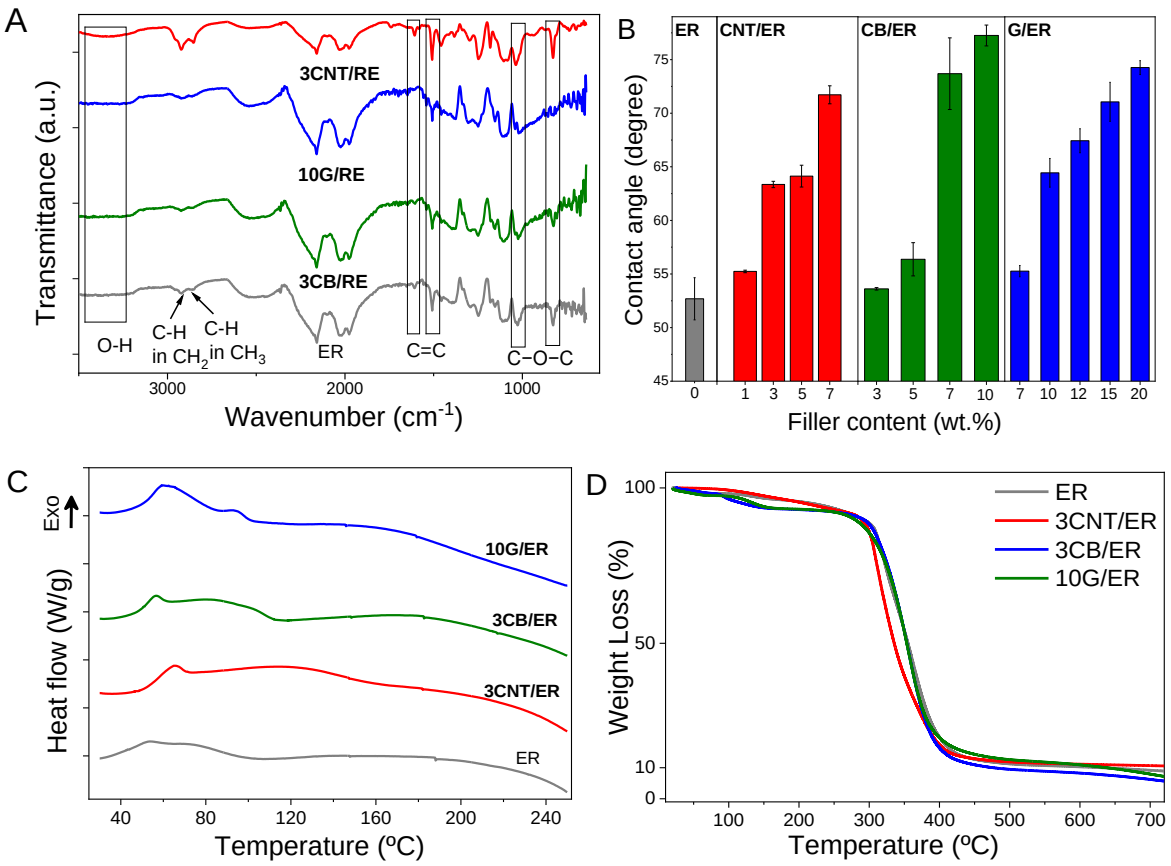


Figure 4.3 - Resin and respective composites with different filler type and content evaluated by: A) FTIR-ATR, B) contact angle, C) DSC and D) TGA.

The chemical structure and composition of the samples has a critical influence on the thermal performance, so the ERs and composites were investigated by DSC and TGA (Figure 4.3C and 4.3D, respectively). In the DSC thermogram, the peak near 50 °C for the ER is the glass transition and ageing peak, which is associated with curing exothermic peaks corresponding to the ring-opening reaction between the amine and ERs functional groups [32-34]. The exothermic peaks for composites increase to 56, 59 and 65 °C for 10G/ER, 3CB/ER and 3MWCNTs/ER respectively. The thermal degradation of the samples was studied by TGA up to 700 °C. First, a decrease of almost 10% of the weight of the samples is observed after 100 °C, related to the evaporation of the adsorbed water from the environment [35]. The second event is between 300 and 400 °C, where more than 80% of their weight is lost, related to the thermal cleavage that occurs between different chemical bonds [35]. The remaining weight at the end is between 5 and 10% of carbonaceous fillers and resin residues [35].

The mechanical properties of the ERs and its composites were evaluated in the uniaxial tensile mode and their behaviour is shown in Figure 4.4A for samples prepared by screen-printing, Figure 4.1B. The fracture strain and stress (Figure 4.4B) for the ERs are approximately 3% and 38 MPa respectively. For the

Composites, the fracture strain is similar to the ER with values below 5%, except for the 20G/ER sample which reaches around 15%. Larger filled composites exhibit plastic behaviour due to voids at the filler-resin and filler-filler interfaces, which hinder entirely stress transfer between nanofillers, along with plasticizing effect [36]. This similarity indicates that the filler content does not limit the ductility of the composites, with the majority of composite samples showing fracture strains between 2 and 3%. The fracture stress is slightly above 40 MPa for the ERs and tends to decrease with increasing filler content, reaching a minimum of ≈ 5 MPa for 7MWCNTs/ER, ≈ 15 MPa for 12CB/ER and ≈ 8 MPa for 20G/ER composites. The low filled samples 1MWCNTs/ER and 3CB/ER show a higher fracture stress than the pure ERs with ≈ 53 and 58 MPa, respectively. These filler contents can be considered as suitable to promote the reinforcement of the maximum strength of the composites, but there is a point at which over-reinforcement can be harmful above which the agglomeration effects are detrimental, as reported in the literature [37, 38]. The mechanical behaviour of the composites is similar for the MWCNTs and CB samples, while the G composites exhibit lower stress at fracture due to the non-compact structure, as shown in the SEM images (Figure 4.2). The Young's modulus (Figure 4.4C) shows the maximum value of ≈ 2.2 GPa for the 1MWCNTs/ER sample, corroborating the idea of the optimum reinforcement percentage, followed by the pure ERs sample with ≈ 1.8 GPa. For the remaining MWCNTs composites, it decreases with increasing filler content to a minimum of ≈ 0.4 MPa for the 7MWCNTs/ER sample. For the CB samples, the initial Young's modulus varies between 1 and 1.5 GPa, with the maximum for the 7CB/ER sample, while for the G samples it varies between 0.4 and 1.4 GPa, with the maximum for the 10G/ER sample. Despite the decline in mechanical properties for the larger filled composites, the results underline the effectiveness of screen-printing additive manufacturing for this type of materials. This method allows for the tailoring of material properties and the fabrication of innovative geometric designs that can be scaled up for industrial processing. This adaptability of screen-printing to maintain mechanical integrity while allowing design flexibility makes it a promising technique for advanced composite applications.

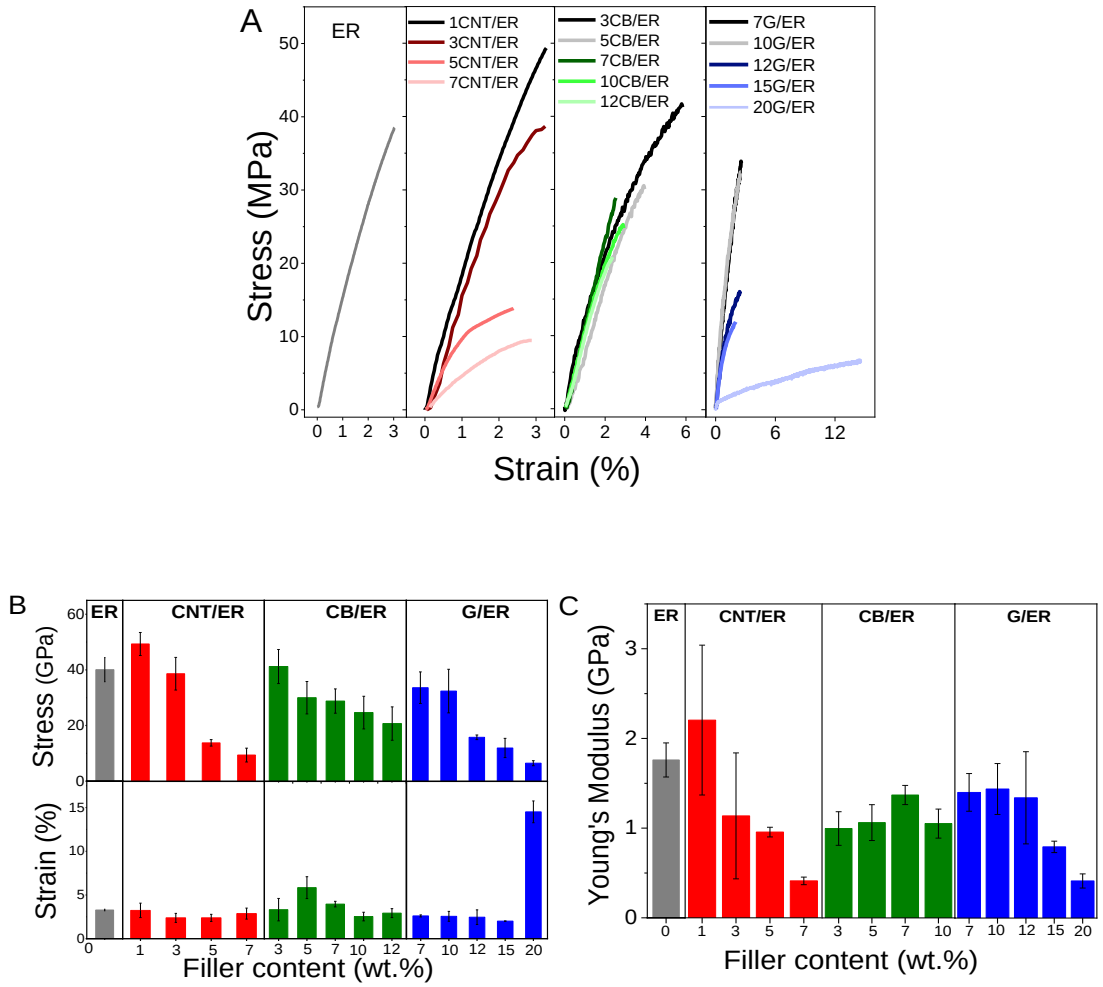


Figure 4.4 - A) Representative stress-strain curves of the resin and composites, B) maximum strength and strain, and C) Young's modulus.

Electrical resistivity was measured on the surface of the samples using the four-point method and the results are shown in Figure 4.5. The ERs exhibits insulating properties with a sheet resistivity of Rs ≈ 8.7×1012 Ω/sq. A significant decrease was observed with the introduction of different fillers into the polymer matrix, with the sheet resistivity decreasing by about 10 orders of magnitude for the most heavily filled composites with MWCNTs and CB, with 7 and 12 wt.% filler, respectively. For the G-reinforced resin, a decrease of about 9 orders of magnitude was recorded for the sample with 20 wt.% filler content. The lower resistivity values are about 112 Ω/sq for 7MWCNTs/ER, 200 Ω/sq for 12CB/ER and 6.6×103 Ω/sq for 20G/ER composites. This behaviour is characteristic of ERs composites reinforced with nanocarbon materials as found in previous studies [39, 40]. The electrical percolation thresholds were found to be below 3 wt.% for MWCNTs composites, below 5 wt.% for CB composites and below 15 wt.% for G composites. The literature reports that these thresholds can range from 1 to 15 wt.%, depending on factors such as resin type, filler type and processing conditions [39]. The low viscosity of the ERs facilitates

effective deagglomeration and dispersion of the fillers, especially for conductive fillers such as MWCNTs and CB. In contrast, G in the form of nanoplatelets may require higher concentrations, above 20 wt.%, to achieve similar conductivity levels.

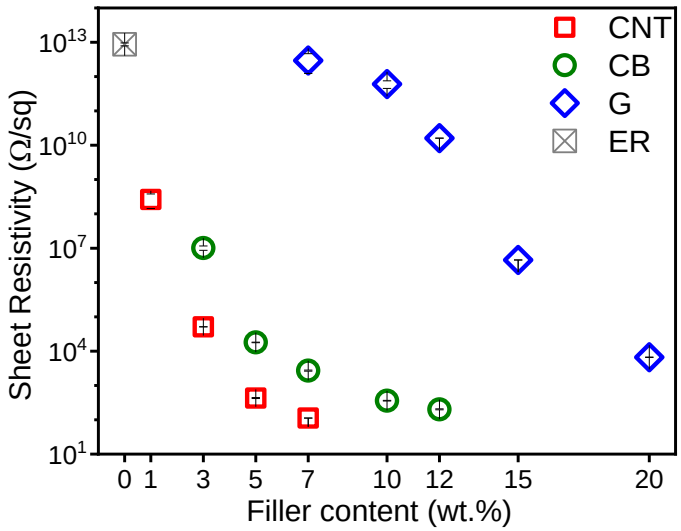


Figure 4.5 - Sheet resistivity measured by the four-point method for ERs composites with MWCNTs, CB and G with different filler contents in two-layer screen-printed samples.

The quality of the printing samples of ERs and composites, a critical step for high performance adhesive coatings, has been evaluated using microindentation. Indentation depth and hardness modulus data at room temperature are derived from the load-displacement curve generated by microindentation studies for composites prior to percolation threshold: 3MWCNTs/ER, 5CB/ER and 15G/ER. The composite samples are based on two screen-printed layers over commercial aluminium, carbon fibre and glass adherends. The representative load-unload curves for the 3MWCNTs/ER samples (also representative for the 5CB/ER and 15G/ER ones) are shown in Figure 4.6A. The curves are composed of an elastic regime (initial part) followed by the plastic regime of the material (last part of the cycle) and the relationship between depth and load is non-linear [41]. The curves are similar between the different composites, varying in the displacement of the tip in the sample, due to the maximum loading force of the equipment at 500 mN and the thickness of the sample. It should be noted that in all tests the force saturates at its maximum. From the analysis of Figure 4.6A, the ERs films with 3% MWCNTs deposited on different substrates showed differences in microindentation behaviour. For all samples, the maximum applied load was around 500 mN, but the stiffness and deformation capacity varied depending on the substrate. The film deposited on aluminium showed the lowest displacement, in the order of 7500 nm, indicating greater resistance to deformation. For the carbon fibre substrate, an intermediate displacement was recorded,

reaching around 9000 nm, while for the glass substrate, the largest displacement was recorded, close to 10500 nm, reflecting a more deformable behaviour.

The higher stiffness observed in the sample on aluminium can be attributed to the high interfacial adhesion between the ERs matrix and the metallic substrate, which favours efficient load transfer. Studies show that the incorporation of MWCNTs in ERs deposited on aluminium increases the modulus of elasticity of the matrix by up to 21% and improves its fracture toughness, reducing the propagation of cracks at the interface [42]. The carbon fibre sample showed an intermediate displacement, reflecting a stiffness lower than that of aluminium but higher than that of the glass sample. The literature shows that the presence of MWCNTs in the ERs matrix influences the thickness and mechanical properties of the ERs-carbon interface, creating a gradual transition of material properties and promoting a better stress distribution. The addition of MWCNTs increased the elastic modulus of the polymer matrix by up to 41% and improved the resistance to plastic deformation by 37%, favouring a more efficient load transfer between the ERs matrix and the carbon fibres [43]. Finally, the samples on glass showed the largest maximum displacement, indicating the lowest stiffness of the three analysed systems. This behaviour may be related to the lower chemical affinity and interfacial adhesion between the ERs matrix and the glassy substrate. Studies suggest that the interface between glass and polymer matrix has lower shear strength and reduced load transfer efficiency [44].

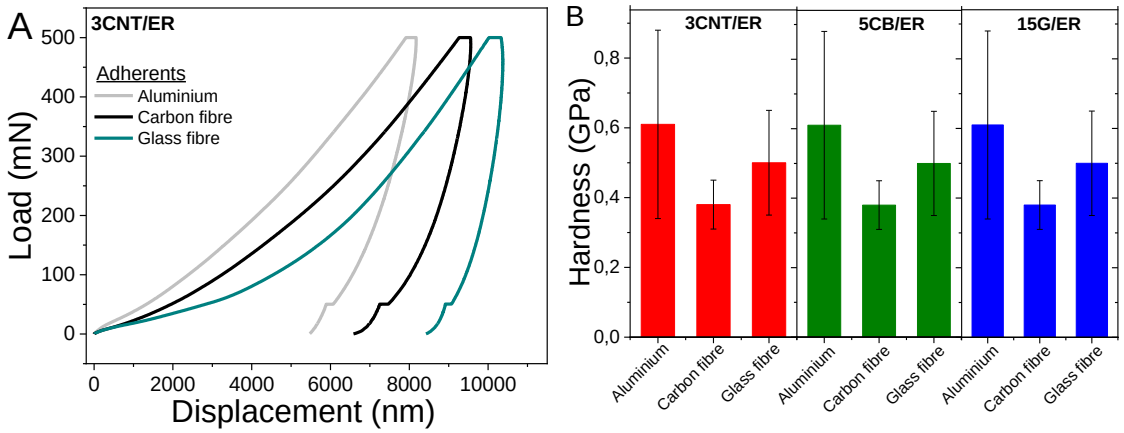


Figure 4.6 - A) Load applied during the indentation procedures as a function of displacement and for the 3MWCNTs/ER sample and the corresponding B) hardness for the different samples, as obtained from the indentation curves.

4.6 Functional piezoresistive and thermoresistive response

The piezoresistive and thermoresistive response of the composites was evaluated with respect to potential multifunctional adhesives with self-sensing sensing properties.

The piezoresistive response, together with its respective sensitivity shown in Figure 4.7 produced by screen-printing Figure 4.1C, was evaluated at different maximum bending displacements from 0.5 to 5 mm for Composites prior to the percolation threshold for each reinforcing filler: 3MWCNTs/ER, 5CB/ER and 15G/ER in Figures 4.7A, 4.7B and 4.7C, respectively. Those concentrations are selected as the piezoresistive response has been demonstrated to be larger around the percolation threshold, which is related to the larger variations of the conductive network upon deformation [24, 45]. The overall performance of the piezoresistive composites shows a linearity between the electrical resistance behaviour and the mechanical stimulus during load-unload cycles, which increases with increasing applied load and vice versa. For the different composites 3MWCNTs/ER composite is the one with the better overall response in terms of linearity, in particular for the higher and medium displacement range.

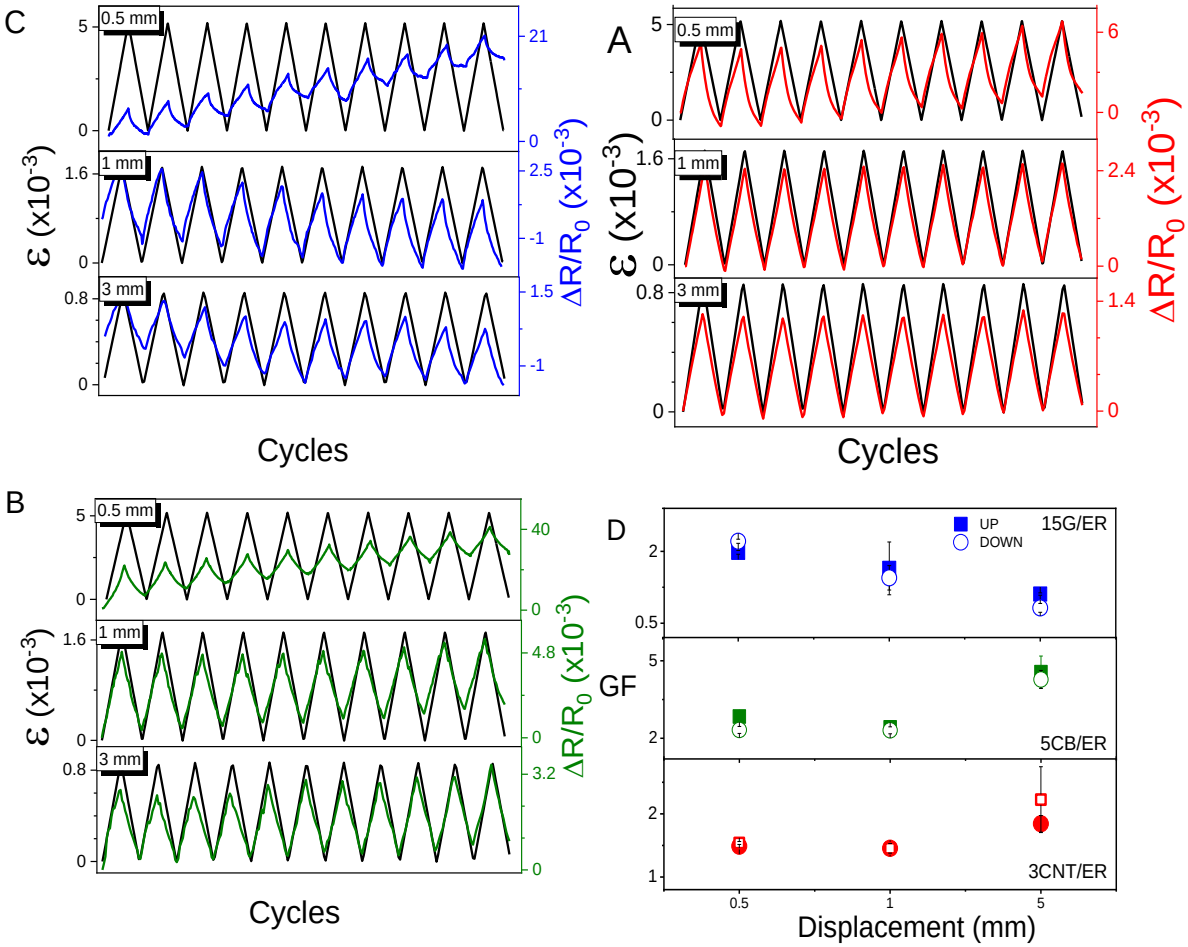


Figure 4.7 - Piezoresistive response under mechanical bending for A) 3MWCNTs/ER; B), 5CB/ER and C) 15G/ER at 0.5, 1- and 3-mm maximum displacement.

The GF of the composites is shown in Figure 4.7D and vary from GF ≈ 1 to 5 for all composites at the different maximum displacements. For the MWCNTs and CB composites, the GF increases with increasing displacement with the 5CB/ER composite showing the higher sensitivity with GF ≈ 2 to 5. The

15G/ER composite shows a slight decrease in sensitivity with increasing displacement, from GF ≈ 2 to 0.8 for 0.5 for 5 mm. This distinct behaviour can be attributed to the non-compact morphology of the G samples, as shown by SEM micrographs, in contrast to the MWCNTs or CB composites (Figure 4.2). Piezoresistive response increases for larger displacements in composites prior the percolation threshold [45], and can be negative for composites beyond the threshold [45].

These results highlight the influence of filler type and content on the piezoresistive performance of composites and show that while MWCNTs composites maintain a consistent linear performance over the range of maximum bending, the CB filler increases sensitivity in certain deformation scenarios.

The thermoresistive properties of the composites were evaluated for 3MWCNTs/ER, 5CB/ER and 15G/ER in the thin films produced by screen-printing. The temperature test ranges included 30 to 50 °C for human temperature sensing applications and 60 to 90 °C for industrial purposes, similar to shown in previous works. The thermoresistive results revealed proportional variation in resistance with a negative temperature correlation, since this effect is mainly driven by the conductive fillers embedded in the polymer matrix, as previously described for contents larger than percolation threshold [46]. At lower temperatures (30 to 50 °C) the relative changes in resistance were less pronounced than at higher temperatures (60 to 90 °C). The sensitivities of the composites were quantified as follows: for the low temperature range S30-50 and high temperature range (S60-90) for 3MWCNTs/ER, the sensitivities were S ≈ 0.09 (%.°C^{-1}) and S ≈ 0.01 (%.°C^{-1}), respectively; for 5CB/ER samples at the low temperature range (S30-50) and high temperature range (S60-90), the sensitivities were S ≈ 0.08 (%.°C^{-1}) and S ≈ 0.11 (%.°C^{-1}) respectively, and for the 15G/ER samples, the low (S30-50) and high temperature range (S60-90) sensitivities were S ≈ 0.28 (%.°C^{-1}) and S ≈ 0.61 (%.°C^{-1}) respectively. The thermoresistive sensitivity increases with increases the filler content in composites this results are similar to chapter 3 Figure 3.9.

4.7 Adhesion and piezoresistive sensing properties of bonded joints

The custom ERs and composites (3 and 5MWCNTs/ER, 5 and 7CB/ER, 12 and 15G/ER) were designed primarily for use in material joints, but also as adhesives to replace conventional fastening methods in bonded structures, with sensing properties to detect fracture, bending or thermal stimuli. Lap shear tests were performed under uniaxial stress-strain, as illustrated in Figure 4.8A, to evaluate the stress at failure (Figure 4.8B). These experiments used commercial carbon fibre reinforced polymer (CFRP) substrates of 10×10 mm2 of bonded area in a single lap joint method [47]. The ERs exhibits in Figure 4.8B a lap shear strength of 1.1 GPa, which is higher than related literature [48, 49] and intrinsic natural resins [49]. The lap shear strength value for the composites is similar to or higher than that of bioresin, except for the

5MWCNTs/ER composite. Reinforced composites with MWCNTs or G near the percolation threshold present a lap shear strength of about 140 MPa, demonstrating the suitable adhesive properties of bioresin and screen-printing as an application technique.

The study indicates that MWCNTs had a negative effect on the bond strength of the ERs matrix, whereas both CB and G improved the lap shear performance. The prevalence of cohesive failure in the adhesive region highlights the potential of these formulations for use in durable adhesive applications. This demonstrates that the strategic selection and concentration of carbon-based fillers can significantly influence the mechanical properties of ERs adhesives.

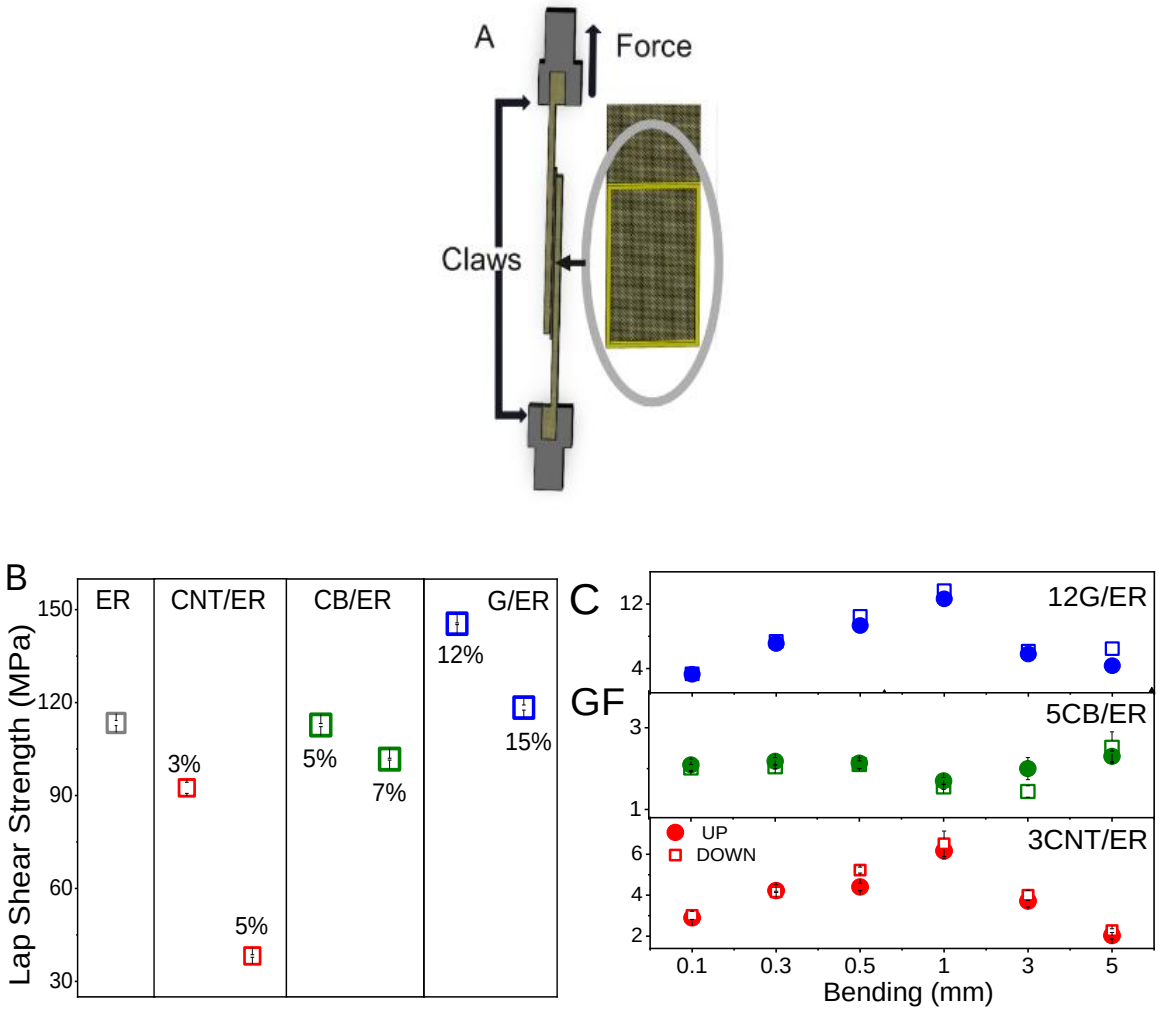


Figure 4.8 - Shear test diagram and B) lap shear strength of bioresin and composite bonded joints. C) Piezoresistive behaviour from 0.1 to 5 mm of displacements in a bonded joint for 3MWCNTs/ER, 5CB/ER, and 15G/ER composites prepared by screen-printing.

The piezoresistive performance of the bonded structures as functional materials for 3MWCNTs/ER, 5CB/ER, and 15G/ER composites present similar behaviour to piezoresistive cycles evaluated in films,

the electrical resistance changes follow linearly the applied bending stimuli, measured in 10 loading-unloading cycles from 0.1 to 5 mm maximum bending for all three adhesive composites (data not shown). The piezoresistive sensitivity shown in Figure 4.8C is larger for bonded joints than films (Figure 4.7), where the sensitivity increases up to near GF ≈13 in bonded joint structure. The piezoresistive sensitivity as a function of bending cycles presents an increase in sensitivity with increasing the applied bending in 3MWCNTs/ER and 12G/ER bond joints until 1 mm of bending, decreasing for larger maximum bending. Further, it exhibits stable performance near GF ≈ 1.5–2.5 for 5CB/ER composite, independently of the maximum bending deformation. Therefore, piezoresistivity is larger for G composite, changing from 4 <GF< 12, than for MWCNTs based composites, in which 2 <GF< 6. Overall, all composites allow to properly evaluate bending deformation in coatings and bonded structures from small to large deformations.

These results highlight the dynamic performance of the piezoresistive materials, revealing not only their sensitivity and response to bending, but also the possibility of tailoring mechanical and electrical response by proper selection of carbonaceous filler.

4.8 Conclusions

The overall properties of sustainable resin and respective composites reinforced with different carbon-based nanofillers (MWCNTs, CB and G) were systematically evaluated. The adhesives were prepared by screen-printing, demonstrating a highly efficient, scalable and reproducible method for the development of sustainable multifunctional adhesives. Morphological analysis confirmed compact films with uniform dispersion of small aggregates for MWCNTs and CB composites, whereas G-based composites exhibited a less compact structure. Mechanical testing showed a decrease in tensile strength for all adhesive composites compared to the pristine ERs (≈ 40 MPa), except for the 1MWCNTs/ER sample, which showed an increase up to ≈ 50 MPa for 1MWCNTs/ER, and a decrease in shear strength for the entire bonded joints compared to bio-ERs (≈ 113 MPa), except for the 12G/ER bonded joint (≈ 154 MPa). Electrical characterisation showed that MWCNTs and CB composites achieved lower percolation thresholds (near 2-3 wt.% for both) compared to G (near 15 wt.%), with the lowest sheet resistance reaching approximately 100 Ω/sq for 7MWCNTs/ER. The adhesive composites exhibited remarkable piezoresistive and thermoresistive properties, with sensitivity values exceeding GF= 4 for 5CB/ER composites and thermoresistive sensitivities up to 0.61 $\%\cdot{}^{\circ}C^{-1}$ for 15G/ER.

The piezoresistive response of the bonded joints demonstrated their potential as integrated structural health monitoring systems. The results indicate that MWCNTs and G offer the best overall performance,

with MWCNTs composites achieving an optimal electrical and mechanical balance with a maximum GF ≈ 6 for 3MWCNTs/ER. G nanoplatelets present larger sensitivity but higher filler contents decrease the mechanical properties.

Overall, this study highlights the potential of bio-based ERs composites as sustainable, multifunctional adhesives with self-sensing piezo- and thermo-capabilities. The results show that screen-printing is a viable approach to produce these materials, allowing precise control of filler distribution and composite thickness, the selection of the filler allowing to tailor overall materials functional response.

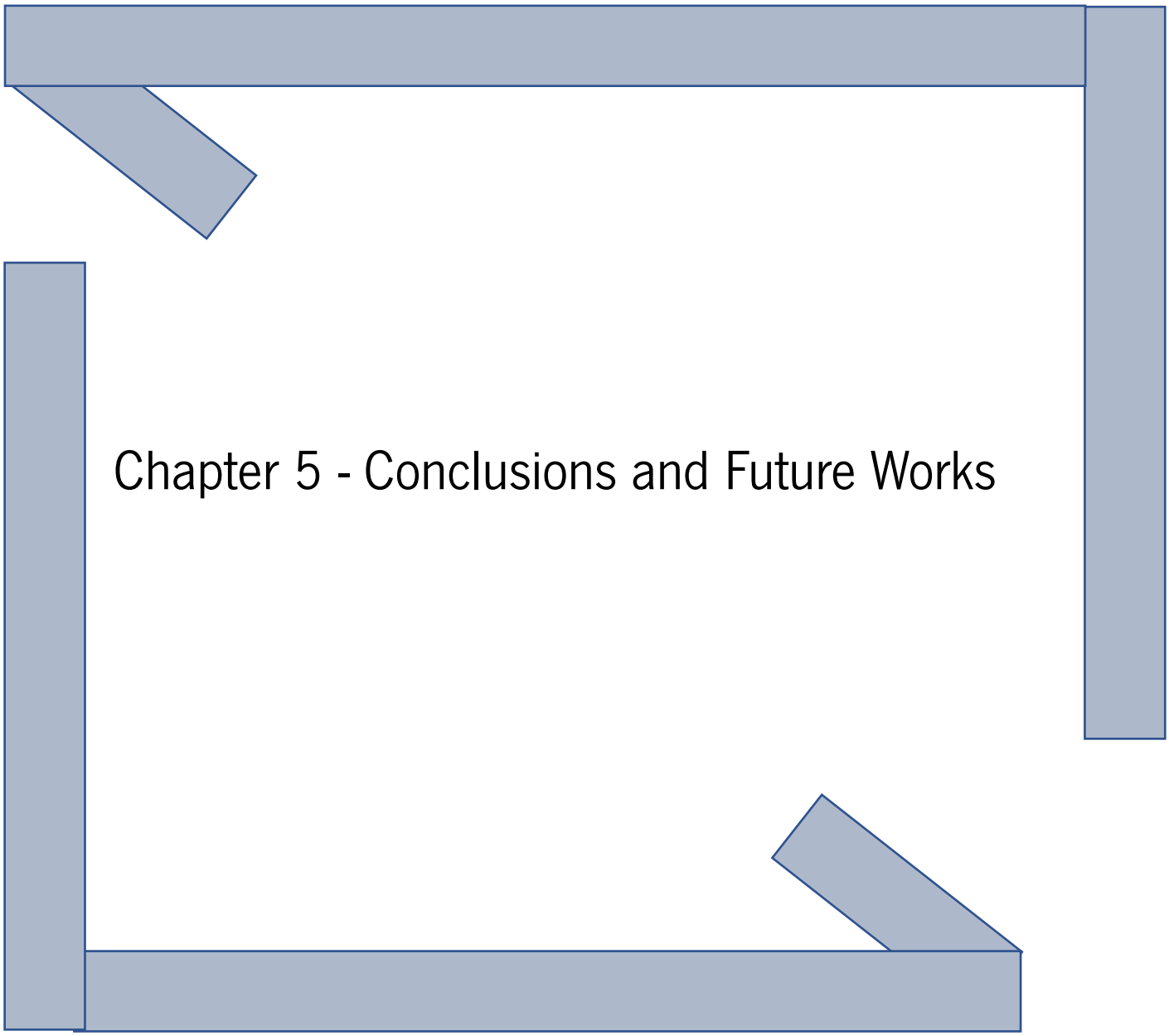
References

1. Zhang, Y., et al., From renewable biomass to bio-based epoxy monomers and bio-based epoxy curing agents: Synthesis and performance. Polymer Degradation and Stability, 2024. 229: p. 110988.
2. Ma, S., et al., Research progress on bio-based thermosetting resins. Polymer International, 2016. 65(2): p. 164-173.
3. Marturano, V., et al., Recent advances in bio-based functional additives for polymers. Progress in Materials Science, 2023. 139: p. 101186.
4. Yang, K., et al., Bio-based epoxy resin demonstrating high breakdown strength and low dielectric loss via intrinsic molecular charge traps construction. Composites Part B: Engineering, 2024. 284: p. 111728.
5. Gong, Y., et al., Enhancing strength, toughness, and flame retardancy of epoxy resins through in-situ interpenetrating network modification. Materials Today Communications, 2024. 39: p. 109233.
6. Prashanth Palani Velayuda Shanmugasundram, H., E. Jayamani, and K.H. Soon, Review: Classification, theories, and methodologies concerning bio-based polymer dielectric composites. Renewable and Sustainable Energy Reviews, 2025. 209: p. 115026.
7. Qiu, X., et al., Self-Compositing: A Efficient Method of Improving the Electrical Conductivity of Graphene Nanoplatelet/Thermosetting Resin Composites. Small, 2023. 19(33): p. 2300931.
8. Yurddaskal, M., M. Erol, and E. Çelik, Development Of The Electrical Conductivity In Carbon Based Polymer Composites. Gazi Mühendislik Bilimleri Dergisi, 2018. 4(2): p. 77-83.
9. Dumas, L., et al., Bio-based high performance thermosets: Stabilization and reinforcement of eugenol-based benzoxazine networks with BMI and CNT. European Polymer Journal, 2015. 67: p. 494-502.
10. Franco-Urquiza, E. and A. Rentería-Rodríguez, Effect of nanoparticles on the mechanical properties of kenaf fiber-reinforced bio-based epoxy resin. Textile Research Journal, 2021. 91(11-12): p. 1313-1325.
11. Gargala, A.N., P.V. Polydoropoulou, and K. Tserpes, Experimental investigation of bio-based polymers reinforced with graphene oxide. Applied Composite Materials, 2024: p. 1-20.
12. Li, Y.-C., et al., Recent advances in improvement of thermal conductivity of epoxy-based nanocomposites through addition of fillers. Polymer, 2024. 313: p. 127678.

13. Lima, R., et al., Additive manufacturing of multifunctional epoxy adhesives with self-sensing piezoresistive and thermoresistive capabilities. Composites Part B: Engineering, 2025. 293: p. 112130.
14. Mousavi, S.R., et al., A review of electrical and thermal conductivities of epoxy resin systems reinforced with carbon nanotubes and graphene-based nanoparticles. Polymer Testing, 2022. 112: p. 107645.
15. Fuseini, M., et al., Review of epoxy nano-filled hybrid nanocomposite coatings for tribological applications. FlatChem, 2025. 49: p. 100768.
16. Ferreira, R.G., A.P. Silva, and J. Nunes-Pereira, Current On-Skin Flexible Sensors, Materials, Manufacturing Approaches, and Study Trends for Health Monitoring: A Review. ACS Sensors, 2024. 9(3): p. 1104-1133.
17. Hao, Q., et al., Progression from graphene and graphene oxide to high-performance epoxy resin-based composite. Polymer Degradation and Stability, 2024. 223: p. 110731.
18. Liu, S., et al., A review of extending performance of epoxy resins using carbon nanomaterials. Composites Part B: Engineering, 2018. 136: p. 197-214.
19. Yildiz, Z., et al., Sustainable fabric printing by using pre-consumed cellulosic textile wastes: The effect of waste particle content. Journal of Cleaner Production, 2024. 448: p. 141635.
20. Khosravani, M.R. and T. Reinicke, On the environmental impacts of 3D printing technology. Applied Materials Today, 2020. 20: p. 100689.
21. Sienkiewicz, N., M. Dominic, and J. Parameswaranpillai, Natural fillers as potential modifying agents for epoxy composition: A review. Polymers, 2022. 14(2): p. 265.
22. Agwa, M., et al., Integrated vacuum assisted resin infusion and resin transfer molding technique for manufacturing of nano-filled glass fiber reinforced epoxy composite. Journal of Industrial Textiles, 2022. 51(3_suppl): p. 5113S-5144S.
23. Franco, M., et al., Environmentally Friendlier Printable Conductive and Piezoresistive Sensing Materials Compatible with Conformable Electronics. ACS Applied Polymer Materials, 2023. 5(9): p. 7144-7154.
24. Arboleda, L., et al., Piezoresistive response of carbon nanotubes-polyamides composites processed by extrusion. Journal of Polymer Research, 2013. 20(12): p. 326.
25. Terry, J.S. and A.C. Taylor, The properties and suitability of commercial bio-based epoxies for use in fiber-reinforced composites. Journal of Applied Polymer Science, 2021. 138(20): p. 50417.

26. Pereira, J.N., et al., Piezoresistive effect in spin-coated polyaniline thin films. Journal of Polymer Research, 2012. 19(2): p. 9815.
27. Cherdoud-Chihani, A., M. Mouzali, and M.J.M. Abadie, Study of crosslinking acid copolymer/DGEBA systems by FTIR. Journal of Applied Polymer Science, 2003. 87(13): p. 2033-2051.
28. Meure, S., D.-Y. Wu, and S.A. Furman, FTIR study of bonding between a thermoplastic healing agent and a mendable epoxy resin. Vibrational Spectroscopy, 2010. 52(1): p. 10-15.
29. María González, G., C. Juan Carlos, and B. Juan, Applications of FTIR on Epoxy Resins - Identification, Monitoring the Curing Process, Phase Separation and Water Uptake, in Infrared Spectroscopy, T. Theophile, Editor. 2012, IntechOpen: Rijeka. p. Ch. 13.
30. Zhu, B., et al., Enhancement of Moisture-Resistant Performance of Epoxy Resins via Introduction of Hydrophobic and Flexible Chains. Macromolecular Chemistry and Physics, 2025. 226(2): p. 2400349.
31. Xie, Z., et al., Molecular design of epoxy resin and the driving forces in adhesion with cementitious materials. Applied Surface Science, 2025. 689: p. 162498.
32. Ruíz de Azúa, O., et al., Improving Glass Transition Temperature and Toughness of Epoxy Adhesives by a Complex Room-Temperature Curing System by Changing the Stoichiometry. Polymers, 2023. 15(2): p. 252.
33. Ghallemohamadi, M.O., et al., Simultaneously cured diglycidyl ethers of bisphenol A and polyethylene glycol: DSC, TGA, and DMA measurements. Polymers for Advanced Technologies, 2023. 34(9): p. 2816-2822.
34. Bockenheimer, C., D. Fata, and W. Possart, New aspects of aging in epoxy networks. I. Thermal aging. Journal of Applied Polymer Science, 2004. 91(1): p. 361-368.
35. Teijido, R., et al., Sustainable Bio-Based Epoxy Resins with Tunable Thermal and Mechanic Properties and Superior Anti-Corrosion Performance. Polymers, 2023. 15(20): p. 4180.
36. Turan, F., et al., The effect of carbon nanotubes loading and processing parameters on the electrical, mechanical, and viscoelastic properties of epoxy-based composites. Journal of the Brazilian Society of Mechanical Sciences and Engineering, 2022. 44(3): p. 93.
37. Parente, J.M., A.P. Silva, and P.N.B. Reis, The influence of carbon and glass fiber hybridization combined with a graphene-enhanced epoxy matrix on bending fatigue response. International Journal of Fatigue, 2025. 193: p. 108782.

38. Parente, J.M., et al., Impact of the Curing Temperature on the Manufacturing Process of Multi-Nanoparticle-Reinforced Epoxy Matrix Composites. Materials, 2024. 17(8): p. 1930.
39. Andreghetto, D.H. and G.d.C. Fuzari, Piezoresistive epoxy resin films with carbon black particles for small-strain sensors. Polymer Bulletin, 2020. 77(7): p. 3725-3734.
40. Imran, K.A. and K.N. Shivakumar, Graphene-modified carbon/epoxy nanocomposites: Electrical, thermal and mechanical properties. Journal of Composite Materials, 2019. 53(1): p. 93-106.
41. Zamfirova, G., et al., Nanocomposites based on epoxy resin. Simulation of microindentation process. Colloids and Surfaces A: Physicochemical and Engineering Aspects, 2014. 460: p. 254-264.
42. Her, S.-C. and P.-C. Chien, Fracture Analysis of MWCNT/Epoxy Nanocomposite Film Deposited on Aluminum Substrate. Materials, 2017. 10(4): p. 408.
43. Mirsalehi, S.A., A.A. Youzbashi, and A. Sazgar, Characterization of the interface and interphase region in the multi-walled carbon nanotube modified epoxy resin/carbon fiber hybrid nanocomposite. Composite Interfaces, 2022. 29(6): p. 675-693.
44. Garg, M., S. Sharma, and R. Mehta, Role of curing conditions and silanization of glass fibers on carbon nanotubes (CNTs) reinforced glass fiber epoxy composites. Composite Interfaces, 2017. 24(2): p. 233-253.
45. Avilés, F., A.I. Oliva-Avilés, and M. Cen-Puc, Piezoresistivity, Strain, and Damage Self-Sensing of Polymer Composites Filled with Carbon Nanostructures. Advanced Engineering Materials, 2018. 20(7): p. 1701159.
46. Dai, H., E.T. Thostenson, and T. Schumacher, Comparative study of the thermoresistive behavior of carbon nanotube-based nanocomposites and multiscale hybrid composites. Composites Part B: Engineering, 2021. 222: p. 109068.
47. Kupski, J. and S. Teixeira de Freitas, Design of adhesively bonded lap joints with laminated CFRP adherends: Review, challenges and new opportunities for aerospace structures. Composite Structures, 2021. 268: p. 113923.
48. Wan, J., et al., Epoxy thermosets and materials derived from bio-based monomeric phenols: Transformations and performances. Progress in Polymer Science, 2020. 108: p. 101287.
49. Oliveira, P.R., et al., Bio-based/green sandwich structures: A review. Thin-Walled Structures, 2022. 177: p. 109426.



Chapter 5 - Conclusions and Future Works

5.1 Conclusions

This thesis provides compelling insights into the development, tailor processing, characterization, and application of three different ERs, including low and larger viscosity ones and a biobased, and Composites reinforced with conductive carbon-based nanofillers, including MWCNTs, CB and G. The development of the thesis led to several overarching conclusions, highlighting the significance of these multifunctional materials in structural adhesives and coatings with self-sensing capabilities.

The excellent mechanical and adhesive properties of thermosetting materials can be enhanced with sensing properties provided by adding conductive nanofillers. Innovation Involves transforming resins into uniformly dispersed composites with a suitable viscosity for screen-printing, ensuring scalability for industrial applications. So, the dissolution process is key step to deagglomerate the nanofillers to obtain composites with superior overall properties. These ERs and composites were tailored to be applied by screen-printing and doctor blade techniques, demonstrating that it is an effective process while maintaining structural integrity in printed thin. The nanofiller dispersion, using acetone as solvent for higher viscosity ERs, has resulted in well-integrated composites, without significant filler agglomeration even at higher filler concentrations. Structural morphology demonstrates compact resin and composites without voids or holes, except for larger filled composites, due to higher viscosity of the materials. These homogeneous properties are confirmed by mechanical properties of epoxies, with a slightly decrease of stress-strain performance in composites compared to ERs, which is accentuated in composites with larger filler content, for all used polymer matrices. The mechanical performance of matrices is superior in strain for low-viscosity ERs, with strain rupture near 10%, and superior stress for bioresin, with stress at rupture near 30-40 MPa for materials. Thermal and chemical properties do not change critically in composites, making it possible to evaluate the capacity of these materials for functional applications.

The composites allow to significantly improve electrical conductivity, while simultaneously revealing reduced mechanical properties related to larger nanofiller concentration. Mechanical testing demonstrated that in-between nanofiller contents achieved a favorable balance between enhanced conductivity and adequate mechanical and adhesive properties. The composites exhibited an electrical resistivity reaching around 100 Ω/sq, for composites reinforced with MWCNTs, independently of matrix or processing. Graphene presents lower conductive properties in thermoset materials. Thus, screen-printed resin or bioresin can be evaluated as a sensing composites.

Taking advantage of the properties of resins, composites with appropriate electrical conductivity were evaluated as functional sensors. Piezoresistive sensitivity, quantified by the gauge factor (GF) for bending

deformations, is observed for bending up to 5 mm for the different matrices in composites above electrical percolation threshold. Loading-unloading piezoresistive cycles have been obtained for composites with all polymer matrices, with linear correlation between mechanical stimuli and electrical resistance changes, mainly for low bending stimuli. The GF performance is larger for bioresin with GF ≈ 1 to 2, and lower than GF< 0.5 for low-viscosity resin. In bioresin, comparing distinct nanofiller types, composites reinforced with CB present larger piezoresistive sensitivity, with GF ≈ 2 to 5. Geometric factor is dominant in rigid matrices, where the GF is lower than GF=2, except for the bioresin. Besides piezoresistivity, these conducive composites also exhibit thermoresistive sensitivity for lower and higher range temperature applications, with sensitivity reaching $S_{35\text{-}40} \approx 0.01$ (%.°C^{-1}) and $S_{60\text{-}90} \approx 0.03$ (%.°C^{-1}) for the two different temperature variation ranges for low-viscosity resin. The thermoresistive response shows a linear variation with a negative temperature correlation, which has been proposed to be dominated by tunnelling effect within the conductive network. The obtaining sensitivity critically depends on filler type and content within the polymer matrix.

Making use of adhesive properties of ERs, bonded joint structures of aluminium, reinforced carbon fibre and reinforced glass fibre, were fabricated using pristine resins and composites to evaluate their mechanical properties, as well as the functional ones. The shear lap tests of bioresins present much larger strength than both traditional resins, with break strength between 90 and 150 MPa for resin and composites with MWCNTs, CB, and G. Also, the bond joints were evaluated as adhesive and sensing materials, simultaneously. Piezo- and thermoresistive measurements were carried out, exhibiting much larger sensitivity, with respect to the pristine sensing materials. Piezoresistive response increases up to l GF ≈ 15 and 30 for low and high viscosity resins, and up to GF ≈ 12 for bioresin. Sandwiched functional composites between fibre or aluminium stripes were tested under compression and bending simultaneous stimuli, increasing the sensitivity of bond joint sensing materials, for all composites, independently of resin or filler type or content. Similar increases in performance for thermoresistive sensors is observed. This ability to integrate sensing functionality into adhesive joints not only enhances operational performance but also aligns with the needed innovations associated with Industry 4.0.

To demonstrate a functional application of the thermoset composites, a bonded cantilever to mimic structural applications was developed. The cantilever system displayed a stable electrical response to bending stimuli after a few cycles. This performance highlights the composites' potential for use in aerospace and automotive industries for structural monitoring. This proof of concept validates the hypothesis that such composite materials can effectively act as smart sensing solutions, enhancing safety and performance in critical structural components.

This study also highlights ERs composites reinforced with conductive carbon nanofillers as potential sustainable materials. Results show that bioresins enables multifunctional adhesives and coatings with self-sensing capabilities. Innovative fabrication, including solvent-free screen-printing, ensures efficient filler distribution and process control. Exceptional electrical resistivity, piezoresistive and thermoresistive sensitivities position these types of composites at the forefront of smart adhesive technology for structural health monitoring and industrial use.

5.2 Future Directions for Research:

Building on this research, several pathways for future investigation are recommended. First, comprehensive studies should be conducted to further examine the effects of filler mixing technology. Utilizing advanced processing techniques, like tip of ultrasound, may improve filler distribution and optimize performance, potentially leading to enhanced gauge factors and stable piezo- and thermoresistivity signalling.

Another area for future exploration is the recycling and reusing of the composites wasting materials. For instance, grinding these materials and mixing them with other polymers could open up new applications in industry. Additionally, conducting long-term stability tests is essential to assess the durability of piezoresistive and thermoresistive responses under operational stresses and varying environmental conditions.

Integrating these multifunctional materials with smart technologies could enable real-time structural health monitoring systems that should be proven in real application scenarios. Collaborating with industries committed to sustainable practices could lead to the development of eco-friendly formulations without sacrificing performance. There are also promising opportunities in specific applications for biomedical devices or energy solutions, leveraging the unique properties of these composites to drive innovation in emerging fields.

Finally, self-healing materials represent an exciting direction for future research, particularly in the context of ERs composites. Incorporating self-healing capabilities could significantly improve performance and longevity, making these materials highly appealing for structural and functional applications. Exploring novel approaches, such as microcapsules containing healing agents or dynamic covalent bonds, could allow for effective repair of cracks or damages upon activation by external stimuli. It will be essential to assess the compatibility of these mechanisms with existing composite materials.

In conclusion, the extensive research presented in this thesis highlights the potential of carbon-based composite materials in combining mechanical strength, adhesive properties, and sensing functionalities, together with improved sustainability. These advancements position ERs composites as valuable contributors to the future landscape of smart materials with far-reaching implications across